Annual Report 2012/2013

PADERBORN
CENTER FOR
PARALLEL
COMPUTING

University of Paderborn
Paderborn Center for Parallel Computing
Warburger Str. 100, D-33098 Paderborn

www.uni-paderborn.de/pc2

Table of Contents

1 FOREWORD 4

2 PC² OVERVIEW 6
- 2.1 PERSONAL 6
  - 2.1.1 Board 6
  - 2.1.2 Advisory Board 8
  - 2.1.3 Staff 9
- 2.2 FUNDED PROJECTS 11
- 2.3 COLLABORATIONS 12
  - 2.3.1 Ressourcenverbund – Nordrhein-Westfalen (RV-NRW) 12
  - 2.3.2 Gauß-Allianz (GA) 14
- 2.4 TEACHING 17
- 2.5 DISSERTATIONS 18
- 2.6 WORKSHOPS 20
- 2.7 COLLOQUIUMS 23
- 2.8 PUBLICATIONS 24

3 PC² SERVICES 25
- 3.1 TESTBEDS AND BENCHMARKING 25
- 3.2 INFRASTRUCTURE 26
- 3.3 OPERATED PARALLEL COMPUTING SYSTEMS 28
  - 3.3.1 Overview 28
  - 3.3.2 Publicly Available Systems 29
  - 3.3.3 Dedicated Systems 34
- 3.4 SYSTEM ACCESS 37
- 3.5 ONLINE DOCUMENTATION 38

4 PC² SELECTED RESEARCH PROJECTS 39
- 4.1 EDGI – EUROPEAN DESKTOP GRID INFRASTRUCTURE 39
- 4.2 ENABLING HETEROGENEOUS HARDWARE ACCELERATION USING NOVEL PROGRAMMING AND SCHEDULING MODELS (ENHANCE) 46
- 4.3 PARALLEL MONTE-CARLO TREE SEARCH AND ITS APPLICATION TO COMPUTER GO 51
- 4.4 GREENPAD 56
- 4.5 SCALUS: SCALING BY MEANS OF UBIQUITOUS STORAGE 61
- 4.6 SIMBA: SIMULATION BACKPLANE AUTOMOTIVE 65

5 SELECTED USER PROJECTS 68
- 5.1 CHEMISTRY 68
  - 5.1.1 Comparative reaction mechanism study of the enzymatic ring-opening polymerization of ε-caprolactone and ε-caprolactam using QM/MM simulations 68
  - 5.1.2 Adhesion and stability of organic adhesion promoters on metal oxide surfaces 74
  - 5.1.3 Theoretical studies on polyfunctional S-N donor complexes 77
  - 5.1.4 Tyrosinase Models as efficient oxidation catalysts 82
  - 5.1.5 Theoretical study on Stereoselective Lactide polymerisations 89
  - 5.1.6 Detailed quantum dynamics study of the H + CH_4 → H_2 + CH_3 reaction on a new potential energy surface 97
  - 5.1.7 Quantum-Chemical Investigation of Bixbyite-Type Vanadium Sesquioxide 101
  - 5.1.8 High Performance Molecular Dynamics Simulations 105

5.2 MATHEMATICS 109
5.2.1 Solution of inverse electromagnetic scattering problems via shape optimization 109
5.2.2 Performance of sparsity exploiting Algorithmic Differentiation on Multicore Architecture 113
5.3 MECHANICAL ENGINEERING 118
5.3.1 Marangoni convection at deformable single rising droplets – a numerical investigation of fluid dynamics and mass transfer 118
5.3.2 Numerical Simulation of Fully-Filled Conveying Elements 121
5.3.3 Thermodynamics of Droplets 125
5.3.4 Crack growth in functionally graded materials and structures 129
5.4 PHYSICS 134
5.4.1 Understanding materials from massively parallel ab initio calculations 134
5.4.2 Lattice QCD on OCuLUS 139
5.4.3 Controlled motion of DNA-molecules through solid-state nanopores 143
5.4.4 Reaction Dynamics of Photochromic Diarylethenes: Non-adiabatic Ab Initio Molecular Dynamics 147
5.4.5 NANOHELIX 153
6 PC^2 BIBLIOGRAPHY 158

1 Foreword

The Paderborn Center for Parallel Computing (PC^2) is the main center for High Performance Computing (HPC) of the University of Paderborn. Our mission is to provide resources for our scientists to work on computationally challenging problems. To this end, we operate our own HPC systems, host and operate systems owned by or dedicated to individual research groups, and provide support to all HPC users. In addition to this service mission, we also pursue research in high performance systems in general, e.g., in the context of resource management systems, the integration of hardware and software into HPC systems, or energy-efficient high-performance and high-throughput systems.

To be able to fulfill this double duty, we need access to appropriate resources, both for service provisioning and experimental research. This task had become increasingly difficult to do in our former location in Fürstenallee, where the necessary prerequisites were simply not fulfilled by the building's infrastructure. This changed when we moved into the new building O in late 2011. In 2012 and 2013 we widely exploited the newly acquired opportunities.

The hallmark of this development was undoubtedly the installation of our new HPC system OCuLUS in March 2013. The proposal had already been submitted to the Deutsche Forschungsgemeinschaft in August 2011 (with the option of building O in mind). It was approved in February 2012 without any cuts at a budget of slightly under four million €. This triggered a considerable amount of work, structuring a European-wide call for offers and contract negotiations, resulting in the production and installation of the new system. Indeed, structuring the call and the installation process turned out to be an interesting challenge – systems of that magnitude cannot simply be ordered off the shelf but have to be adapted to the particular building setup, especially with respect to cooling. Needing to know about air circulation, cold and warm water supply, dew points, water pump parameters, etc. has introduced some seemingly old-fashioned aspects of plumbing to the job of a computer scientist. However, the risk of a powerful, yet terribly inefficient machine would have otherwise been very high. Fortunately, we were lucky enough to be able to draw on the help of many experts of our University's administration, providing good advice and great support for both technical and legal/administrative questions.

In the end, we successfully installed a system that vastly outperforms our earlier setups. This is evidenced by rank 173 in the worldwide list of super computers, published in July 2013, corresponding to rank 7 in Germany. Not only does this system provide conventional HPC services, it is also accompanied by a dedicated setup for Big Data processing, opening the door to a new class of services for everyday use and research.

It is worthwhile to point out that this new system is not only a technological but also a collaborative innovation. Unlike prior efforts, this proposal, both its content and its financing, was a joint effort of the University of Paderborn as a whole and its research groups interested in HPC. Furthermore, it also comprised several of our neighboring universities; in particular the Bielefeld University and the Universities of

Applied Science in Bielefeld, Hamm-Lippstadt and Ostwestfalen-Lippe contributed to the proposal and are, of course, entitled to use a corresponding share of our resources. We are very grateful to our University's Executive Board and administrative experts, who have made this new form of collaboration possible and helped it along in its early stages.

But moving into a new building has not only opened technical possibilities. It has also fostered opportunities for collaboration. In particular, the collaboration with the IMT, our mainstream data center, has benefitted considerably from sharing some of the same infrastructure and rooms. This has led to many small improvements as well as to joint projects, e.g., the GreenPAD project or the campus storage system based on the Isilon technology, the use of which was pioneered in Paderborn by the PC^2.

Similarly, the collaboration with the computer engineering group, in particular the group of Prof. Plessl, has been improved. This has boiled down to the new EU project SAVE, led by Prof. Plessl and supported by us. The project will investigate self-adapting systems in the context of heterogeneous computing resources.

Additionally, we are experimenting with new forms of cooperation. For example, in the technical context of SAVE, we are currently financing an FPGA expert, with the goal to better advise our users on the use of this promising technology as well as a kick-start funding for new projects.

These activities have also been reflected in a formal way. Prof. Plessl was elected part of the executive board in August 2013. Also, Dr. Simon, Tobias Beisel, Axel Keller and Oliver Rabe have been (re-)elected to serve on this board. On the other hand, Prof. Fels left the board after his retirement – we cordially thank him for his continuing support over the years and wish him all the best!

Akin to the executive board, the advisory board has seen some changes, too. With the end of their term, Prof. Lippert and Dr. Sack have been followed up by Prof. Rückert (Bielefeld University) and Mr. Rüther (IBM). We thank our former advisors and look forward to working with the new ones. Not only our boards have changed: Dr. Birkenheuer defended his PhD thesis in September 2012 and Dr. Niehörster in January 2013; Mrs. Bolaji and Mr. Altstädt completed their vocational training as IT specialists.

Notwithstanding these positive events, one intended change at the PC^2 did not come to pass. In 2012 we were not successful in hiring a director, a position that was combined with a W1 junior professorship. Since then we have struggled to find new options and managed, with the support of the Institute for Computer Science, to upgrade this position to a W2 professorship. This necessitated a new application process, which has its inevitable time constant. Nevertheless, we are hopeful to conclude this new hiring process with an excellent candidate in the first half of 2014. We are optimistic that with a new leadership and the current excellent infrastructural setup, the PC^2 will be able to contribute to the success of the university and its researchers.

Prof. Dr. Holger Karl

Chairman of the Board

2 PC^2 Overview

2.1 Personal

2.1.1 Board

An interdisciplinary board comprising professors from various working groups heads the PC². The following people were assigned to the PC^2 board in 2012/2013.

Prof. Dr. Holger Karl (Chairman)
Faculty of Electrical Engineering, Computer Science and Mathematics

M.Sc. Tobias Beisel (since October 2013)
Assistant researchers' representative

Prof. Dr. Michael Dellnitz
Faculty of Electrical Engineering, Computer Science and Mathematics

Prof. Dr. Gregor Fels (until October 2012)
Faculty of Science, Department of Chemistry

Dipl.-Inform. Axel Keller
Paderborn Center for Parallel Computing
Non-researchers' representative

Prof. Dr. Burkhard Monien
Faculty of Electrical Engineering, Computer Science and Mathematics

Prof. Dr. Gudrun Oevel
Zentrum für Informations- und Medientechnologien (IMT) representative

Prof. Dr. Marco Platzner
Faculty of Electrical Engineering, Computer Science and Mathematics

Jun-Prof. Dr. Christian Plessl (since August 2013)
Faculty of Electrical Engineering, Computer Science and Mathematics

Oliver Rabe (since October 2013)
Students' representative

Prof. Dr. Franz Josef Rammig
Faculty of Electrical Engineering, Computer Science and Mathematics

Dipl.-Inform. Lars Schäfers (until September 2013)
Assistant researchers' representative

Prof. Dr. Wolf Gero Schmidt
Faculty of Theoretical Physics

Dr. Jens Simon
Paderborn Center for Parallel Computing
Assistant researchers' representative

Jörn Tilmanns (until September 2013)
Students' representative

Prof. Jadran Vrabec
Thermodynamics and Energy Technology

Prof. Andrea Walther
Faculty of Electrical Engineering, Computer Science and Mathematics

Prof. Dr. Hans-Joachim Warnecke
Faculty of Science, Department of Chemistry

2.1.2 Advisory Board

Dr. Karsten Beins
Senior Director Portfolio & Technology
Fujitsu Technology Solutions, Paderborn

Dr. Horst Joepen
Chief Executive Officer
Searchmetrics GmbH, Berlin

Prof. Dr. Dr. Thomas Lippert (until September 2012)
Director of Institute for Advanced Simulation, Head of Jülich Supercomputing Centre,
Jülich Supercomputing Centre, Jülich

Prof. Dr. Alexander Reinefeld
Head of Computer Science, Zuse-Institut Berlin
Humboldt Universität Berlin

Prof. Dr.-Ing. Michael Resch
Director of the High Performance Computing Center Stuttgart
HLRS Höchstleistungsrechenzentrum Stuttgart

Prof. Dr. Nikolaus Risch
President of the University of Paderborn
Universität Paderborn

Prof. Dr.-Ing. Ulrich Rückert (since October 2012)
Faculty of Technology, Cognitronics & Sensor Systems
Universität Bielefeld

Dipl. Phys. Thomas Rüter (since October 2012)
Leading Technical Sales Professional, Certified IT Architect
IBM Deutschland, Ehringen

Dr. Werner Sack (until September 2012)
Miele, Gütersloh

2.1.3 Staff

In the years 2012 and 2013, the PC² employed

- 23 research associates,
- 5 non research associates,
- 4 trainees qualified IT-specialists (Fachinformatiker),
- 14 students and graduate assistants.

Jannic Altstädt (Trainee until June 2013)
Justin Amedick (Trainee since August 2013)
Dipl.-Inform. Bernard Bauer
M.Sc. Tobias Beisel
Fabian Berendes (Trainee)
Dr. Georg Birkenheuer (until September 2012)
Jennifer Bolaji (Trainee until June 2013)
Birgit Farr
Rafael Funke (May to December 2013)
M.Sc. Ramy Gad (until March 2012)
Dipl.-Inform. Yan Gao (until January 2012)
M.Sc. Matthias Grawinkel (until March 2013)
M.Sc. Jürgen Kaiser (until December 2012)
Dr. Server Kasap (since September 2013)
Dr. Paul Kaufmann (until April 2012)
Dipl.-Inform. Axel Keller
Michaela Kemper
Dipl.-Inform. Tobias Kenter (until March 2012)
Dipl.-Ing. Andreas Krawinkel
Dipl.-Inform. Fabio Margalia (until September 2012)
Dipl.-Ing. Sebastian Meisner (until December 2012)
Dr. Dirk Meister (until April 2012)
Dipl.-Inform. Björn Meyer (until March 2012)
Dr. Oliver Niehörster (external PhD student until January 2013)
Holger Nitsche
M.Sc. Federico G. Padua (December 2012 to November 2013)
Dipl.-Inform. Ivan Popov (until July 2012)
M.Sc. Heinrich Riebler (since September 2013)
Dipl.-Inform Lars Schäfers
Dr. Jens Simon
M.Sc. Gavin Vaz (since December 2013)
Dipl.-Inform. Tobias Volkhausen (June to September 2012)

Additional support was provided by students and graduate assistants who were engaged part time (9.5 h/week and 19 h/week) and working in the fields programming, user support, or system-administration.

Gregor Best	Hubert Dömer	Christoph Kleineweber
Michael Meier	Markus Pargmann	Christof Possienke
Inga Poste	Anika Schediwy	Jörn Schumacher
Johannes Schuster	Sebastian Surmund	Alexander Weinhold
Tobias Wiersema		
Markus Pargmann		

2.2 Funded Projects

Projects started in 2012 and 2013

Funding agency	*Projectname*	*Start of the Project*	*End of the Project*
EU	SAVE	September 2013	August 2016
Land NRW/EFRE	SMART EM	February 2013	April 2015

Ongoing Projects

Funding agency	*Projectname*	*Start of the Project*	*End of the Project*
EU	EPiCS	September 2010	August 2014
BMWi	GreenPAD	June 2011	May 2014

Projects finished in 2012 and 2013

Funding agency	*Projectname*	*Start of the Project*	*End of the Project*
EU	Scalus	December 2009	November 2013
EU	Edgi	June 2010	August 2012
DFG	Smash	January 2011	December 2012
BMBF	DGSI	May 2009	April 2012
BMBF	Enhance	April 2011	December 2013
BMWi - ZIM	Simba	April 2011	March 2013
BMWi - ZIM	ProAdapt-2	July 2009	January 2012
Microsoft Ltd.	GOmputer	March 2009	February 2012

For current information about our projects please refer to our website.

2.3 Collaborations

2.3.1 Ressourcenverbund – Nordrhein-Westfalen (RV-NRW)

Supervisor:	Dr. Jens Simon, PC², University of Paderborn
Members:	Axel Keller, PC², University of Paderborn
	Andreas Krawinkel, PC², University of Paderborn
	Holger Nitsche, PC², University of Paderborn

Abstract
The Ressourcenverbund – Nordrhein-Westfalen (RV-NRW) is a network of university computer centers of the state North Rhine-Westphalia. It provides a network of excellence and cooperative resource-usage of high performance compute systems [1]. Targets of this network are:

- Outsourcing of work besides the main focus of each computer center.
- Providing access to short and expensive resources.
  Active member organizations of the RV-NRW are:
- RWTH Aachen
- University Köln
- University Paderborn
- University Münster
- University Siegen
- University Dortmund
- University Duisburg-Essen
- Ruhr-University Bochum
- Open University Hagen

In general, all systems and services of the RV-NRW are available for all scientists of RV-NRW members. The use of the resources is free of charge for this community.

Project Description
The RV-NRW excellence network provides different kind of services to researchers of universities and institute of the state North Rhine-Westphalia.

The RV-NRW provides a primary point of contact for users for all resources provided within the network. Expert advice is provided by the appropriate compute center staff. PC² provides all technical services and user support for its systems. Additionally, courses and material concerning high performance computing are offered to increase the skills and qualifications of the users.

The *Rechen- und Kommunikationszentrum* of the RWTH Aachen, the University Siegen, and the *Paderborn Center for Parallel Computing* provide resources to the RV-NRW.
The following centers are providing resources to RV-NRW, but they are up to now not integrated in the unified user management: The *Zentrum für Informationsverarbeitung* of the University Münster, the *Zentrum für Angewandte Informatik* of the University Köln, the University Dortmund, and the University Duisbur-Essen. Interested scientists apply for access to the RV-NRW compute resource at their local compute center.

Certificate Registration Authority: The Open University Hagen provides a Public Key Infrastructure (PKI) for an automatically issue of X.509v3 certificates. Members of the RV-NRW are free to use the dedicated certificate-server.
The University Paderborn, PC² is a registration authority for Grid certificates. The standard DFN certificates, used for the encryption of e-mails, cannot be used for grid services.

Resource Usage
PC² provided about 30 percent of the compute resources of the Arminius cluster to users of universities and institutes of North Rhine-Westphalia. Researchers from University Wuppertal and Ruhr-Universität Bochum were using RV-NRW accounts to access the PC² cluster system.
Further information about the RV-NRW network of excellence is available on the web pages of the Ressourcenverbund-NRW [1].

References

[1] Ressourcenverbund Nordrhein-Westfalen, http://www.rv-nrw.de

2.3.2 Gauß-Allianz (GA)

Supervisor: Dr. Jens Simon, PC², University of Paderborn

Abstract
The Gauß-Allianz was funded to promote research and development in the field of HPC and to coordinate the HPC related activities in Germany, a further important goal is to increase the visibility on an international level by bundling the expertise of the participating centers.

Project Description
Two years after the Gauss-Centre has been created to coordinate the European supercomputing activities, Germany took the next step to shape the future of high performance computing (HPC) on a national level. On December 3rd 2008 the German leading supercomputing centers met in Bonn to create the Gauß-Allianz. While the Gauss-Centre was successfully addressing the needs on the top end, it was clear from the beginning that an additional layer of support was required to maintain the longevity with a network of competence centers across whole Germany. This gap is now addressed by the Gauß-Allianz, where regional and topical centers team up to create the necessary infrastructure.

With the foundation of the Gauß-Allianz, the HPC community creates the organizational framework to continue the successful collaboration of the past and implements the recommendations given in the BMBF study “HPC in Germany – Reasons for a Strategic Alliance”. On the other hand BMBF recognizes the important role of HPC in science and industry, where sufficient computing power and advanced computational methods are inevitable to drive research and development. This demand also motivates the research in HPC that is necessary to continue the exponential growth in compute power while maintaining and improving usability, productivity and efficiency.

Supercomputing is a key technology of modern science and engineering to solve critical problems of high complexity. Computer simulation and modeling have become indispensable supporting pillars for modern science and engineering, joining the traditional methods of theory and experiment as an additional partner. The application areas range from physics, materials science, chemistry, biology and medicine, to fluid dynamics and structural mechanics. These areas pose equally increasing challenges on the precision of scientific and technical modeling, the efficiency of the mathematical methods and the innovative power of the computer architecture.

The mission of the Gauß-Allianz is to coordinate the HPC related activities of the members. With the provision of versatile computing architectures and by combining the expertise of the participating centers, this creates the ecosystem necessary for computational science.
Strengthening the research and increasing the visibility to compete on an international level are further goals of the Gauß-Allianz. It is especially an important milestone to maintain the leading role of Germany in the European supercomputing activities.

The Gauß-Allianz is getting involved with the

- Promotion of High Performance Computing as an independent strategic research activity
- Improvement of the international visibility of the German research efforts
- Accomplishment of scientific events
- Consulting of research groups, economy, German federation, German countries and supporting organizations
- Publication of scientific results of the Allianz

The full members are:

- Gauss Centre for Supercomputing (GCS)
- Center for Computing and Communication of RWTH Aachen University
- Norddeutscher Verbund für Hoch- und Höchstleistungsrechnen (HLRN) consisting of Konrad-Zuse-Center for Information Technology Berlin (ZIB) and Regional Computer Centre for Lower Saxony (RRZN)
- Center for Information Services and High Performance Computing (ZIH) at TU Dresden
- Rechenzentrum Garching (RZG) of the Max-Planck Society
- Deutscher Wetterdienst (DWD)
- German Climate Computing Centre (DKRZ)
- Steinbuch Centre for Computing at KIT (SCC)
- Forschungszentrum Computational Engineering, Kompetenzgruppe Wissenschaftliches Hochleistungsrechnen der Technischen Universität Darmstadt (CE)

The associated members are:

- Deutsches Elektronen-Synchrotron (DESY)
- German Research and Education Network (DFN)
- Gesellschaft für wissenschaftliche Datenverarbeitung Göttingen mbH (GWDG)
- Goethe Center for Scientific Computing (G-CSC) at Frankfurt University
- Johannes Gutenberg-Universität Mainz
- Paderborn Center for Parallel Computing (PC^2)
- Regionales Rechenzentrum Erlangen (RRZE)
- Regionales Rechenzentrum der Universität Köln

References

[1] Gauß-Allianz, http://www.gauss-allianz.de
[2] Gauss Centre for Supercomputing, http://www.gauss-centre.eu

2.4 Teaching

Lectures

- Architektur Paralleler Rechnersysteme
  WS11/12, WS12/13,WS13/14
  Dr. Jens Simon

Master Theses

- Ashish Chopra
  Simulation of Workloads for Performance Evaluation of Storage Systems: Modeling and Implementation, 2013
- Christoph Kleineweber
  Robust Feedback Control for Virtualized Applications, 2012
- Sebastian Moors
  Advice-Based Caching in NFS Environments, 2012
- Markus Maesker
  Overcoming Write Penalties of Conflicting Client Operations in Distributed Storage Systems, 2012
- Gregor Best
  Energy Efficient Storage Allocation Schemes for Disk Based Archival Systems, 2013

Bachelor Theses

- Felix Bröker
  Konzept und Implementierung eines Systems zur Anforderung und Verwaltung von virtuellen privaten Clustern, 2012

2.5 Dissertations

Dr. Georg Birkenheuer: „Risk Aware Overbooking for SLA Based Scheduling Systems“

Abstract
Academia as well as the economy profit from the abilities of todays computer-aided design processes and simulations. When the need for compute resources is not continuous but occurs in peak loads, it is more efficient for a large number of research groups to share an infrastructure or to rent the compute power on demand instead of maintaining an own infrastructure.

Compute resource providers cover the resulting demand. They trade compute power on the basis of automatically negotiable contracts including estimated resources, fees and penalties, runtime, and deadlines. Statistics show that users lack the ability to accurately estimate a jobs runtime and tend to overestimate. This leads to low utilization of the provider’s infrastructure. However, a high utilization is important to be competitive and profitable.

This thesis introduces two overbooking approaches for the scheduling and negotiation mechanisms of a compute provider. Overbooking exploits the runtime overestimations by using statistics on the user estimation quality to calculate the probability of failure and success when a job is planned with less runtime. Accepting additional, promising jobs increases the utilization of the underlying compute infrastructure, increases the provider’s profit, and minimizes the risk of job failures due to overload. The potential of the presented overbooking approaches is shown based on simulations with real-world job traces. The evaluation demonstrates that academic and commercial resource providers can benefit from overbooking. Careful overbooking allows to successfully executing more jobs even if a few of the additional accepted jobs fail. It is possible to double a provider’s utilization and profit by overbooking

Dr. Oliver Niehörster: Autonomous Resource Management in Dynamic Data Centers

Abstract

Software as a Service (SaaS) providers offer customers easy and spontaneous access to applications that are usually run on virtualized hardware. While virtualization enables flexible administration and better hardware utilization, it turns the data centers into stochastic environments where it is hard to avoid overprovisioning and at the same time guarantee an agreed quality of service (QoS). The number of users and services increases, which makes it impossible to manage user requests manually.

This thesis presents a control theory framework for ensuring the QoS for any given SaaS. For this the resources of the system – such as resource allocations and configuration parameters – are adapted during runtime. The framework supports the adjustment of multiple resources and, in contrast to previous work, also allows for resources whose reconfiguration causes long delays.

The concepts are integrated into a multi-agent system consisting of a scheduler agent and multiple worker agents. Each user request is controlled by an autonomous worker agent, which is equipped with controller implementations and application-specific knowledge allowing it to estimate the type and number of necessary resources. All worker agents interact with the scheduler agent, which takes care of limited resources and does a cost-aware scheduling by assigning jobs to times with low costs. The lowest layer of the system has a rule-based mapping algorithm assigning virtual machines (VMs) to the hosts according to different policies.

The control cycles have been evaluated with two different applications, a high performance computing (HPC) software and an e-commerce benchmark. An energy-aware and SLO fulfilling SaaS stack was built up including a scheduler agent that assigns jobs according to an energy function and a mapper that considers an energy metric.

2.6 Workshops

OpenMP Workshop
May, 7th 2012

Christian Terboven, RWTH Aachen
OpenMP provides a standard, well-known easy-to-use parallel programming model for shared-memory multiprocessors and is supported by all major compilers. However, it is sometimes being said that this is not scalable enough for HPC. The goal of this tutorial is to educate programmers for better understanding of language characteristics and the implications of their decisions when choosing different parallelization patterns with OpenMP, both in terms of correctness and performance. After reviewing key OpenMP concepts, we will cover particularly tasking and the new features of OpenMP 3.1. A selection of tools supporting OpenMP debugging and correctness analysis will be presented as well. After the hands-on session, the tutorial will close with an outlook on upcoming features of OpenMP 4.0.

Christian Terboven is the deputy head of the HPC department at the Center for Computing and Communication at RWTH Aachen University. His research interests are centered around Parallel Programming, with a focus on shared-memory architectures, paradigms, programming languages, and related software engineering aspects. Christian Terboven has been involved in the analysis, tuning, and parallelization of several large-scale simulation codes for various architectures. Since 2006, he is a member of the OpenMP Language Committee. In this context he is involved in the Affinity subcommittee, working on explicit support for NUMA architectures, and the Interoperability and Composability subcommittee, taking care of integration with other parallel programming models and developments in the base languages.

ZKI-Supercomputing
March, 14th to March, 15th 2013

Twice a year the working group “Supercomputing” of the “Zentren für Kommunikation und Informationsverarbeitung e.V.” (ZKI) calls a meeting for all members and other persons interested in exchanging information about HPC topics. The spring meeting of 2013 was held at the Paderborn University and organized by the PC².

The following talks have been given:

- *Wissenschaftliches Rechnen im Paderborner Umfeld*
  Holger Karl, Universität Paderborn
- *Entwurf von Hardwarebeschleunigern für FPGA-basierte HPC-Systeme*
  Christian Plessl, Universität Paderborn

- *Accelerating Bioinformatics Tools for High-throughput DNA Sequence Analysis*
  Alexander Goesmann, CeBiTec Bielefeld
- *Rechenbeschleunigung mit FPGA auf hybrider Plattform (FPGA/x86/GPU)*
  Michele Mazzante, EUROTECH
- *Speicherverbrauchsanalyse von Nutzerprogrammen im Hinblick auf die Eignung für Beschleuniger sowie erste Erfahrungen mit Intel Xeon Phi Beschleunigern*
  Holger Angenent, Universität Münster
- *Scalable I/O Best Practices mit IBM GPFS*
  Klaus Gottschalk, IBM
- *Ausblick auf den HLRN III - Die neue HPC-Ressource für Norddeutschland*
  Holger Naundorf, RRZN
- *Neues von den LIKWID-Tools: Unterstützung aktueller Architekturen und Einsatz in der Praxis*
  Georg Hager, Universität Erlangen
- *Lösung kombinatorischer Probleme durch numerische Algorithmen: Ein anschauliches Beispiel aus der Lehre*
  Martin Bücker, Universität Jena
- *Erfahrungsbericht zum Prorammieren mit Vector-Intrinsics*
  Hinnerk Stüben, Universität Hamburg
- *Beschleunigung von Molekülgeometrie-Optimerungen mit Hilfe von GPUs*
  Lennart Heinzerling, Universität Hamburg
- *IBM GPFS Storage Server*
  Karsten Kutzer, IBM
- *Immerson Cooling*
  Arno Ziebart, ClusterVision

Trainee Crash Course
August, 19th-30th 2013

Since 1998, PC² trains qualified IT specialists in the discipline systems integration (Fachinformatiker Systemintegration). Yearly, about six trainees in this disciplin begin their three years education at the University of Paderborn finishing with an examination at the Chamber of Industry and Commerce.

In 2013 the PC², the Center for Information and Media Technology (IMT), the Heinz Nixdorf Institute (HNI), and the IT service of the Department of Mathematics together organized a two-week crash course for all new trainees.
The course took place at the PC^2.

Goal of the crash course was to lead the trainees in the very beginning to the complex eduational objectives. In addition to a presentation of the particular tasks in the different IT areas of the university, the topics hardware, operating systems, and network were addressed. Due to the limited time the contents could only be superficially addressed. Anyhow, this training facilitated the apprentices' start and showed impressively the opportunities provided by the heterogeneous hardware and software environment of the university.
This workshop not only improved the quality of education but also enhanced the continued cooperation of the departments involved in the training.

2.7 Colloquiums

2012

- *Robust Feedback Control of Virtualized Applications*
  Christoph Kleineweber, Universität Paderborn
- *Risk Aware Overbooking*
  Georg Birkenheuer, PC²
- *A Chemical Approach to Packet-Flow Engineering*
  Dr. Thomas Meyer, University of Basel
- *Herausforderungen der Bereitstellung cloud-basierter Infrastrukturen*
  Dr. Matthias Hovestadt, Technische Universität Berlin
- *Virtualisierung und Daten-Intensive Systeme in Hochleistungsumgebungen*
  Dr. Ilia Petrov, Technische Universität Darmstadt

2013

- *Services des PC²: Status und zukünftige Entwicklung*
  PC² gurus
- *Accelerating Lattice QCD simulations with GPU clusters*
  Dr. Mathias Wagner, Universität Bielefeld
- *Parallele Performance-Analyse - Stand der Technik und aktuelle Trends*
  Dr. Andreas Knüpfer, Technische Universität Dresden
- *Hochleistungs-IT-Systeme zur besseren Skalierung von Simulationen und Datenanalysen*
  Prof. Dr. Kay Hamacher, Technische Universität Darmstadt
- *Challenges and Opportunities for Exascale Computing*
  Dr. Karl Fürlinger, Ludwig-Maximilians-Universität München
- *Autonomic Cloud Computing*
  Dr. Ivona Brandic, Vienna University of Technology
- *Towards Interactive HPC for Large-Scale Applications*
  Dr. Ralf-Peter Mundani, Technische Universität München
- *Ganzheitliches Verständnis von Nutzungs- und Systemverhalten als Zugang zu effizienterem Hochleistungsrechnen*
  Julian Kunkel, Deutsches Klimarechenzentrum Hamburg
- *Complex Data Object Analysis: Determining Memory Footprint and Data Direction*
  Sebastian Dreßler, Konrad-Zuse Zentrum für Informationstechnik (ZIB), Berlin
- *Autonomous Resource Management in Dynamic Data Centers*
  Oliver Niehörster, PC²
- *Konzept und Implementierung eines Systems zur Anforderung und Verwaltung von virtuellen privaten Clustern*
  Felix Bröker, Universität Paderborn

2.8 Publications

In 2012 and 2013 the staff of the Paderborn Center for Parallel Computing published, 2 dissertations, 1 book article, 11 journal papers, 12 conference papers, 10 workshop papers, and one technical report.
All publication references can be found in the bibliography at the end of this report.

3 PC² Services

3.1 Testbeds and Benchmarking

The development of software components for high complex networked systems requires besides analytical and simulation-based evaluation methods more and more experiments in large real live environments. One method to build a new system on top of an existing system is to use virtualization. Virtualization of resources can be found in all areas of computing. In the domain of networking, virtualization is used to hide the characteristics of network resources (like routers, switches, etc.) from the way in which other systems interact with them. The PC² is engaged in investigating how virtualization can be utilized as a concept in the context of building new network testbeds.

The PC² benchmarking center is specialized in evaluating the performance of high-speed networks and parallel computer systems. Typically, these are based on cluster technology. Functional parts or complete systems are evaluated with the help of so-called low-, system-, and application-level benchmarks. The results affect the next generation system architectures. In addition, the PC² offers assistance in finding a high-performance and cost efficient solution for parallel computers for already existing application programs and those under development.

3.2 Infrastructure

In October 2011, the PC² moved from Fürstenallee to the new building O at Pohlweg. After 16 years located in the building of the Heinz Nixdorf Institute, the PC² is back to its roots on campus, close-by the building E, where the first system was launched in 1991. To keep the down time of our services low, the removal of the larger computer systems from the under-dimensioned computer room to the technically well equipped new computer center was organized in three “waves”. The last computer system reached its final position in January 2012.

The new location provides 160m² floor space for offices and additional space for laboratories, training and meeting rooms.

The compute center consists of five computer rooms, with 195m² floor space for HPC systems operated by the PC² and 160m² floor space for systems operated by the IMT (Zentrum für Informations- und Medientechnologien). The building infrastructure provides a redundant cooling system (pipelines to the central cooling facility of the campus and chillers on the roof) and a fault tolerant electrical system with battery backup and emergency power generator. Now, together with state-of-the-art security and fire protection equipment, we are able to provide reliable services and HPC systems with up to 550 kWatt of electricity consumption.

Fig. 1: The computer room in preparation

Fig. 2: Building O. The compute center is located behind the Alan Kay quote

Fig. 3: One of two uninterruptible power supply units (UPS)

Fig. 4: The emergency power system (Diesel engine)

Fig. 5: One of two chillers on the roof

Fig. 6: Cooling and Heating central in the cellar

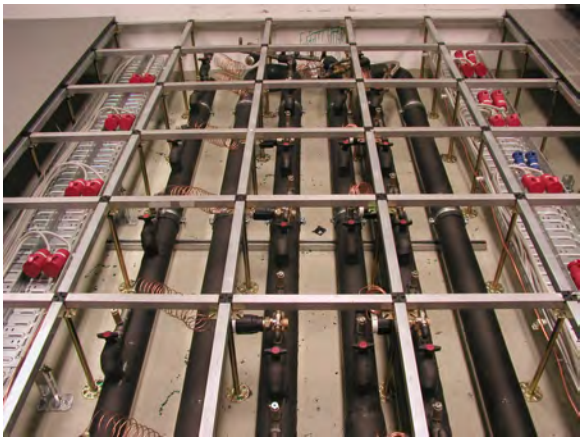

Fig. 7: Tichelmann ring and power supply of OCuLUS

Fig. 8: Nitrogen fire suppression

3.3 Operated Parallel Computing Systems

3.3.1 Overview

In 2012 and 2013 the PC² operated seven high performance computing systems and one parallel file system. Three systems were dedicated to specific projects and/or working groups. Four systems were available for all internal and external researchers of the University.

Publicly Available Systems

Name	Years of Operation	Number of Nodes	Number of Cores	Main Memory per node	Processor Types	Interconnect	Machine
OCuLUS	2013 -	616	9920	64GB 256GB 1TB 4TB	Intel Xeon E5-2670, Intel Xeon E5-4670	InfiniBand QDR	diverse
Arminius+	2010 -	60	720	36GB	Intel X5650 2.67GHz	InfiniBand QDR	Fujitsu RX200S6
High Throughput Cluster (HTC)	2009 -	depends on availability	depends on availability	up to 8GB	Intel or AMD x86-64bit	only for sequential jobs	diverse
SMP Compute Server	2009 -	1	24	128GB	Intel X7542 2.67GHz		Fujitsu RX600

Dedicated Systems

Name	Years of Operation	Number of Nodes	Number of Cores	Main Memory per node	Processor Types	Interconnect	Machine
HPC Cloud	2010 -	38	304	16GB	Intel E5506 2.13GHz	Gigabit-Ethernet	Fujitsu CX1000 CX120S1
Pling2	2009 -	57	456	24GB 48GB	Intel E5540 2.53GHz, Intel X5570 2.93GHz	InfiniBand SDR	Fujitsu RX200S5
BisGrid	2008 -	8	64	64GB	AMD Opteron 2220, 2.8GHz	InfiniBand DDR	Supermicro 2041M-T2R

File Systems

Type	Manufacturer	Years of Operation	Capacity	Protocols	Available on
Network Attached Storage	Isilon	2009 -	54TB	NFS, CIFS	all systems
Parallel File System	FhGFS	2013 -	500TB	FhGFS	OCuLUS

3.3.2 Publicly Available Systems

For all systems, we provided standard system software. A Linux operating system with its software development tools was installed. Additionally, some MPI message passing libraries optimized for InfiniBand were available. Scientific libraries for numerical applications were provided and the Intel compiler suite optimized for the Intel Xeon processor could be used.

OCuLUS Cluster

With the financial support of the state North Rhine-Westphalia and the federal republic of Germany, the PC² established 2013 the OCuLUS cluster. The official opening was April 16th 2013.

Peak performance	200 TFLOP/s (CPU) and > 40 TFLOP/s (GPU)
Processor cores	9.920 Intel Xeon "Sandy Bridge"
Total main memory	45 TByte
Cabinets	12 racks - backdoor cooling, 2 racks - air cooling
Compute nodes (small)	552, each with two Intel Xeon E5-2670 (16 cores), 2.6 GHz, 64 GByte main memory
Compute nodes (large)	20, each with two Intel Xeon E5-2670 (16 cores), 2.6 GHz, 256 GByte main memory
GPU nodes Typ 1	32, each with two Intel Xeon E5-2670 (16 cores), 2.6 GHz, 64 GByte main memory, nVIDIA K20 (2.496 cores, 5 GByte)
GPU nodes Typ 2	8, each with two Intel Xeon E5-2670 (16 cores), 2.6 GHz, 64 GByte main memory, Intel Xeon Phi (60 cores, 8 GByte)
SMP nodes	4, each with four Intel Xeon E5-4670 (32 cores), 2.7 GHz, 1 TByte main memory
Service nodes	6, frontend and admin nodes
Interconnect	QDR InfiniBand PCIe3, 40 Gbit/s Mellanox
Storage system	500 TByte parallel file system, FhGFS 54 TByte PC^2 NAS

Table 1: Hardware specification of the OCuLUS cluster

OCuLUS Utilization

Fig. 1 depicts the daily utilization of the system in 2013. The average load was 57.98%. Table 2 depicts the dates in 2013 the whole system was not accessible (marked with numbers in Figure 1).

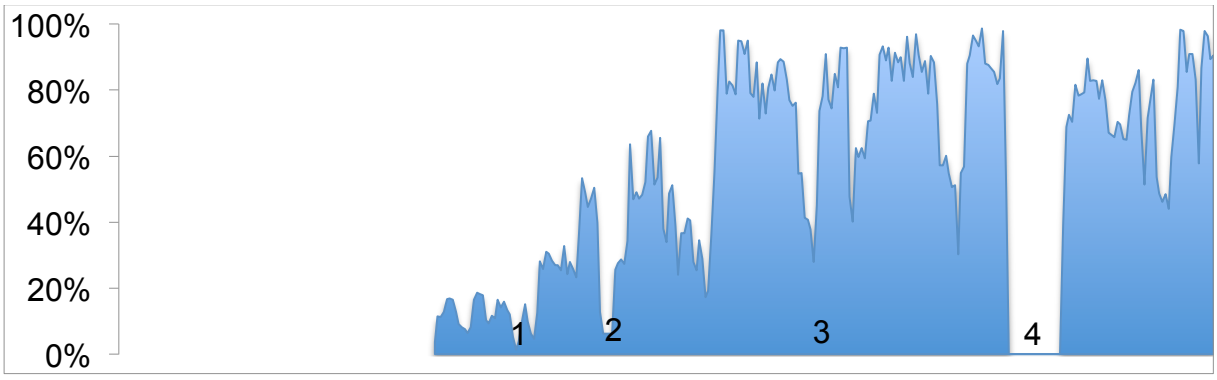

Fig. 1: OCuLUS utilization 16.04.2013 - 31.12.2013 (24h per day)

Event	Date	Reason
1	14.05.13	Upgrade of the FhGFS meta-data servers
2	18.06.13 – 19.06.13	Failure in the internal network configuration
3	20.08.13 – 21.08.13	Maintenance
4	23.10.13 – 11.11.13	Basic system software update and hardware extensions

Table 2: Dates, OCuLUS was not available

Arminius+ Cluster

With the financial support of the state North Rhine-Westphalia and the federal republic of Germany, the PC² established 2010 the ARMINIUS+ cluster. The official opening was October 20th 2010.

Peak performance	7.7 TFLOP/s
Processor cores	720 Intel Xeon "Nehalem"
Total main memory	2.1 TByte
Cabinets	2 racks
Compute nodes	60, each with two Intel Xeon X5650, 2.67GHz, 36 GByte main memory 1, with four Intel Xeon X7542, 2.67GHz, 128GByte main memory
Service nodes	3, frontend and administration
Interconnect	QDR InfiniBand, 40 Gbit/s Mellanox
Storage System	54 TByte PC² NAS

Table 3: Hardware specification of the Arminius+ cluster

Arminius+ Utilization

Fig. 2 depicts the daily utilization of the system in 2012. The average load was 72.93%. Fig. 3 depicts the daily utilization of the system in 2013. The average load was 53.11%. Table 4 depicts the dates in 2012 and 2013 the whole system was not accessible (marked with numbers in Figures 2 and 3).

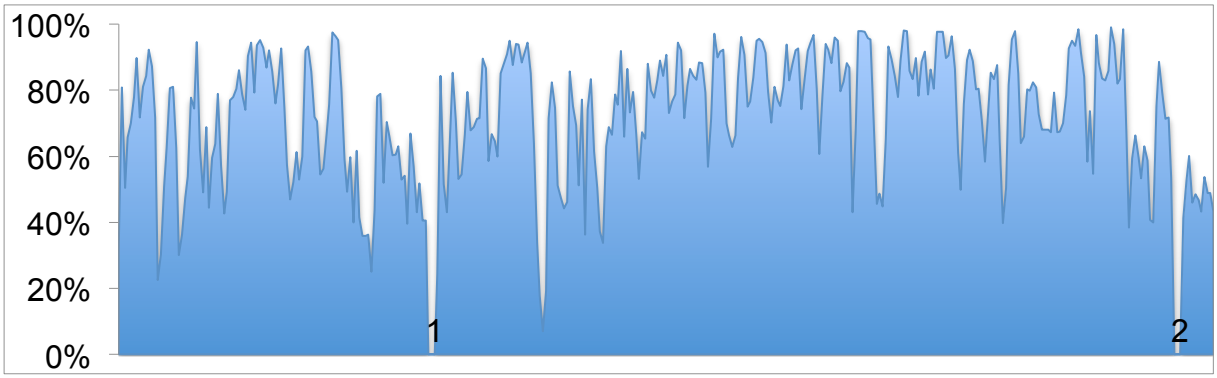

Fig. 2: Arminius+ utilization 2012 (24h per day)

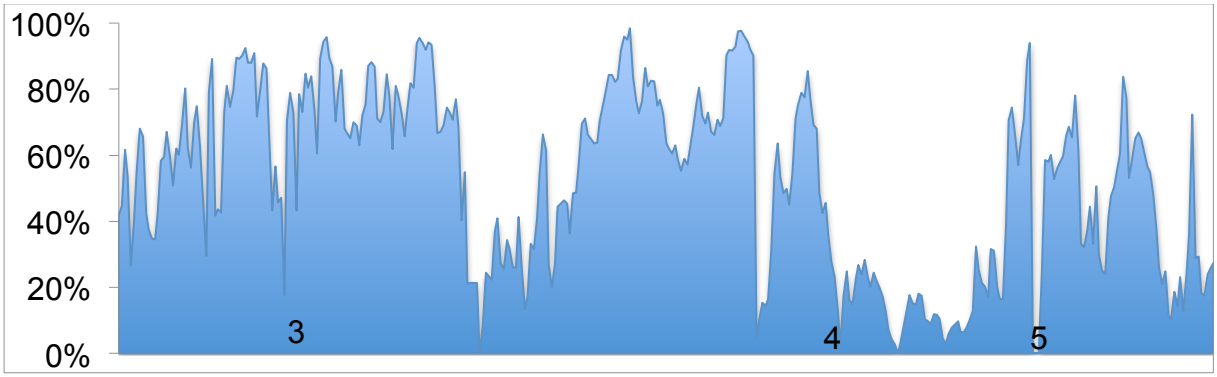

Fig. 3: Arminius+ utilization 2013 (24h per day)

Event	Date	Reason
1	13.04.12 – 16.04.12	Update of the Isilon Filer
2	17.12.12 – 20.12.12	Update of OpenCCS
3	01.03.13	Power failure in Paderborn
4	29.08.13 – 30.08.13	Update of OpenCCS
5	31.10.13 – 04.11.13	Failure in the PC^2 network due to an external maintenance

Table 4: Dates in 2012 and 2013, the system was not available

High Throughput Cluster (HTC)

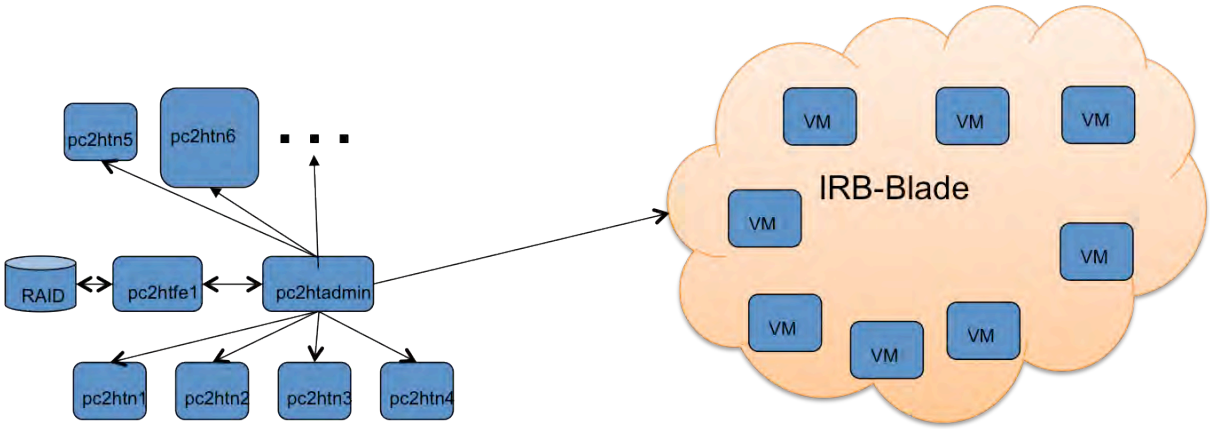

This system has been established in 2009 and is intended to run only sequential jobs with no timeout (i.e., sequential throughput computing). The HTC provided access to about 140 CPUs. Most of them were running as virtual machines on a blade system of the computer science department.

The HTC comprised:

- **A frontend node**
  - name: pc2htfe1, accessible via ssh from 131.234.
  - hosting the cluster local homes and the pre-installed software
- **A server (admin node)**
  - hosting the batch system (Torque)
- **The physical worker nodes**
  - pc2htn*
  - up to 8GB main memory
- **The virtual worker nodes hosted on a blade system of the computer science department**
  - 4GB main memory

The HTC is only dedicated to members of the University of Paderborn. To be able to use the HT-Cluster one has to have an IMT account and has to be member of a special LDAP group.

3.3.3 Dedicated Systems

Paderborn HPC Cloud

Peak performance	2.6 TFLOP/s
Processor cores	304 Intel Xeon "Nehalem"
Total main memory	0.6 TByte
Cabinets	1 rack
Compute nodes	38, each with two Intel Xeon E5560, 2.13GHz, 16 GByte main memory
Interconnect	Gigabit Ethernet

Table 5: Hardware specification of the HPC cloud system

The system is mainly used for research purposes in the cloud field.

Physics InfiniBand Cluster (Pling2)

Peak performance	4.7 TFLOP/s
Processor cores	456 (392 Intel Xeon E45540 and 64 Intel Xeon X5570)
Total main memory	1.5 TByte
Cabinets	2 racks
Compute nodes	49, 2 Intel Xeon E5540, 2.53 GHz, 24 GByte main memory 8, 2 Intel Xeon X5570, 2.93 GHz, 48 GByte main memory
Service nodes	2, frontend and administration
Interconnect	Infiniband SDR and Gigabti Ethernet
Storage System	54 TByte PC^2 NAS

Table 6: Hardware specification of PLING2

BisGrid Cluster

Peak performance	360 GFLOP/s
Processor cores	64 AMD Opteron
Total main memory	512 GByte
Cabinets	1 rack
Compute nodes	8, each with one Opteron 2.8GHz, 64 GByte main memory
Interconnect	Infiniband DDR and Gigabti Ethernet
Storage System	10TByte Fibre Channel SAN

Table 7: Hardware specification of BisGrid

The BisGrid cluster consists of a frontend system and 8 compute nodes. All nodes are connected via InfiniBand HCAs to a 24 port InfiniBand 4x DDR switch, via Gigabit Ethernet to a control network, and via FibreChanel to a Storage Area Network. The Storage Area Network consists of a switched 4Gbit/s Fibre Channel fabric and 10 TByte disk storage. The parallel file system GPFS is used for high performance disk access.

The system is available as a Grid resource operated with UNICORE.

3.4 System Access

All publicly available systems at the PC² can be utilized free of charge from academic users e.g. universities or colleges. In return the users have to provide status reports and references to their research publications.

Users from commercial sites are also welcome but may have to pay a fee for using the systems. Please send a request email to pc2-info@uni-paderborn.de for more information.

Access to restricted systems, e.g. dedicated to specific user groups, can be granted in cooperation with the owner.

Interested parties can apply for an account to access systems at the PC^2 by completing a small application form, available on our web server. Refer to http://pc2.uni-paderborn.de/become-a-pc2-user

After processing the application we will send all necessary information via email within a few days.

The registration information is kept private and will not be disclosed to third parties. It helps us to keep track about the usage of our parallel systems.

Specialist counseling is available for the following fields:

- Compiler
- Debugging
- Grid Computing
- MPI
- Optimization
- Performance Profiling
- System Access
- System-Benchmarking and -Evaluation

Please ask questions and report problems about our systems and services to: pc2-gurus@uni-paderborn.de

3.5 Online Documentation

The PC^2 offers two sources of online documentation. One is the website http://pc2.uni-paderborn.de for general information about the PC^2.

Fig. 1: The PC^2 homepage

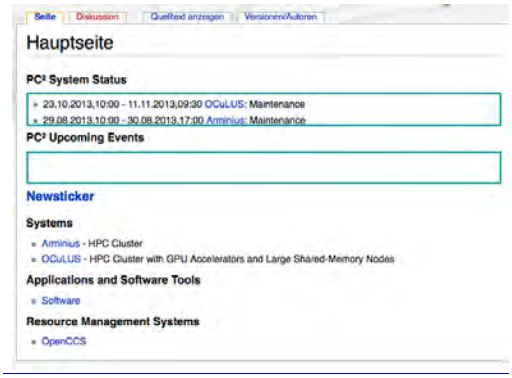

Fig. 2: The PC^2 Wiki

Since 2013 the Paderborn Center for Parallel Computing also utilizes a Wiki as a second source to provide up to date information about our publicly available systems. Refer to https://wikis.uni-paderborn.de/pc2doc. In the Wiki we document relevant hardware and software changes, inform about system status (e.g., maintenance or failures), describe the system architecture, available software packages and available file systems.

Further we provide HowTos, FAQs and give hints for tuning application performance.

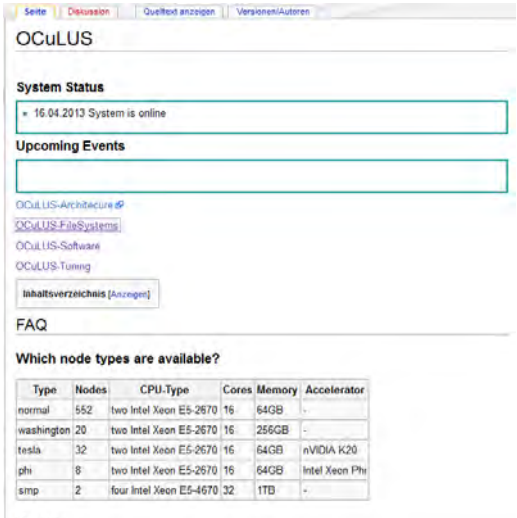

Fig. 3: The PC^2 System FAQs

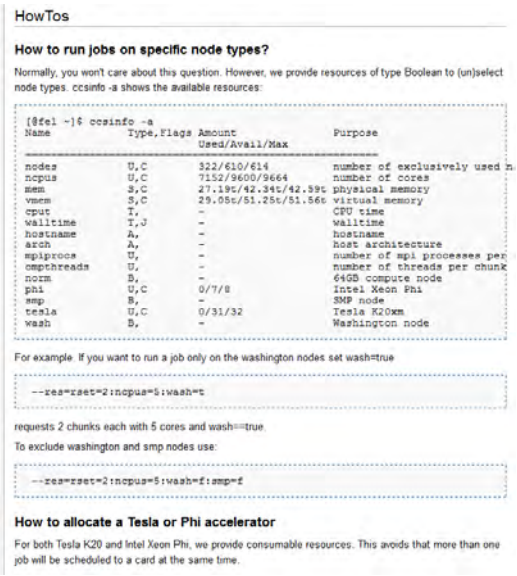

Fig. 4 The PC^2 System HowTos

4 PC^2 Selected Research Projects

4.1 EDGI – European Desktop Grid Infrastructure

Supervisor:	Prof. Dr.-Ing. André Brinkmann, Johannes Gutenberg-Universität Mainz
Members:	Dipl.-Inform. Matthias Keller, University of Paderborn
Supported by:	The FP7 Capacities Programme under grant agreement no. RI-261556

Abstract

Research communities from high-energy physics to humanities utilize grid infrastructures to support and accelerate their research. Their computations can be executed by different grid technologies: Grids of cluster systems, like the German D-Grid, grids of supercomputers, like the Distributed European Infrastructure for Supercomputing Applications (DEISA), or desktop grids consolidated in the International Desktop Grid Federation (IDGF). UNICORE is one of the three grid middleware environments supported by the European Middleware Initiative (EMI) for managing a set of clusters or supercomputers, but desktop grids are currently unsupported. Our work within the EDGI project fills this gap by enabling UNICORE to support all three kinds of grid technologies of the European Grid Infrastructure (EGI). This unified interface enables European scientists to access web services, portals, and applications on all grid technologies in the same way.

Project Description

The European Grid Infrastructure (EGI) creates and provides an eScience infrastructure for European research communities. Those communities, reaching rom high energy physics to humanities, can choose from different grid technologies to execute their computations: Grids of cluster computers, like the German D-Grid, supercomputers, like the Distributed European Infrastructure for Supercomputing Applications (DEISA), or desktop grids consolidated in the International Desktop Grid Federation (IDGF). Each of the technologies has different properties concerning access limitations, amount and types of available resources, and privacy properties.

UNICORE [1] supports both clusters and supercomputers, which are also known as service grids (SGs). Extending UNICORE to support desktop grids is the final step to enable UNICORE to operate with all available grid resources. This extension enables European eScience communities, especially UNICORE virtual organizations, to access all available grid resources from one middleware.

Desktop grids (DG) collect idle resources from loosely coupled desktop computers. Each DG client only has to install a small client software to run computations. DGs exploit the compute capacities of modern computers. Often they are rarely exhausted while performing daily tasks, like reading mails and websites or writing texts. The DG client software now allows the utilization of idle capacities for scientific computations. The desktop computers form either an institutional / private / campus or a voluntary / public desktop grid. The first scenario aggregates idle resources out of computer pools of a university or out of employees' computers of a company. The second scenario motivates the general public to install DG client software on their home computers and therewith to donate compute resources for science similar to popular projects like SETI@home [2].

Since there is no high-speed network between the desktop computers, only a subset of applications is applicable to them, like parameter studies. Parallel applications, which require a high-speed interconnect should still be executed on service grids. However, parameter studies running on service grids can be outsourced to DGs, leaving more available resources for researchers in need of highly interconnected nodes. The power of the DG is the potential to collect and utilize millions of desktop computers owned by citizens. A typical public desktop grid can collect hundreds of thousands or even millions of computers from the volunteers worldwide, depending on how appealing the supported applications are for the citizens. In case of a campus desktop grid, the typical size is several thousands since they are collected within an institute/company.

The aim of the European Desktop Grid Initiative (EDGI) is to deploy desktop grid and cloud services for EGI user communities that are heavy users of distributed computing infrastructures (DCIs) and require an extremely large multi-national e-infrastructure. In order to achieve this goal, software components of ARC, gLite,

UNICORE, BOINC, XWHEP, ATTICS, 3G-Bridge, OpenNebula, Eucalyptus and OpenStack will be integrated into a platform, which can move jobs from service grids to desktop grids. Therefore, EDGI extends ARC, gLite, and UNICORE grids with gateways to volunteer and institutional DG systems. EDGI also integrates a bridge between service grids and cloud environments to be able to support Quality of Service for the DG environments. This enables EDGI to explore new service provision models in order to ensure a harmonized transition from service grids to desktop grids. EDGI will also provide a workflow-oriented science gateway to enable user communities to access the EDGI infrastructure more easily. EDGI establishes the IDGF organization to coordinate DG-related activities in Europe, both for solving technical issues as well as to attract volunteer DG resource donors by disseminating results of the EDGI and EGI projects. IDGF and EDGI will work in strong collaboration with EGI, EMI, NorduGrid, the UNICORE Forum, and interested national grid initiatives.

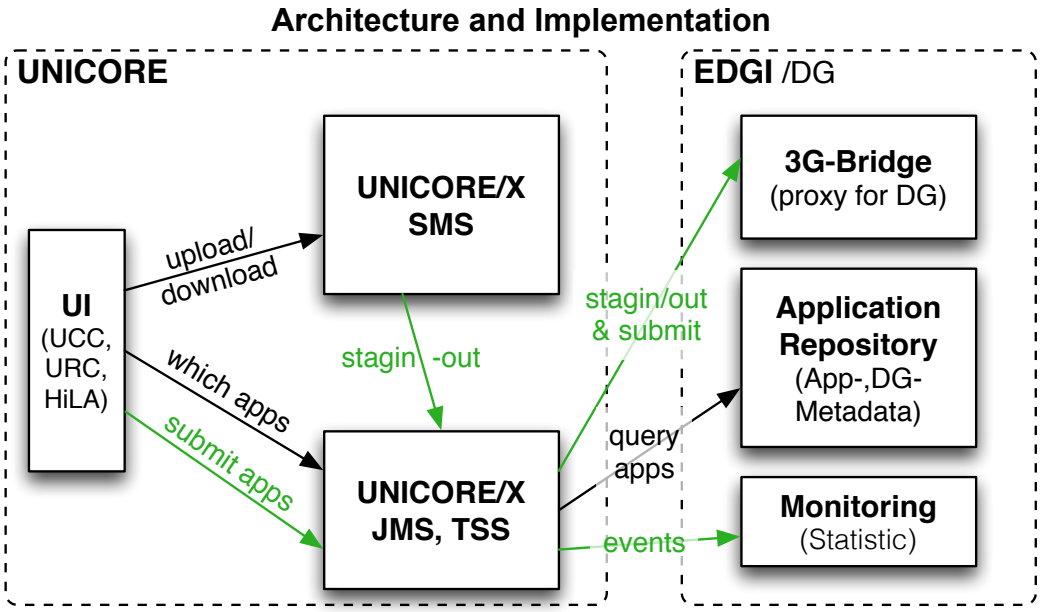

Fig1: Architecture and interaction of UNICORE and EDGI components

This section describes the changes to UNICORE services required to enable DG job submission and is based on [3]. Figure 1 shows UNICORE and EDGI components and their interactions. With the User Interface (UI), a user can upload his input data to an Storage Management Service (SMS), query a UNICORE/X server for available applications, and submit jobs using those applications and input data. The UNICORE/X server (specifically the XNJS through the TSI) will download the input data from the SMS and submit the job to the 3G-Bridge, which forwards the job to the target DG. After the job terminates on a DG client, the UNICORE/X server downloads the output data from the DG and stores it on the given target storage. Later, the user can download the results from the target UNICORE storage.

Typically, an UNICORE/X site represents a single cluster. The extension keeps this architecture by wrapping a single DG installation. Therewith, querying each UNICORE/X for application or resource information results in individual data for each DG. Additionally to submit a job, a user can choose a DG installation. Connecting a target system is usually done by implementing a Target System Interface (TSI). Rather than using a Perl script and executing command line applications, we decided to implement a Java based TSI, which is less error prone. This also includes a full reimplementation of the TSI for accessing remote components like the application repository and the 3G-Bridge, which is SOAP-based.

The remainder of this section describes critical points of the implementation in detail: the special data flow, processing information from the application repository, communication with external components, URL-pass-through realization, and installation.

The staging process is slightly different from a standard UNICORE system, because data has to be transferred additionally to and from the DG head node. The control

flow during a job submission is shown in Figure 2. Figure 3 shows related interactions from an architectural point of view. Through the TSI, the backend component XNJS initiates through the TSI a stage-in process (b),(c). This creates a working directory for the job and downloads every input file into this directory (c). In contrast to the stage-out process, this stage-in process is unchanged and works by using existing code supporting every UNICORE file transfer protocol.

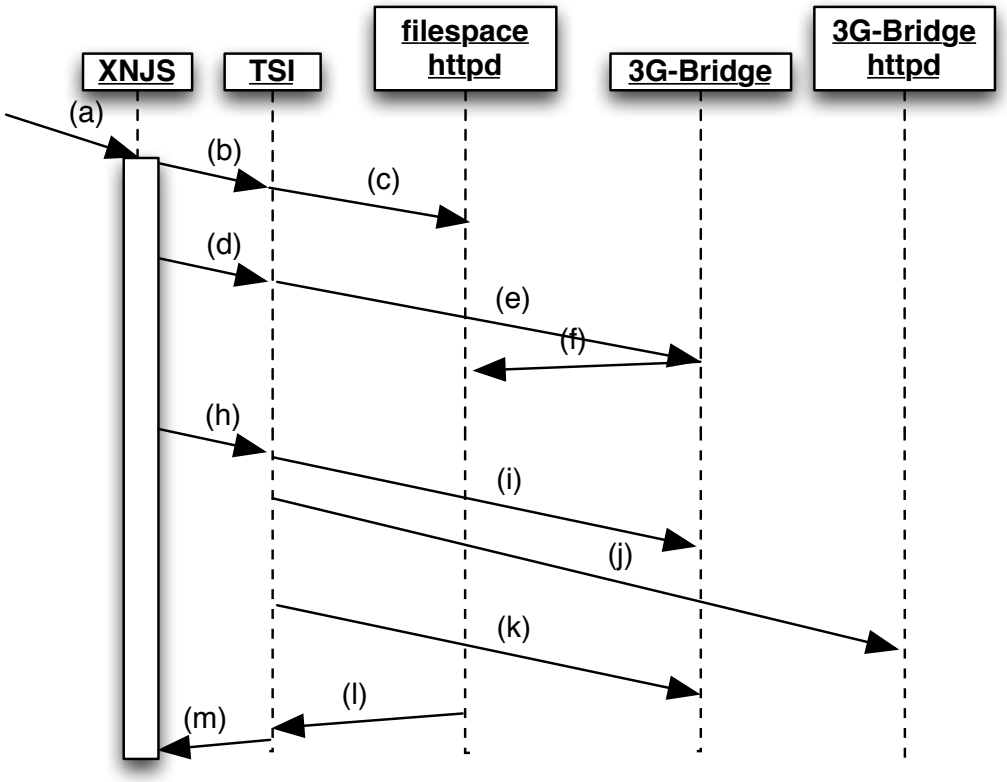

Fig2: Control flow between UNICORE and EDGI components

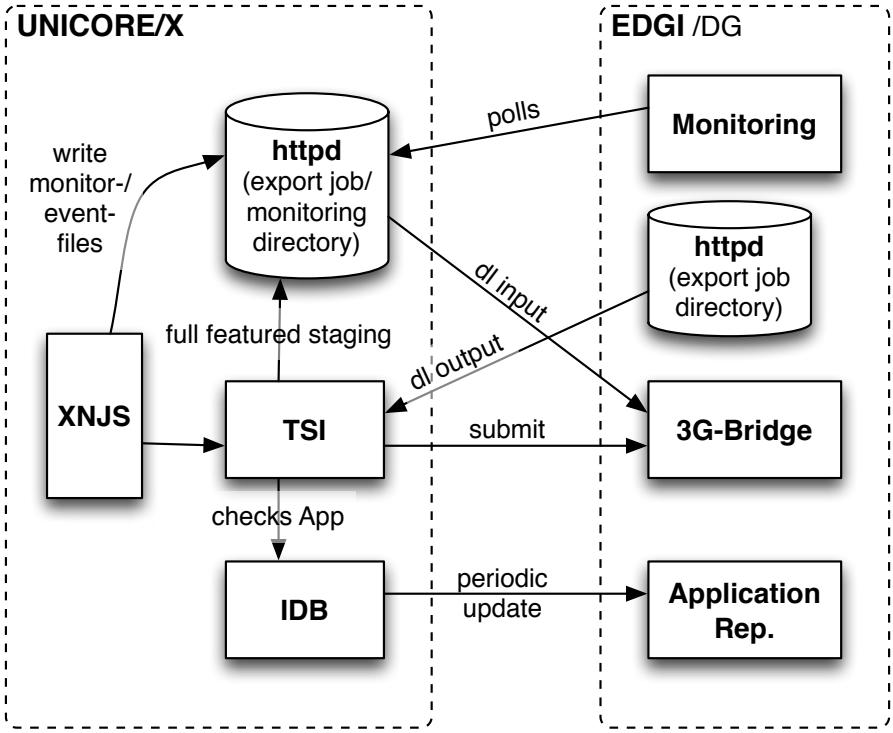

Fig. 3: Interaction of components during job submission

Afterwards, the XNJS triggers a job submission (d). The new TSI transforms the UNICORE job request into a 3G-Bridge request (e). This request cannot contain input data, which is probably hundreds of megabytes large. Thus, the 3G-Bridge expects an alternative way to fetch the input data, e.g., via HTTP (f). The 3G-Bridge is typically collocated with the DG management software on the DG head node, so the 3G-Bridge moves these files to the correct place. To enable fetching input files, the directory, in which UNICORE creates working directories, is exposed via an HTTP-server. To inform the 3G-Bridge about the download location, the input file location of the request (e) is replaced by the corresponding remote URL.

If nothing unexpected happens, the status will change from PENDING to RUNNING and FINISHED. The new TSI observes this by polling the 3G-Bridge (h),(i). If FINISHED is reached, the 3G-Bridge provides a list of output data with HTTP URLs. This data is downloaded to the job's working directory (j). This functionality is hooked in prior to UNICORE's normal stage-out process to enable a fully supported file transfer. Thus, the XNJS believes the computation is not finished until the output file downloading from the remote HTTP server (j) is finished. After every file transfer is finished (j), the job and its files are deleted on the DG site (k), and the normal XNJS functionality continues: stage-out after job computation (l), (m).

This implementation preserves the UNICORE/X stage functionality and supports different target and source storage systems. It also cleans up the 3G-Bridge or the DG head node. Thus overall storage load is minimized. The job data is stored (for later download) in only one place, at the UNICORE side. To download data from the 3G-Bridge site, the implementation reuses UNICORE's File Transfer Services to have stable and concurrent download capabilities.

The Incarnation Database (IDB) is basically an XML-file read by the XNJS. The IDB is used to describe native or local properties of the target system, for which the UNICORE Atomic Services (UAS) provide an uniform interface. The IDB has roughly three parts describing the kind of local resources, CPU architecture, cluster size, the available applications, and specific execution environments used by applications, e.g., MPI. Based on a JSDL-extension, the IDB can specify how to invoke POSIX-like applications.

A viable solution is to introduce a new JSDL-extension for DG-like applications and fill them with data and properties from the application repository. This solution is postponed after the first version is running stable because it introduces additional efforts of creating the specification and verifying it. The current solution updates the

IDB at UNICORE/X start time with information from the application repository, which relates to the currently accessed DG. This can also be triggered from command line, deactivated in the XNJS configuration file, and continuously updated if an interval is specified (default are daily updates). This eases the administrative effort because newly available applications for DGs are automatically available for UNICORE users without involving manual actions. However, this manual step is still needed for submission via gLite and ARC.

An additional benefit of utilizing the IDB system is that information about the accessed DG instance is available from inside the UNICORE system. This not only enables the UNICORE users to access the new type of resources as usual but also frees them to look up DG application specific information from the application repository (another website) and to write a correct job description for submission.

Communication with external components is wrapped inside border classes. The communication is written in pure Java so that no command line calls for clients are involved. This makes the implementation more stable and reliable and exceptions can be handled better. For communication with the 3G-Bridge, UNICORE's SOAP communication capabilities are reused and the application repository is accessed via HTTP requests. A third border class handles the EDGI internal monitoring system, but does not need to communicate with external components, because the monitoring system follows a pull model for observed nodes. For this, a directory is exposed by an HTTP server and the border class writes monitoring events in files, handling the special format for the monitoring internally.

The benefit of encapsulating the handling of external components is that changes to the interface are most probably restricted to local changes within these border classes. Thus, the remaining code stays unchanged. This was observed by updating the monitoring format and SOAP-interface for a new 3G-Bridge version.

URL-pass-through is a concept realized in EDGI for gLite to bypass local staging processes. Publicly available data can directly be downloaded by DG clients.

Otherwise, those data have to be downloaded to a UNICORE/X side, then to a DG head node, from which the DG clients could fetch them. This would result in a waste of bandwidth and potentially cause network bottlenecks on the UNICORE/X site or the DG head node.

Conclusion

We have described the motivation for and the implementation of a UNICORE extension, which directly supports desktop grids from within this service grid middleware. The extension will have a release version, which will be integrated in a productive environment. The stability of the extension is ensured by several unit tests and also by EDGI's work package to test the developed infrastructure. Thus, an active cycle between test engineers and developers is established.
Additional concurrent project efforts port a lot of application to run on desktop grids, so that the UNICORE community can choose from a rich set of applications to submit to new resources. These new resources will boost research, not only for those who use the additional desktop grid resources, but also by leaving more capacity for the rest of the users. In summary, the release quality, the broad application spectrum, and newly available resources make this extension a valuable contribution to the UNICORE community.

References

[1] Streit, A.; Bala, P.; Beck-Ratzka, A.; Benedyczak, K.; Bergmann, S.; Breu,R.; Daivandy, J.; Demuth, B.; Eifer, A.; Giesler, A.; Hagemeier, B.; Holl, S.; Huber, V.; Lamla, N.; Mallmann, D.; Memon, A.; Memon, M.; Rambadt, M.; Riedel, M.; Romberg, M.; Schuller, B.; Schlauch, T.; Schreiber, A. and Soddemann, A.: Unicore 6 - Recent and Future Advancements. Berichte des Forschungszentrums Jülich, 65, 2010.

[2] Anderson, D.P.: Boinc: A system for public resource computing and storage. Proceedings of the 5th IEEE/ACM International GRID Workshop , pp. 1–7, 2004.

[3] Keller, M.; Kovacs,J. and Brinkmann,A.: Desktop Grids Opening up to UNICORE. Proceedings of the UNICORE Summit 2011, pp. 67-76, Torun, Poland, 2011.

4.2 Enabling Heterogeneous Hardware Acceleration Using Novel Programming and Scheduling Models (ENHANCE)

Supervisor:	Jun.-Prof. Dr. Christian Plessl, PC², University of Paderborn
Members:	Tobias Beisel, PC², University of Paderborn
Supported by:	Federal Ministry of Education and Research (BMBF)

Abstract

ENHANCE was a research project carried out by German academic as well as industrial partners. The project aimed on a better integration and simplified usage of heterogeneous computing resources of current and upcoming computing systems.
Heterogeneous systems contain multiple computing resources like multi-core processors, complemented by graphics processing units (GPUs) and/or field-programmable gate arrays (FPGAs). Employing such hardware architectures raises several challenges in programmability, performance estimation, and scheduling that have been approached within the ENHANCE project and resulted in a framework enabling the development and use of applications on heterogeneous systems.
The Paderborn Center for Parallel Computing's role within the project was a to contribute in research and to manage the cooperation of the partners as the official coordinator of the consortium.
The research contribution focused on the efficient and transparent use of the available heterogeneous devices, which is addressed by a novel scheduler that directly cooperates with the operating system. We have developed both, a kernel space and a user space scheduler that use customized scheduling algorithms to map available tasks to supported hardware devices. We could demonstrate that the scheduler improves on state of the art solutions both in the responsiveness of the tasks and the total runtime of a batch of tasks. In addition, the utilization of available computing devices can be increased through dynamic scheduling of tasks to all available resources at runtime. By providing a simple programming model we are able to keep the barrier of entry for users very low.

Project Description

The project was funded by the German Federal Ministry of Education and Research (BMBF) under grant number 01|H11004 and was running from April 2011 to December 2013. ENHANCE was one of twelve projects sponsored within the "HPC-Software für skalierbare Parallelrechner" program that aimed and aims on promoting the high performance computing (HPC) community in Germany. The projects website can be found at [1].

Heterogeneous accelerator systems are commonly used since the appearance of multicore CPUs and general-purpose graphics processing units (GPUs). Multi-core

CPUs combined with GPUs are even provided in standard configurations of personal computers. Also data centers starting to provision experimental cluster systems, which use a combination of multi-core processors, GPUs, and specialized co-processors, such as FPGAs. This is particularly interesting for solving medium-sized scientific computing problems in a cost- and energy-efficient way without accessing large and expensive computing systems. This enables nearly every scientific and industrial institution to access significant computing power to address increasingly complex simulations.

In the state of the art before starting the project the usage of such systems was still limited, since most accelerators need to be programmed with proprietary and unfamiliar programming languages and Application Programming Interfaces (APIs). Efficiently developing software for these architectures is highly challenging for inexperienced developers and requires knowledge about the underlying hardware and software components. Hence, the research effort within the ENHANCE project addressed the challenges in development and use of hardware accelerated code.

Detailed Ideas of the Project

Facing the first challenge to simplify software development for heterogeneous systems we developed a tool-flow that automatically parallelizes loops within an application. We therefore perform the following steps to automate the source-to-source code transformation:

- First, we use a source code parser to analyze the application and translate the code into a polyhedral representation.
- This intermediate representation is then optimized by index transformations to maximize the number of independent indices.
- We developed tools to map the generated index paths to different hardware based on existing tools (PLUTO, CLooG) that work on polyhedral models. These were extended to support heterogeneous systems by automating the transformation of sequential code to parallelized CPU code (OpenMP) and GPU code (CUDA).

In a second major part of the project we approached the challenge of performing scheduling decisions at runtime. To this end we treat hardware accelerators as peer computation units that are managed by the scheduler like CPU cores. The goal of scheduling tasks in the context of heterogeneous systems is to assign tasks to compute units in order to enable time-sharing of accelerators and to provide fairness among tasks that compete for the same resources. We therefore

- include the current utilization of automatically detected heterogeneous compute units
- exploit knowledge about the availability and suitability of a task for a particular hardware accelerator from the application

- introduce a scheduling and programming model that allows preemption and migration for accelerators
- evaluate different scheduling policies to be used for the scheduling decisions
- implement a scheduler to support heterogeneous computing components.

Both of these parts had a strong demand of profiling data to optimize their results and a need for well-defined interfaces between application and operating system.

In a third part of the ENHANCE project we therefore developed a performance model to collect according information, which precisely measures and provides runtimes, input- and output data volumes and uncovers hotspots of an application.

The ENHANCE project resulted in a complete framework (cf. Figure 1) allowing both automatic parallelization and scheduling of applications on heterogeneous hardware architectures and optimizing the results with an included performance model. Intermediate results were iteratively evaluated by incorporating the industrial partner's challenging applications on bio-informatics, automotive computing, pollutant dispersion, and thermodynamics.

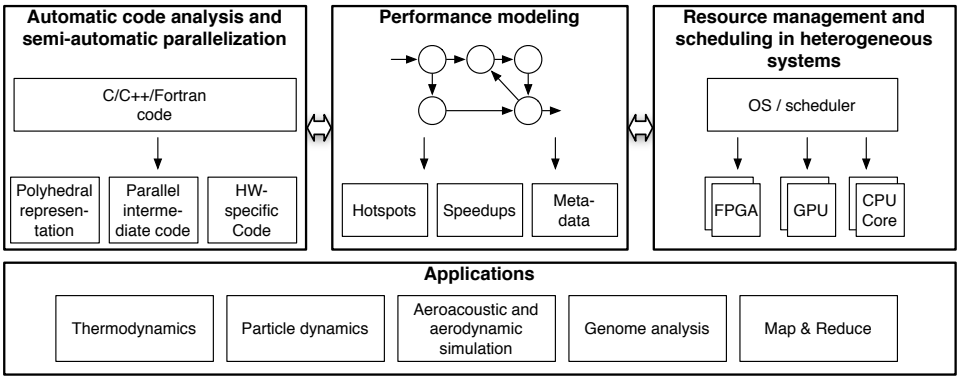

Fig 1: General structure of the ENHANCE project

Scheduling on Heterogeneous Systems

The Paderborn Center for Parallel Computing set its main focus within the project on the development of a scheduler for the heterogeneous target systems. This included developing a scheduling framework, designing and evaluating scheduling algorithms and providing a convenient programming model to be used with the scheduler. Scheduling such heterogeneous systems is more difficult than traditional CPU scheduling due to several reasons:

1) Accelerators typically do not have autonomous access to the shared memory space of the CPU cores and require explicit communication of input data and results.
2) Most accelerators do not support preemption but assume a run-to-completion execution model. While CPU computations can be easily preempted and resumed by reading and restoring well-defined internal registers, most hardware

accelerators neither expose the complete internal state nor are they designed to be interrupted.

3) Heterogeneous computing resources have completely different architectures and ISAs. Hence, a dedicated binary is required for each combination of task and accelerator, which prevents migrating tasks between arbitrary compute units. Even if the internal state of the architecture is accessible, migrating a task between different architectures is far from trivial, as the internal task state representation is different.

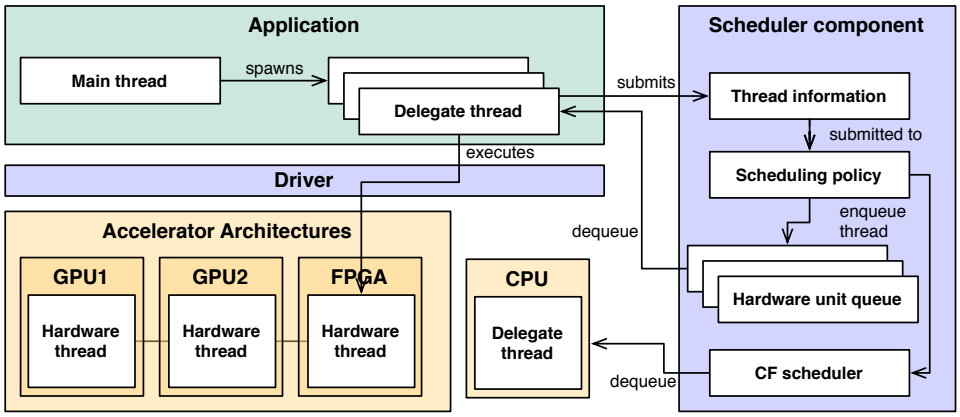

Fig 2: General scheduling model for heterogeneous systems

Our developed scheduler extends the Linux Completely Fair Scheduler (CFS) to treat accelerators as peer computation units that may be used almost equally to the available CPUs. Augmenting the operating system to be aware of available compute units and being able to use these as allocatable compute units allows scheduling decisions to not only incorporate the applications inputs but also the state of the accelerators and the operating system. This approach implies to use the scheduling model of the CFS that uses preemptive multitasking with time-sharing.

We overcome the absence of preemption on some accelerators by introducing the use of cooperative multitasking with checkpoints to the programming and scheduling models. Tasks voluntarily release accelerator architectures at application-defined checkpoints and thus allow to be “preempted” and suspended at these points and to be enqueued again for later continuation or being migrated to a different architecture.

As operating systems cannot directly handle “hardware threads”, i.e., the threads executed on the accelerator, we introduce so-called “delegate threads” that are a logical representation of their hardware counterparts running on the accelerators. These CPU threads are handled by our scheduler and used as communication partners to the application. The application still handles all functionalities that have to be carried out by using the vendor specific APIs. Our scheduler therefore is used as thread and hardware management entity that is able to handle any type of application and hardware. The application execution is mostly hidden behind a scheduling library simplifying the use of the scheduler and prevents applications from major changes.

We developed both a kernel space CFS extension and a user space scheduler. The latter avoids the limitations of the kernel space approach by simplifying the use of the

scheduler for the applications but being slightly less applicable for short-term inclusion of the system status and utilization.

Based on these ideas a scheduler and a corresponding programming model was implemented as a direct extension for Linux and presented in [2]. Its general architecture is shown in Figure 2. Our user space implementation of such a scheduler was submitted for publication recently. Figure 3 shows the reduction of the total runtime of a batch of tasks using the user space scheduler. The two leftmost approaches were compared to state of the art solutions and show a reduction of runtimes on small, medium, large problem sizes and also set of mixed problem sizes.

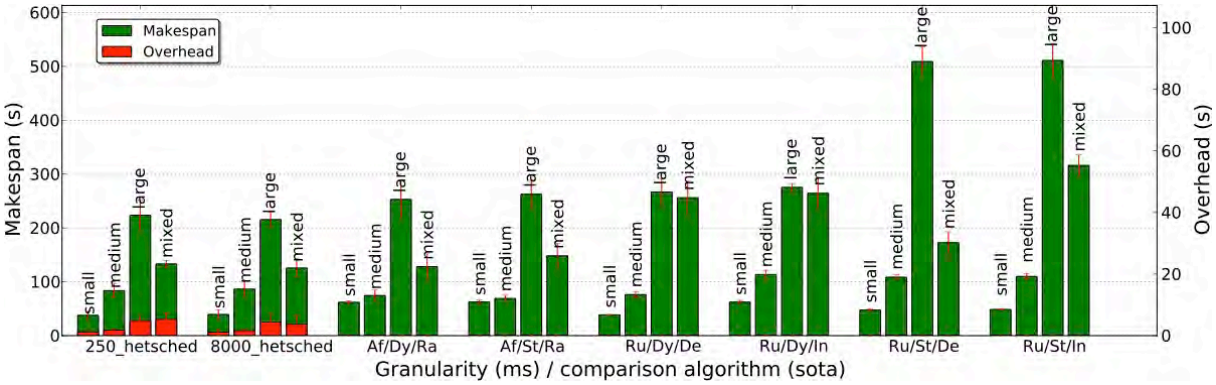

Fig 3: Reduced total runtimes (makespan) using the scheduler (*hetsched*)

Resource Usage

The funding of the project included the purchase of a GPU cluster system. Two nodes, each equipped with 2 INTEL XEON E5620 CPUs, 4 NVidia C2070 GPUs and 48GB main memory are provided by the PC² to the partners for the development and evaluation of parallel applications within the project. In addition, a Convey HC-1 equipped with several FPGAs was used to test parts of the workflow.

References

[1] www.enhance-project.de

[2] Beisel, T.; Wiersema, T.; Plessl, C. and Brinkmann, A.: Programming and Scheduling Model for Supporting Heterogeneous Accelerators in Linux. Proceedings of 3rd Workshop on Computer Architecture and Operating System Co-design (CAOS). Paris, France, January 2012.

4.3 Parallel Monte-Carlo Tree Search and its application to Computer Go

Supervisor:	Prof. Dr. Marco Platzner, University of Paderborn
Members:	Dipl.-Inform. Lars Schäfers, University of Paderborn
Supported by:	Microsoft Ltd.

Abstract

Monte-Carlo Tree Search (MCTS) is a class of simulation-based search algorithms that brought about great success in the past few years regarding the evaluation of deterministic two-player games such as the Asian board game Go. The development of MCTS is said to have started in 1993 with a seminal paper of Bernd Brügmann about a simulated annealing based method that he used with his Go playing program Gobble. It was only in 2003 that Bouzy and Helmstetter took up Brügmann's approach and extended it with an efficient way to grow and store a game tree in memory. In 2006, Rémi Coulom managed to further improve the concept and developed his Go program CrazyStone that was able to compete with the strongest traditional Go programs at that time. This marked the start of a terrific revolution in the development of Computer Go that persists until today. In the field of Computer Go, MCTS highly dominates over traditional methods such as alpha-beta search.

Over the years, MCTS found applications in several search domains. A recent survey of MCTS methods lists almost 250 MCTS related publications originating only from the last seven years, which demonstrates the popularity and importance of MCTS. It is currently emerging as a powerful tree search algorithm yielding promising results in many search domains such as connection games Hex and Havannah, combinatorial games Othello and Amazons as well as General Game Playing, and real-time games. Apart from games, MCTS finds applications in combinatorial optimization, constraint satisfaction, scheduling problems, sample-based planning, and procedural content generation.

In our project we developed a parallelization of the most popular MCTS variant for large HPC compute clusters that efficiently shares a single game tree representation in a distributed memory environment and scales up to 128 compute nodes and 2048 cores in self-play experiments. It is hereby one of the most powerful MCTS parallelizations to date. We empirically confirmed its performance with extensive experiments and showed our parallelization’s power in numerous competitions with solutions of other research teams around the world.

In order to measure the impact of our parallelization on the search quality and remain comparable to the most advanced MCTS implementations to date, we implemented it in a state-of-the-art Go engine Gomorra, making it competitive with the strongest Go programs in the world. We proved the strength of Gomorra in several international

computer Go tournaments, most recently in 2013 by winning a silver medal at the 13th Computer Olympiad in Yokohama, Japan.

Project Description

We developed an empirically analyzed a novel data-driven parallelization approach for Monte Carlo Tree Search (MCTS) algorithms targeting large HPC clusters with fast network interconnect. The power of MCTS strongly depends on the number of simulations computed per time unit and the amount of memory available to store data gathered during simulation. High-performance computing systems such as large compute clusters provide vast computation and memory resources and thus seem to be natural targets for running MCTS.

Parallelization of traditional alpha-beta search is a pretty well solved problem. While for alpha-beta search it is sufficient to map the actual move stack to memory, MCTS requires us to keep a steadily growing search tree representation in memory.
Targeting at optimal utilization of the available resources our algorithm spreads a single search tree representation among all compute nodes (CNs) and guides simulations across CN boundaries using message passing. In the context of MCTS, sharing a search tree as the central data structure in a distributed memory environment is rather involved and only few approaches have been investigated so far [1][2]. A comparable approach used with traditional alpha-beta search was termed transposition table driven work scheduling (TDS) [3]. Computing more simulations in parallel than distinct compute resources are available allows us to overlap communication times with additional simulations, a technique commonly known as *latency hiding*.

We integrate our parallel MCTS approach termed UCT-Treesplit in our state-of-the-art Go engine Gomorra [4] and measure its strengths and limitations in a real world setting. Our extensive experiments show that we can scale up to 128 compute nodes and 2048 cores. The generality of our parallelization approach advocates its use to significantly improve the search quality of a huge number of current MCTS applications.

Our Go engine Gomorra has proven its strength at the Computer Olympiad 2010 in Kanazawa, Japan, the Computer Olympiad 2011 in Tilburg and several other international Computer Go tournaments. Gomorra is regularly placed among the strongest 6 programs and recently won a silver medal at the Computer Olympiad 2013 in Yokohama, Japan.

Experimental Results

We performed extensive experiments with our Go engine Gomorra that incorporates our parallelization. In the following we show experimental results concerning the scalability of our parallelization in terms of search quality that were produced by

Gomorra playing against itself. Then we present more detailed insights by showing the development of achieved simulation rates, measured workloads and network bandwidth usage for varying numbers of MPI ranks. Whenever provided confidence intervals are given with a 95% confidence level.

For our experiments we use up to 160 CNs of the OCuLUS cluster, each one equipped with 2 Intel Xeon E5-2670 CPUs (16 cores in total) running at 2.6 GHz and 64 GByte of main memory. A 4xQDR Infiniband network connects the CNs. We use OpenMPI (version 1.6.4) for message passing.

We examine our parallelization's overall performance characteristics with Gomorra playing games against itself with varying numbers of compute nodes.

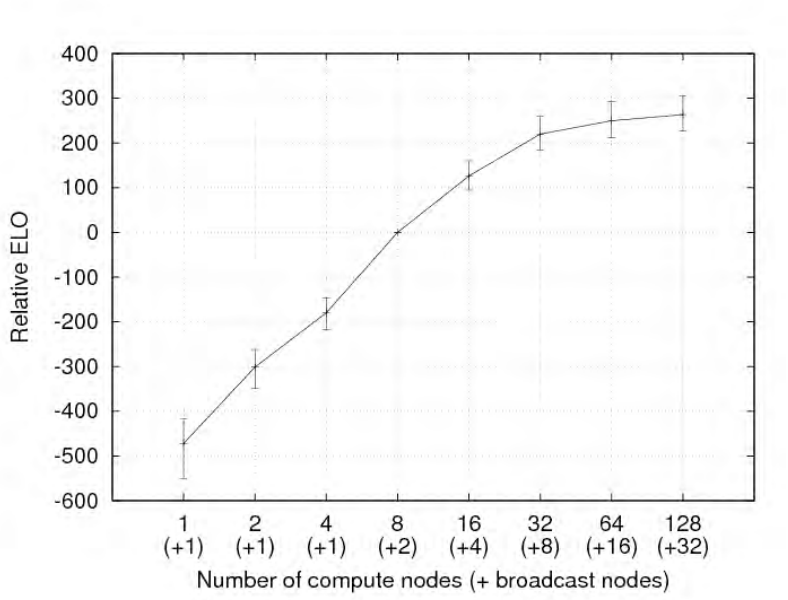

Fig 1: Evaluation of Gomorra's playing strength when playing against itself using parallel UCT-Treesplit for varying numbers of compute nodes

The most important measure for the performance of a parallel MCTS algorithm and its scalability is the development of playing strength with an increasing number of CNs. We measured the playing strength in ELO [5].
Figure 1 shows the strength development for the parallel version when using varying numbers of CNs. All games played for these figures were games against Gomorra itself. The reference configuration for the parallel version used 8(+2) CNs. Here, we write 8(+2) for 8 search CNs and 2 additional broadcast CNs that assist broadcast operations. As we can see, the parallel version improves by about 700 ELO from 6 doublings of the number of CNs.
We additionally look at the simulation rate, i.e. the number of simulations that can be computed per time unit for varying numbers of CNs.

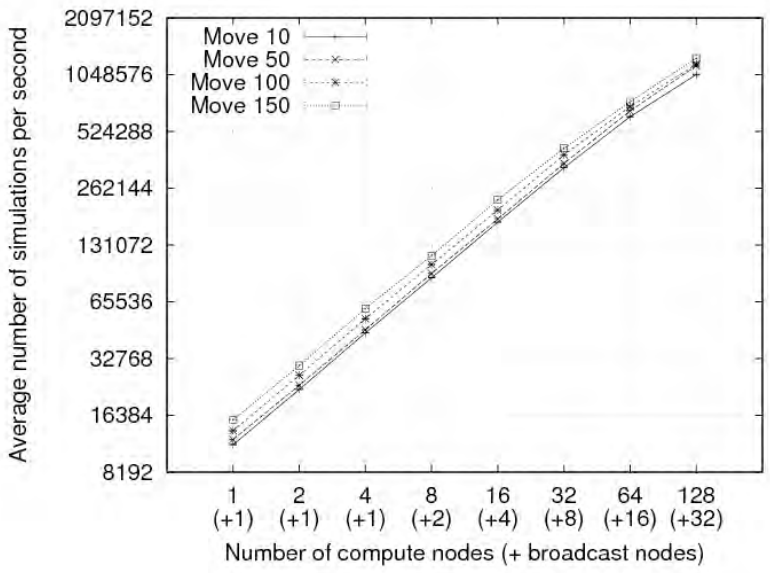

Fig. 2: Scalability of simulation rate with increasing number of CNs at different game phases

Figure 2 shows the scalability of the simulation rate and Figure 3 the development of the average workload measured at the worker cores. Both diagrams show 4 curves for measurements at different phases of the game: At moves number 10, 50, 100 and 150. We can see that the number of simulations scales uniformly for up to 32(+8) CNs and observe a slightly degraded scalability for more nodes. Figure 3 in contrast shows a more remarkable drop of measured workloads when using more than 32(+8) CNs. This observation also matches the reduction of playing strength scalability observed in Fig. 1.

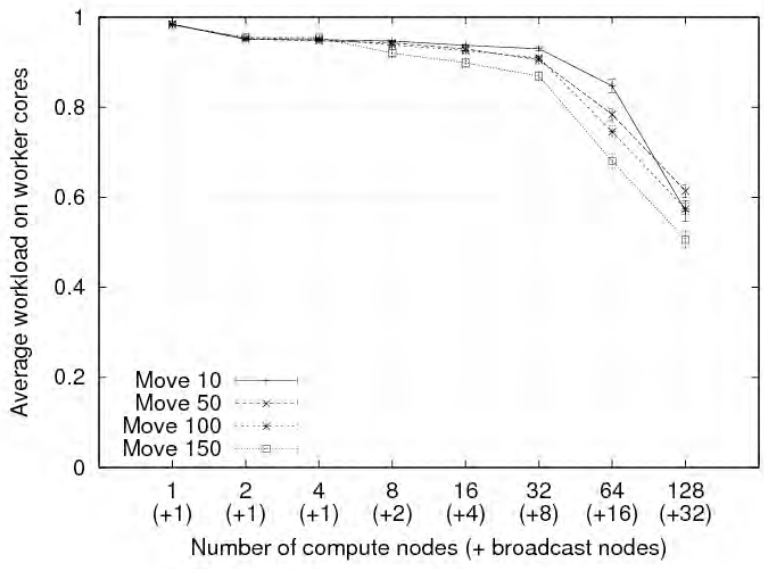

Fig. 3: Average workload at worker cores with increasing number of CNs at different game phases

References

[1] Bourki, A; Chaslot, G.M.-B.; Coulm, M.; Danjean, V.; Doghmen, H.; Hoock, J.B.; Hérault, T.; Rimmel, A.; Teytaud, F.; Teytaud, O.; Vayssiére, P. and Yu, Z.: "Scalability and Parallelization of Monte-Carlo Tree Search". International Conference on Computers and Games, pp. 48–58, 2010.

[2] Yoshizoe, K.; Kishimoto, A.; Kaneko, T.; Yoshimoto, H. and Ishikawa, Y.: "Scalable Distributed Monte-Carlo Tree Search". SOCS, Borrajo,D.; Likhachev,M. and López,C.L.: Eds. AAAI Press, pp. 180–187, 2011.

[3] Romein, J.W.; Plaat, A.; Bal, H.E. and Schaeffer, J.: "Transposition Table Driven Work Scheduling in Distributed Search". National Conference on Artificial Intelligence, pp. 725–731, 1999.

[4] Graf, T.; Lorenz, U.; Platzner, M. and Schaefers, L.: "Parallel Monte-Carlo Tree Search for HPC Systems". Proceedings of the 17th International Conference, Euro-Par, ser. LNCS, vol. 6853. Springer, Heidelberg, pp. 365–376, Aug 2011.

[5] Elo, A.E.: "The Rating of Chessplayers, Past and Present". New York: Arco Publishing, 1986.

4.4 GreenPAD

Supervisor:	Prof. Dr. Gudrun Oevel, University of Paderborn
Members:	Rainer Funke, University of Paderborn
	Holger Nitsche, PC^2, University of Paderborn
	Sabine Mennen, University of Paderborn
	Frederik Möllers, University of Paderborn
	Sebastian Porombka, University of Paderborn
Supported by:	Bundesministerium für Wirtschaft und Energie (BMWi)

Abstract

The main idea behind our project "GreenPAD" is to examine the possibility of using regionally produced renewable energy in data centers. Although most servers should be available 24 hours a day throughout the year, we ask if it is possible to schedule jobs and equipment in such a way that the available renewable energy is maximally used.

The Paderborn part of the project concentrates on energy efficient computer centers and racks, network components their load, and corresponding energy consumption as well as virtual desktop infrastructures and thin client solutions compared with classical desktops. Also cloud infrastructures as a way to concentrate equipment for regional Small and Medium-sized Enterprises (SME) were addressed and examined. As a last step we try to develop price models for cloud services in which the usage of regionally produced renewable energy is rewarded.

Project Description

GreenPAD (www.green-pad.de) is a project funded by the German Federal Ministry of Economics and Energy. It started in June 2010 and the project partners are the Universities of Mainz and Paderborn, unilab AG, Fujitsu technologies, and E.ON Westfalen Weser AG.

As a first step the newly built computer center at the University of Paderborn underwent a review from an energy efficiency perspective. Also, the computer rooms of some small and medium-sized enterprises were reviewed regarding their so-called PUE (power usage efficieny) coefficient. Energy efficient servers were bought and built up. As we tried to power-off servers during low demand times we had to realize that our rack model CoolTherm did not support parts of the equipment to be powered-off. In cooperation with the producer (Co. Knürr) we developed a zoning model for racks that is under further examination now (see figure 1a, 1b).

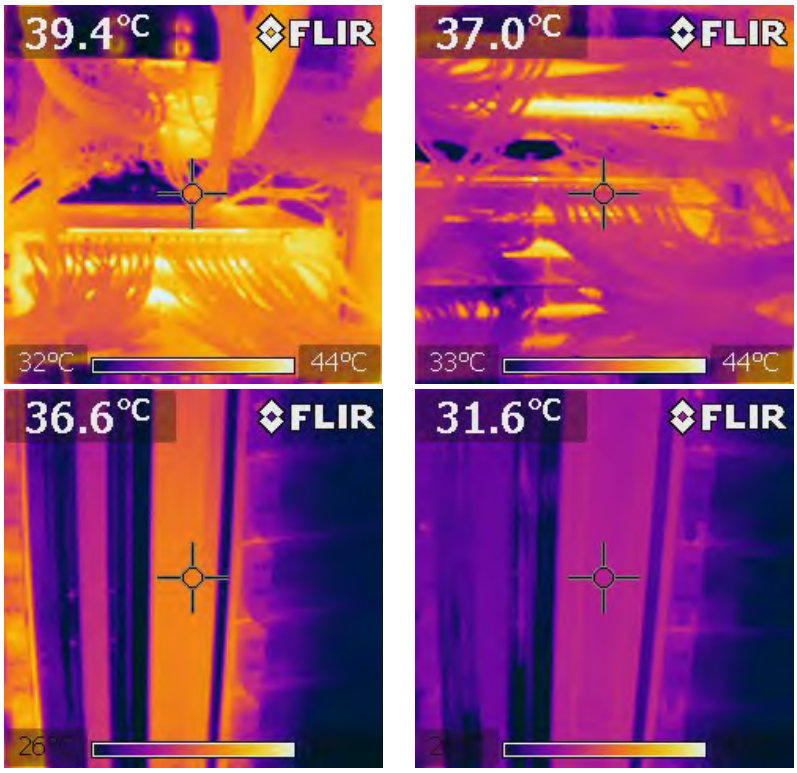

Fig 1a: Before and after: Top of the rack mounted equipment and cabling heated up unintentionally by lack of thermal zoning between high energy HPC nodes and low power networking.

Fig 1b: Before and after: With thermal zoning, fore parts of the installed racks are significant cooler, indicating less thermal short between cold and warm side.

We conducted a deeper examination of network equipment and found that in contrast to energy efficient servers or laptops network components still waste energy.

Figure 2 shows a comparison between different connection speeds and the energy consumption, where in figure 3 the behavior under load is demonstrated for different Cisco switches.

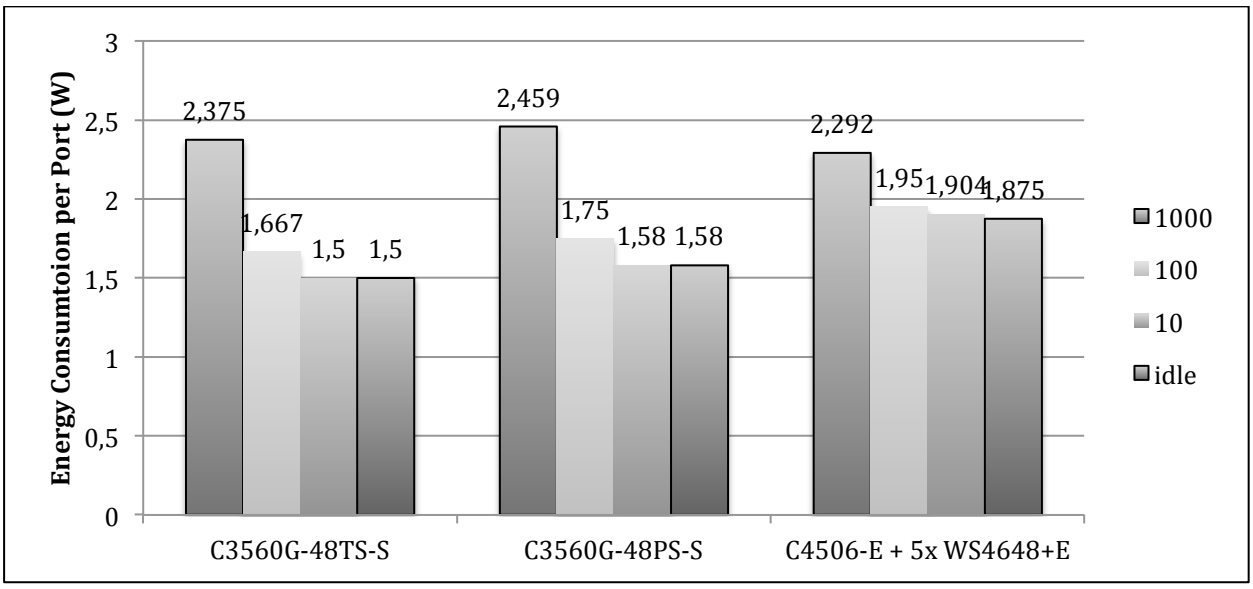

Fig 2: Energy consumption per port depending on connection speed

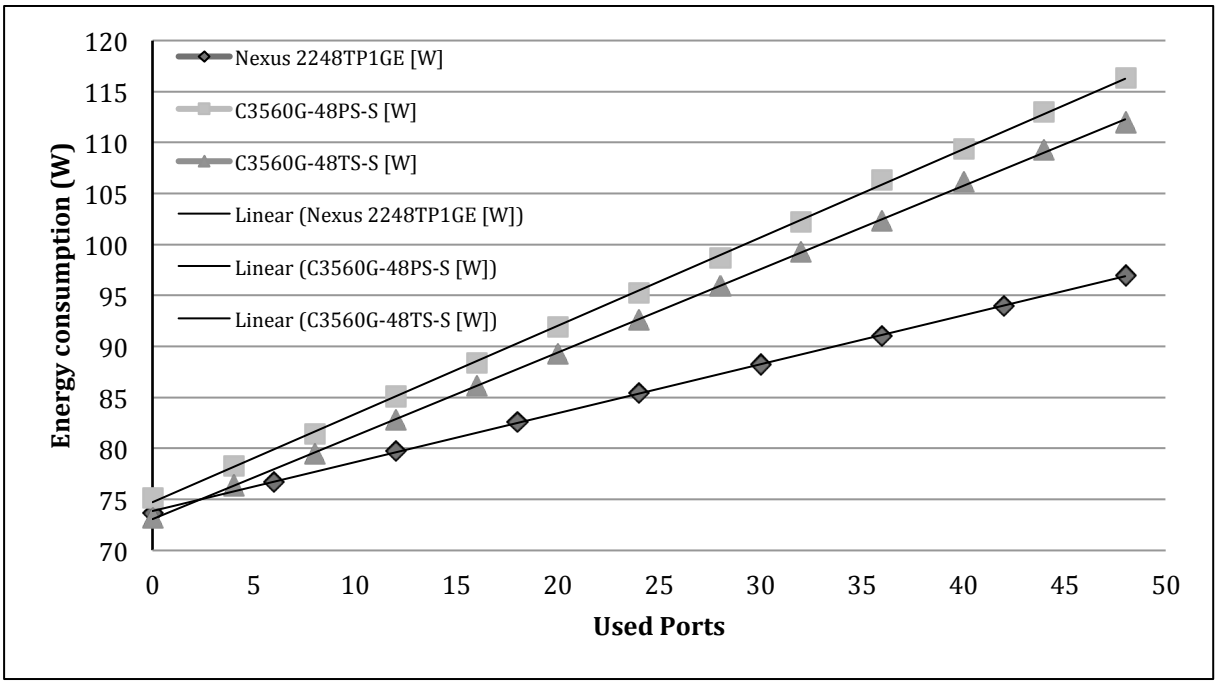

Fig 3: Energy Consumption of Different Cisco Switches

Figure 4 shows a compares the efficiency of the modular Cisco switch C4506 and a stacked architecture with C3560 switches.

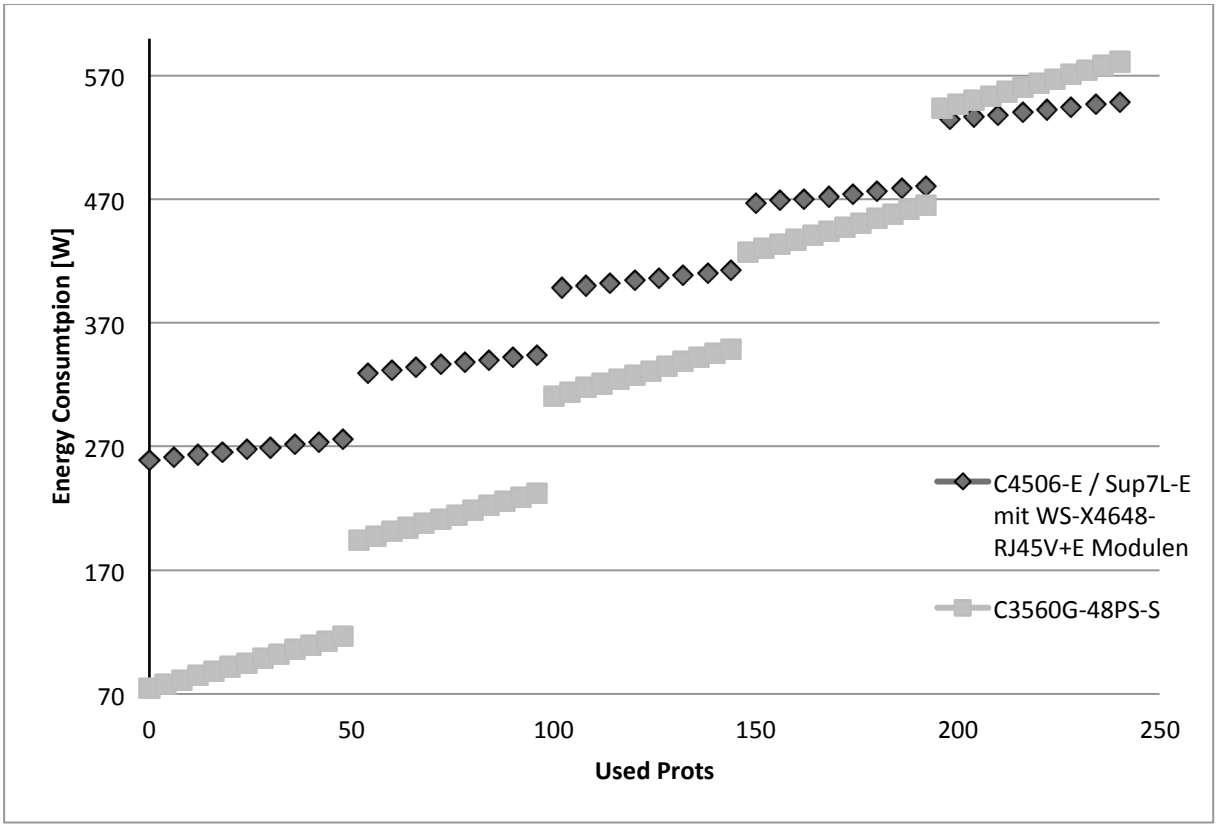

Fig 4: Energy consumption of a modular switch vs. a stacked architecture

Also our Wireless LAN (WLAN) infrastructure was taken into consideration. As part of his master thesis Maximilian Boehner[3] could show that the university's infrastructure is designed to handle peak demand just like Jardosh et al.[1] stated but

leaving significant parts of these deployments idle for long time of periods. A study of Lanzisera et al.[2] indicates that in 2012 enterprise WLAN devices consumed 2.3 TWh worldwide, which accounts for roughly 2% of the overall energy consumed by network devices.

For a campus case study it was estimated that the portion of WLAN energy-consumption is around 5%. Jardosh et al.[1] proposed a green-clustering algorithm to schedule the operating times of access points according to demand. Maximilian Boehner was able to improve this algorithm and developed a new algorithm called green star clustering using mathematical optimization software (see figure 5).

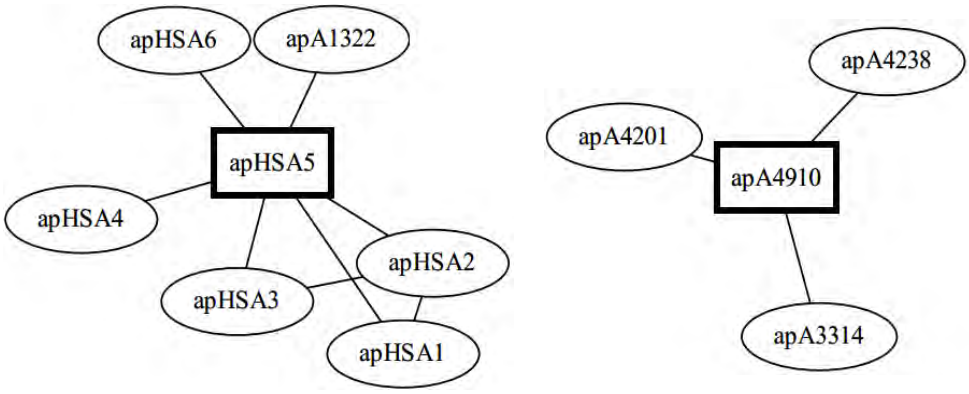

Fig 5: Clustering of access points by green star clustering

He showed that according to his schedule one is able to save up to 15% of the energy consumption by WLAN infrastructures while still maintaining a good service quality. Compared with potential savings of 25% for a complete power-off during six hours by night, this is quite a good result. We are sure we can find analogous savings when we start to examine the LAN infrastructure accordingly.

Also we built up a virtual desktop infrastructure for computer classrooms at the university. At the moment we look deeper into the energy consumption of these virtual infrastructures and the corresponding applications.

As already mentioned we engaged ourselves in price models, too. We try to formulate service level agreements, which allow the usage of regionally produced renewable energy. Using weather forecasts our project partner in Mainz developed a scheduling algorithm to distribute computer jobs according to the expected amount of renewable energy.

During the coming and last year of the project we hope to bring all these ends together in a tool we call the green control panel in which the expected regionally-produced renewable available energy, the actual energy consumption in the computer center and a simulation of possible job schedules help to run an energy-efficient computer center.

References

[1] Jardosh et al.:Towards an Energy-Star WLAN Infrastructure, Mobile Computing Systems and Applications, 2007.

[2] Lanzisera, S.; Nordman, B. and Brown, R.E.: Data network equpiment energy use and savings potential in buildings. *Energy Efficiency*, 5(2), 2012, S. 149-162.

[3] Boehner, M.: Optimization the Energy-Consumption of WLAN-Infrastructures, Master thesis, Universität Paderborn, 2013

4.5 SCALUS: *SCAL*ing by means of *U*biquitous *S*torage

Supervisor:	Prof. Dr. André Brinkmann, University of Mainz
Members:	Fabio Margaglia, M.Sc., PC^2, University of Paderborn
	Federico Padua, PC^2, University of Paderborn
Supported by:	The EC FP7 Marie Curie Initial Training Networks (ITN) SCALUS – SCAling by means of Ubiquitos Storage under Grant Agreement no. 238808

Abstract

Storage research increasingly gains importance based on the tremendous need for storage capacity and I/O performance. Over the past years, several trends have considerably changed the design of storage systems, starting from new storage media, like Flash-based disks, over the widespread use of storage area networks (SANs), up to grid and cloud storage concepts.

Furthermore storage systems are increasingly assembled from commodity components to achieve cost efficiency. Thus, we are in the middle of an evolution towards a new storage architecture made of many decentralized commodity components with increased processing and communication capabilities, which requires the introduction of new concepts to benefit from the resulting architectural opportunities.

The consortium of this Marie Curie Initial Training Network (MCITN) ”SCALing by means of Ubiquitous Storage (SCALUS)” aims at elevating education, research, and development inside this exciting area with a focus on cluster, grid, and cloud storage. The vision of this MCITN is to deliver the foundation for ubiquitous storage systems, which can be scaled in arbitrary directions (capacity, performance, distance, security). Providing ubiquitous storage will become a major demand for future IT systems and leadership in this area can have significant impact on European competitiveness in IT technology. To get this leadership, it is necessary to invest into storage education and research and to bridge the current gap between local storage, cluster storage, grid storage, and cloud storage. The consortium will proceed into the direction by building the first interdisciplinary teaching and research network on storage issues. It consists of top European institutes and companies in storage and cluster technology, building a demanding but rewarding interdisciplinary environment for young researchers.

As part of the SCALUS project, the PC^2 is working on development and optimization of new storage technologies, in particular Flash memory technology.
Flash memory is growing in popularity after its adoption in Solid State Drives as a mass storage technology. Even though a Solid State Drive presents the same interface as a traditional disk based Hard Disk, the operation granularity and

semantics of Flash technology are profoundly different. For this reason, there is a lot of room for optimization at every level of the storage stack, and at the application layer. In this project we study deeply how Flash memory works. Based on our findings we optimize some popular data structures and algorithms to adapt to this memory technology.

Traditionally Flash devices are used with Erase-Write cycles, although under certain circumstances is possible to perform more Write operations without an Erase first. Our goal is to analyze in which circumstances is possible to perform more Write operations without Erasing first, and to show that this reduces Flash wear-out while increasing performance.

Project Description

The last years have faced a continuously increasing adoption of NAND flash technology in mass storage devices, typically in the form of Solid State Drives (SSD). Although other types of flash memory exist, we address only the NAND type, thus for simplicity we will just use the term flash.

Flash memory comes in form of silicon chips. Its behavior is way different from traditional disks. In the first place, while a disk has many moving parts, a flash chip has none. For this reason it can reach better access times, especially for random access patterns. Secondly, the access methods are totally different. A disk can be seen as a long array of blocks, typically 512 Byte each, that can be read or written without particular restrictions. A flash chip is a long array of big blocks of pages. Typically a page is 8 KB or more, and a block contains 128 pages. The minimum unit for a read or write operation is a page. A write operation can be performed arbitrarily only after the entire block has been erased. The erase operation has block granularity, and is the most time consuming. Furthermore, erase operations physically wear the silicon, and eventually break the Flash cells. For these reasons decreasing the number of erase operations will increase the lifetime of Flash devices, while improving the performance.

A possible way to reduce the number of erase operations is allowing more writes to occur before an erase takes place. In order to understand why a page must always be erased before being written, we analyze the behavior of a flash cell using a SSD prototype aimed to develop new SSD firmware. The prototype platform we used is the OpenSSD board [1]. Given our Flash cell analysis results, we define *overwrite compatible writes* as write operations that do not force a ‘0’→‘1’ transition of any of the bits involved in the operation.

		Page content	
		0	1
New data	0	✓	✓
	1	✗	✓

Table 1: Overwrite compatibility

In general applications do not respect this rule. To take advantage of this, they must be modified accordingly. To give examples of application modifications, in the following we show how data structures can be adapted to generate overwrite compatible accesses to the underlying storage medium. We focus in particular on two popular data structures: Bloom Filters and B-Trees.

A Bloom Filter [2] is a data structure used to efficiently test the set membership of an element. It consists of an array of bits initially all set to '0'. To state the set membership of an element, it will be fed to a number (*k*) of hash functions and the resulting *k* values are the indexes of the bits that will be set to '1'. An element is a member of the set if when fed to the *k* hash functions, the *k* bits indexed by the hash output values are all '1'. Two important features of this data structure are the possibility of false positives and the impossibility of removing an element from the set. In particular, the second property means that a bit that is set to '1' can never be reset to '0'.

This data structure already performs overwrite compatible operations. There is no need for a real modification, just inverting all bits, so that inserting a bit in the filter will result in '1'→'0' transitions.

The B-Tree data structure [3] is widely used in databases and file systems. The data structure is a good candidate for overwrite operations because it modifies the data in-place. However, without modifications a B-Tree will not generate overwrite-compatible operations.

Traditionally, B-Trees store keys in the nodes in a sorted order. By relaxing this constraint, it is possible to append new keys at the end of the node. An append operation always results in *overwrite compatible writes*.

We evaluated the behavior of these data structures on a SSD simulator. Figure 1 shows the fraction of erase operations needed by our system compared to a traditional one, for different B-Tree workloads. Our simulator is able to set a maximum number of write operations on a page before an erase operation is forced. The X-axis shows different values of this parameter. As the figure shows, it does not make sense to allow too many overwrites per page, as the situation does not improve significantly after 8 overwrites.

In general the erase reduction is dramatic. On every workload only less than 20% of the original erases are needed.

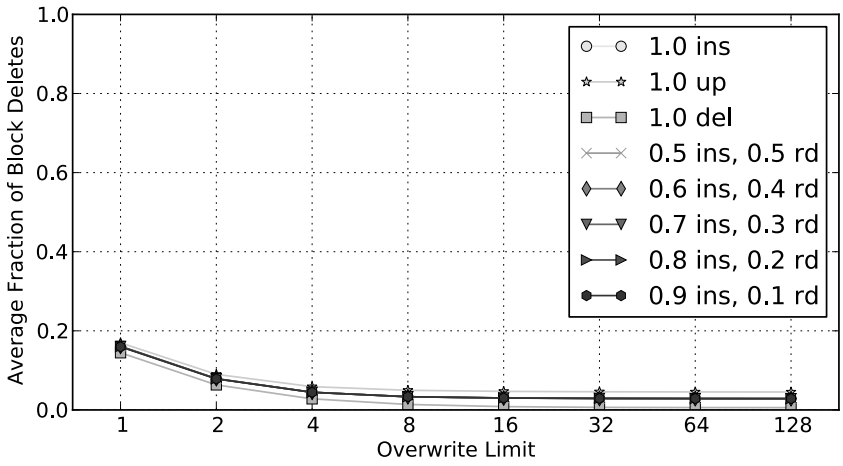

Fig.1: Number of erase operations when running our modified B-Tree

Results of this project have been presented at the Systor 2013 conference [4].

References

[1] http://www.openssd-project.org

[2] Bloom, B.H.: *"Space/time trade-offs in hash coding with allowable errors"*. Communications of the ACM, vol. 13, no. 7, pp. 422–426, Jul. 1970.

[3] Comer, D.: *"The Ubiquitous B-Tree".* ACM Computing Surveys (CSUR), vol. ll, no. 2, pp. 121–137, 1979.

[4] Kaiser, J.; Margaglia, F. and Brinkmann, A.: *"*Extending SSD lifetime in database applications with page overwrites*"*. Proceedings of the 6th Annual International Systems and Storage Conference (SYSTOR), Haifa, Israel.

4.6 SIMBA: *SIM*ulation *B*ackplane *A*utomotive

Supervisor:	Prof. Dr. André Brinkmann, University of Mainz
Members:	Matthias Grawinkel, M.Sc., University of Mainz
	Jürgen Kaiser, M.Sc., University of Mainz
Supported by:	BMWi / ZIM – Kooperationsprojekte (Fz.: KF2159005KM1)

Abstract

Today, the development of vehicles is not possible without simulation tools and frameworks. Development teams use these tools independently from each other for their assigned tasks. However, a real integration of the developed software-based components happens only after the corresponding hardware is available. The reason is that simulation of a full vehicle is too expensive in terms of complexity and computation overhead.

The goal of this project is to develop a central multi-user-appliance, which enables real simulation of a complete vehicle-system. The appliance could greatly reduce development time. This was achieved by designing a hardware-software solution, which allows cooperative development in the cloud. The software allows performant interaction of different simulation environments and developed vehicle components. A co-design hardware platform supports efficient storage, processing, and simulation of the developed vehicle components.

Project Description

Vehicle design includes several simulation tools which have to interact with each other. The base of this cooperation is a common specification-language. In SIMBA, we developed a new language, SIMBA-DSL, which is based on Autosar and SYSML. The goal was a simple representation of communication and a simple configuration of complex system architectures.

The project also required several interfaces to simulation frameworks. The software supports the following simulators: AVL Cruise, Dart, Dymola, FileSource, Flowmaster, GT-Suite, KULI, Simulink, and TIM. All simulators can be connected via a common simulation-backplane, which is the centerpiece of all communications among the implemented modules. In total, 50 submodules can be connected and 200 signals processed. The cycletime was reduced from 10ms to 100µs. The backplane can be controlled via a configuration interface over LSF or a TCP-based protocol.

The graphical configuration interface is an Eclipse-plugin based on the EMF- and GMF framework. The Eclipse Modeling Framework (EMF) is an open source java-framework for automatically generating of source code based on models. The

Graphical Editing Framework (GMF) is a framework for generating of graphical model editors. With both technologies, the project partners developed an editor for creating and modifying of simulation models (full vehicles or simple workflow managements, for example).

The graphical interface and the backplane communicate via XML. The system supports multi-user and version control management. Additionally, internal state and log events can be fetched via protocols.

Hardware

The system uses virtual machines to distribute the simulation overhead and for load balancing purposes. The project partners evaluated different hardware setups for these tasks including common server setups, custom hardware, and processor-based nodes based on GPUs and FPGAs. The partners aimed for a volume reduction of 65% and a 30% better system efficiency compared to COTS-hardware. Both was achieved. However, the goal of a 30% cheaper hardware setup was missed because the higher hardware complexity compared to COTS. The reduction is 10-15%. The nearly cable-free infrastructure allowed an operation- and maintenance costs reduction of 15%.

The computation nodes communicate via a central communication backplane. For the plane, the project partners evaluated different communication protocols (PCI-Express, Infiniband, several Ethernet-standards) and chose to develop a new backplane-solution because of operating system incompatibilities in the virtualization environment. The solution can be configured via a specific network node. The focus of the first lies on 1- and 10 Gbit interconnects in the first network modules.

The computation nodes are connected to the backplane via a basis board. This connection doesn't require any cable. Additional hardware accelerators can be connected via further PCI-express interfaces on the base boards. This modular architecture allows many different combinations of FPGA Systems, GPU-accelerators and processor boards.

All computation nodes can be monitored and controlled via a dedicated monitoring network that was integrated into the backplane. The network consists of several low-power microcontroller, which preprocess and send the data over an other central microcontroller to the user. The microcontroller are interconnected with an I2C-bus. The user receives the data over an Ethernet connection.

In addition, the hardware allows to connect control units or: HiL-simulators. For this, the partners created gateways, which convert the signals from the bus-system LIN or CAN into the TISC-format. This format allows a direct communication of standard simulators with the hardware.

Storage

The computations generate and require redundant data, especially in form of the virtual machines, which mostly run the same operating system. The PC2 supported the project with its experience in deduplication systems, which efficiently exploit data redundancy to save storage capacity.
In detail, the PC2 developed a distributed backup deduplication system based on its Dedupv1-Project. The system deduplicates incoming data live. For this, it first divides newly written data into chunks with an expected size of 8KB. All chunks then are fingerprinted with a cryptographic hash function. The fingerprints are used as identifiers. If a fingerprint appears for the first time, the system stores the chunks; otherwise it only saves a reference to the already stored chunk.

For this project, the PC2 aimed for a system that performs exact deduplication and can scale up to 100 nodes. In addition, it must be fault tolerant against single node crashes. The resulting project was called distributed dedupv1 (diderupv1).

The final didedupv1 system uses a series of storage nodes, which provide their storage via a SAN. With this, all storage can be accesses by all servers in the system. However, the system prohibits to let more than one server use a specific storage range at a time. For this, it divides the storage of the storage servers into equally-sized partitions and assigns these to other servers. The assignment is established for a long time and prevents several scalability issues. It also simplifies the error case because a server directly can overtake partitions of a crashed node.

Another cornerstone of the system is its communication protocol, which prevents the node interconnect to become a performance- and scalability bottleneck. The protocol ensures that chunk data never crosses the network and only is sent to the storage servers if at all. This only holds for the write case, which, however, is the common case in backup systems.

The didedupv1 system provides virtual block devices via iSCSI. Client nodes only see these devices. The nodes providing the devices receive the data and deduplicate and distribute the load as mentioned above. The system was presented at the MSST 2012 conference.

5 Selected User Projects

5.1 Chemistry

5.1.1 Comparative reaction mechanism study of the enzymatic ring-opening polymerization of *ε*-caprolactone and *ε*-caprolactam using QM/MM simulations

Supervisor:	Prof. Dr. Gregor Fels, University of Paderborn
Members:	Dr. Brigitta Elsässer, University of. Paderborn
	Dr. Iris Schönen, University of. Paderborn
Supported by:	University of Paderborn

Abstract

Polyesters and polyamides are important biomaterials for medical purposes, due to their biodegradability, and good mechanical strength and also because they are non-toxic. Therefore, these materials can be employed e.g. as surgical sutures, screws and reinforcing plates. The polymers can be prepared by conventional chemical polymerization, and, alternatively, by “green polymer chemistry” through lipase catalyzed polymer synthesis. In contrast to the chemical procedure, *in vitro* enzymatic catalysis is characterized by mild reaction conditions, and high enantio-, regio-, and chemoselectivity.

The literature provides numerous examples of enzymatic polyester formations,[1-12] which usually proceed through either a ring-opening polymerization (ROP)of lactones, or by polycondensation of carboxylic acids or esters with alcohols. In contrast, little is known about enzyme catalyzed polyamide formation.[13-15] Recently, our cooperation partner, the research group of Prof. Katja Loos at the University of Groningen, has described the first successful synthesis of a polyamide, particularly for the unbranched poly(*β*-alanine), nylon 3, by enzymatic ring-opening polymerization starting from unsubstituted *β*-lactam (2-azetidinone) using *Candida Antarctica lipase* B (CALB) immobilized on polyacrylic resin (Novozyme 435).[15] The polymerization, however, proceeds with poor yield and with a maximum chain length of only 18 units and an average length of 8. There is, obviously, a need for a better understanding of the reaction mechanism of this enzymatic process and for enzymatically catalyzed polyamide formation in general in order to produce an industrially useful polymer.

Theoretical studies help understanding the underlying reaction mechanism at atomistic details and can pave the way to optimize the enzymatic process. We have applied docking tools to generate the reactant state complex and have performed QM/MM calculations at DFT/PBE0 level of theory to simulate the acylation of Ser105 by the lactone and the lactam, respectively, via the corresponding first tetrahedral intermediates. We found that the polymerization of *ε*-caprolactone proceeds

according to the widely accepted pathway via the catalytic triade of Ser105, His224 and Asp187. However, the formation of the first tetrahedral intermediate in case of ε-caprolactam is hindered, which can be explained by the disfavored proton transfer during this part of the reaction. Since the crucial step of the polymerization procedure is the generation of an acylated Ser105 species, our results explain why the enzymatic polyamide formation is so poor and does open up new possibilities for targeted rational catalyst redesign in hope of an experimentally useful CALB catalyzed polyamide synthesis.

Project Description

In order to generate the initial complexes of ε-caprolactone and ε-caprolactam (Fig. 1), respectively, for further QM/MM reaction mechanism studies, docking experiments were applied. Although currently available crystal structures from the PDB data base provide fundamental information about the three dimensional structure and the active site of CALB it is not possible to generate the coordinates of their reactant state complex experimentally since the ligand either reacts to form the corresponding polymer or does not polymerizes but rather leaves the binding pocket. Therefore, the use of docking programs to build a productive initial complex structure is crucial. According to the experience in the research group of Prof. Fels, the software packages MOE2010.10[16] and QXP-Flo+0802[17] yield the best results for an initial guess of the starting configuration of the enzyme-ligand complex of lipases. In the docking simulations we started from the available X-ray structure of CALB.[18] After adding hydrogens to the heavy atoms the enzyme was optimized by force field methods since the accuracy of the docking process is also at this level of theory. The different placement methods afford an unbiased setup for the evaluation of the docking hits and the scoring function. The resulting structures were analyzed by comparison of the relevant enzyme–ligand–conserved active site water molecules. In the productive reactant state the carbonyl group of the lactam or lactone was coordinated by Ser105 and Thr40 and the unprotonated His224 is to be H-bonded to the nitrogen of the lactam ring.

The best hits of the docking procedure were the starting point for the investigation of the reaction mechanism. Prior to these calculation the complex structures were optimized by the following stepwise procedure: Counter ions were added to maintain neutrality and the complete system was solvated in an 80 Å cubic box of waters, followed by dividing the system into a QM region, which comprises the most important active site amino acid residues, and the ligand, while the rest of the enzyme was considered as the MM subsite. The bonds between the QM and MM subsystems were capped with H atoms.[19] In the first step of the optimization the entire solvent-enzyme-substrate structure was equilibrated by performing a series of molecular dynamics annealing runs at different temperature followed by a full QM/MM optimization at DFT/PBE0 level of theory (using the Ahlrich's pVDZ basis set) by applying the multi-region optimization algorithm of NWChem.[20]

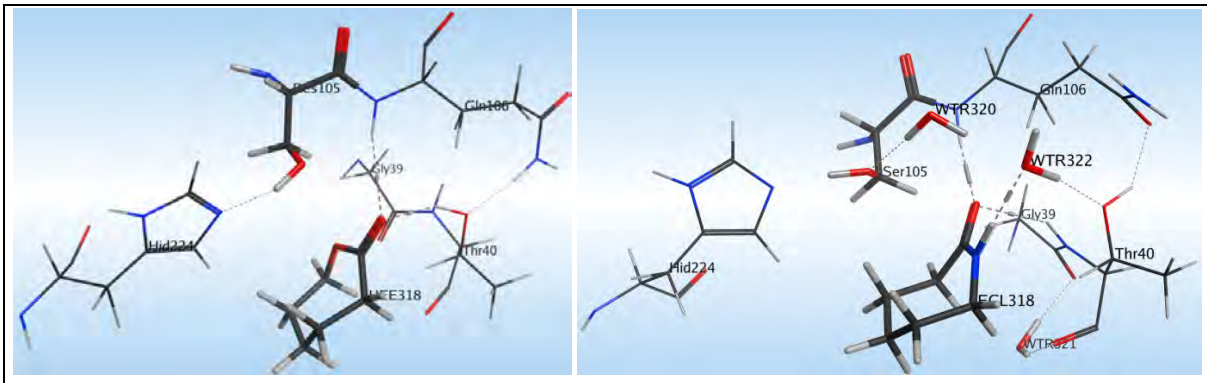

Fig 1: QM/MM optimized reactant state of the enzyme substrate complex for the lactone (left) and lactam (right).

The objective of the comparative simulation of the Ser105 attack at ε-caprolactone and ε-caprolactam, respectively, was to understand the enzyme's action and selectivity in such detail that rational protein engineering can be used to develop more effective enzymes for polyamide formation.The most crucial stationary points of the reaction coordinates along the catalytic cycle is the generation of the first stabile intermediate (analogue to TI1, Scheme 1) which was modelled using the "spring method" as implemented into NWChem.[20] According to this method harmonic restraints were applied to drive the system over the reaction barrier of the transition state to the desired product while at the same time allowing the MM system (initially equilibrated to the reactant structure) to adjust to the changes. When a reasonable estimate of each stage was obtained, the constraints were lifted, and the system was optimized using a sequence of optimizations and dynamic relaxation steps similarly to those discussed above.

Starting from the reactant state (Figure 1) resulting from the docking and optimization process described above, a sequence of constrained optimizations was performed to study the nucleophilic attack. First, to simulate the attack of Ser105 at the substrate carbonyl, a spring of 1.5 Å between OG(Ser105) and the lactam/lactone carbonyl was applied, which is supposed to yield the first stabile tetrahedral intermediate (**TI1**, Scheme 1). As expected, in case of ε-caprolactone the proton transfer of HG(Ser105) to NE2(His224) took place automatically. Afterwards, in a second set of calculations the lactone ring was opened by transferring a proton from NE2(His224) to the lactone oxgen using a constraint of 0.97 Å between HE2(His224) and O(lactone) to form the acyl-enzyme complex as depicted on Scheme 1. During this processes the negatively charged oxygen was stabilized within the oxy-anion-hole made up by the amino acids Thr40 and Gln106.

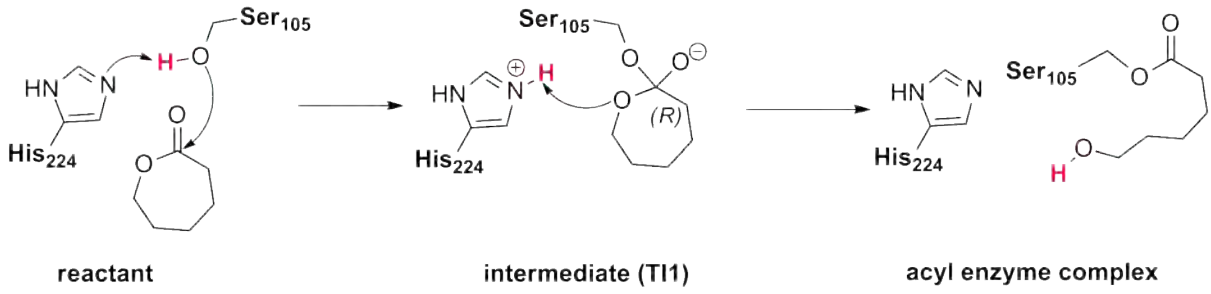

Scheme 1. Mechanism of the acyl-enzyme formation with ε-caprolactone.

HN(Gln106) to the carbonyl oxygen of the lactam leaving a negative charge on the Glutamate nitrogen, N(Gln106). In the intermediate (Scheme2, **TI1**) the H-bond from the former carbonyl group of the lactam to N(Gln106) is reduced to 2.77 Å while still being 3.09 Å to N(Thr40). Although, the proton transfer from the Glutamate nitrogen, N(Gln106), (Scheme 2) occurred spontaneously, this reaction step is very unusual. Therefore, in a consecutive calculation we have tried to move the migrating HN(Gln106) proton back to the glutamate nitrogen N(Gln106) by using constraints. However, none of these attempts was successful but rather resulted in the displacement of the lactam from Ser105 and restoring of the reactant state.

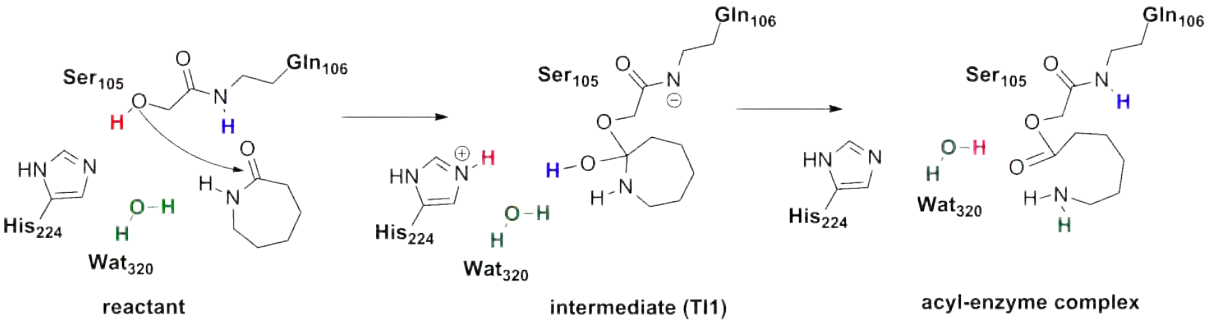

Scheme 2. Acylation of Ser105 by caprolactam: Generation of the first tetrahedral intermediate (**TI1**) and ring opening to the acyl-enzyme complex.

The lactam ring was opened similarly to that of the lactone and during optimization several proton transfers occurred. The proton from the carbonyl has shifted back to Gln106, a water proton has been transferred to the lactam nitrogen and the HE2(His224) proton has moved to neutralize Wat320.

Calculation of the reaction energies supports the findings of the reaction mechanism simulations and is in excellent agreement with all experimental studies.[11, 21, 22] The free energy profile of the NEB (nudged elastic band)[23, 24] optimized pathway was obtained by calculating free energy difference between the consecutive NEB beads (points, calculation steps) in all cases.

Figure 2. shows the QM/MM energy profile for the two polymerization reactions. As a result we calculated the reaction barrier of the nucleophilic attack of Ser105 on the lactone and lactam carbonyl generating the intermediate (**TI1**). This barrier is in case

of the lactone polymerization only 12 kcal/mol (Fig. 2, left) and thereby much lower than for the lactam, which is as high as 27 kcal/mol (Fig. 2, right). It is rater unlikely that such a high reaction barrier can be overcome in an enzymatic reaction which suggests, that the experimentally shown hindrance of the CALB catalyzed polyamide synthesis from caprolactam presumably does not proceed because of an energetically unlikely ring opening step.

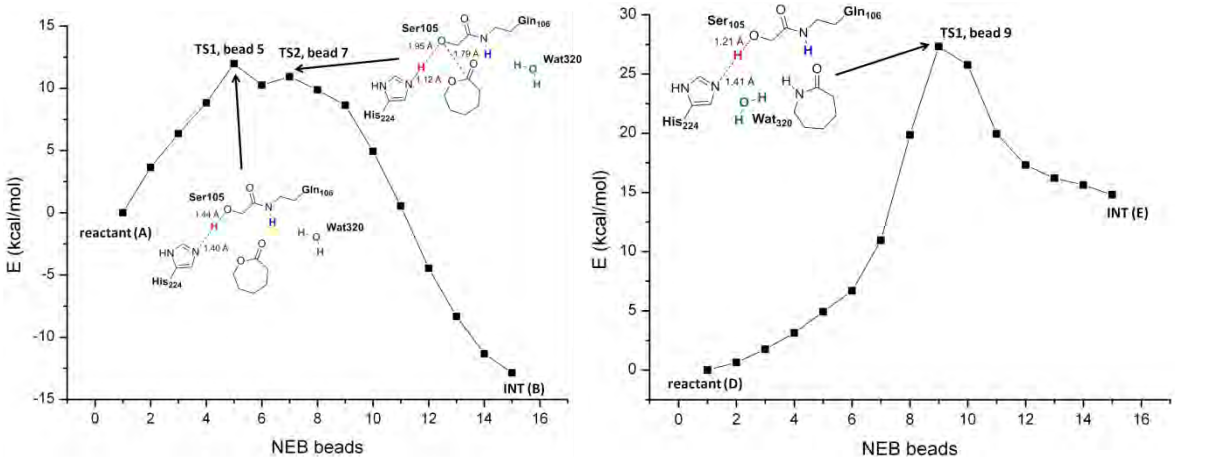

Fig 2: Comparing the reaction energies for the formation of the first tetrahedral intermediate (**TI1**) for the lactone (left) and the lactam (right).

Based on the molecular modeling results, as a future work, the enzyme shall be redesigned as a catalyst for the ring opening polymerization of *ε*-caprolactam. In a preparative synthesis of the corresponding polyamide by our cooperation partner promising mutants can then be tested for improvement of the polymerization. In addition, other available lipases can eventually also be examined by molecular modeling for a more appropriate reaction with *ε*-caprolactam and could be suggested for immobilization and experimental testing.

For our calculations the highly parallel software package of NWChem[20] was used installed on the Arminius cluster at the Paderborn Centre for parallel computing (PC^2) (60 nodes Fujitsu RX200S6, 2.67 GHz, Infiniband Switch Fabric, 7.7 TFlops Cluster with 720 cores).

References

[1] Al-Azemi, T.; Kondaventi, L. and Bisht, K.: *Macromolecules* **2002,** 35, 3380-3386

[2] Binns, F.; Harffey, P.; Roberts, S.M. and Taylor, A.: *J. Pol. Sci. Part A,* **1998,** 36, (12), 2069-2079.

[3] Gross, R.A.; Kumar, A. and Kalra, B.: *Chemical Reviews* **2001,** 101, (7), 2097-2124.

[4] Jääskeläinen, S.; Linko, S.; Raaska, T.; Laaksonen, L. and Linko, Y.Y.: *Journal of Biotechnology* **1997,** 52, (3), 267-275.

[5] Kikuchi, H.; Uyama, H. and Kobayashi, S.: *Macromolecules* **2000,** 33, 8971-8975.
[6] Kobayashi, S.: Recent *Macromolecular Rapid Communications* **2009,** 30, (4-5), 237-266.
[7] Kobayashi, S. and Uyama, H.: *ACS Symposium series* **2003,** 840, 128-140.
[8] Kumar, A. and Gross, A.: *Biomacromolecules* **2000,** 1, 133-138.
[9] Thurecht, K.J.; Heise, A.; deGeus, M.; Villarroya, S.; Zhou, J.X.; Wyatt, M.F. and Howdle, S.M.: *Macromolecules* **2006,** 39, (23), 7967-7972.
[10] Uyama, H. and Kobayashi, S.: *Enzyme-Catalyzed Synthesis of Polymers* **2006,** 194, 133-158.
[11] van der Mee, L.; Helmich, F.; de Bruijn, R.; Vekemans, J.A.J.M.; Palmans, A.R.A. and Meijer, E.W.: *Macromolecules* **2006,** 39, 5021-5027.
[12] Varma, I.K.; Albertsson, A.-C.; Rajkhowa, R.; and Srivastava, R.K.: *Prog. Polym. Sci.* **2005,** 30, 949-981.
[13] Cheng, H.N.; Maslanka, W.W. and Gu, Q.-M.: *[US 6677427* **2004,** Hercules Inc., invs.
[14] Gu, Q.-M.; Maslanka, W.W. and Cheng, H.N.: *Polymer Biocatalysis and Biomaterials II, ACS Symposium series* **2008,** 999, Chapter 21, pp 309-319.
[15] Schwab, L.W.; Kroon, R.; Schouten, A.J. and Loos, K.: *Macromol. Rapid Commun.* **2008,** 29, 794-797.
[16] http://www.chemcomp.com.
[17] McMartin, C. and Bohacek, R.S.: QXP: Powerful, rapid computer algorithms for structure-based drug design. *Journal of Computer-Aided Molecular Design* **1997,** 11, (4), 333-344.
[18] Uppenberg, J.; Ohrner, N.; Norin, M.; Hult, K.; Kleywegt, G.J.; Patkar, S.; Waagen, V.; Anthonsen, T. and Jones, T.A.: C *Biochemistry* **1995,** 34, (51), 16838-16851.
[19] Valiev, M.; Garrett, B.C.; Tsai, M.K.; Kowalski, K.; Kathmann, S.M.; Schenter, G.K. and Dupuis, M.: *J. Chem. Phys.* **2007,** 127, (5), 51102.
[20] Valiev, M.; Bylaska, E.J.; Govind, N.; Kowalski, K.; Straatsma, T.P.; Van Dam, H.J.J.; Wang, D.; Nieplocha, J.; Apra, E.; Windus, T.L. and de Jong, W.A.: *Computer Physics Communications* **2010,** 181, (9), 1477-1489.
[21] Kobayashi, S.: *Macromolecular Symposia* **2006,** 240, 178-185.
[22] Panova, A.A. and Kaplan, D.L.: *Biotechnology and Bioengineering* **2003,** 84, (1), 103-113.
[23] Henkelman, G. and Jonsson, H.: *J. Chem. Phys.* **2000,** 113, (22), 9978-9985.
[24] Henkelman, G.; Uberuaga, B.P. and Jonsson, H.: *J. Chem. Phys.* **2000,** 113, (22), 9901-9904.

5.1.2 Adhesion and stability of organic adhesion promoters on metal oxide surfaces

Supervisor:	Guido Grundmeier, Technical and Macromolecular Chemistry, University of Paderborn
Members:	Ozlem Ozcan, Technical and Macromolecular Chemistry, University of Paderborn

Abstract

The design of successful bi-functional organic thin film surface treatments leading to improved adhesion and higher corrosion resistance requires a profound knowledge on the binding mechanisms and stabilities of such molecules on the metal oxide surface. The possible binding modes of selected organofunctional molecules on different crystalline orientations of relevant metal oxides were investigated by means of DFT calculations. AFM-based chemical force microscopy (CFM) measurements were performed to assess the bond strengths of selected molecules and functionalities on metal oxide surfaces to enable the experimental verification of the simulation results.

In general, the changes in the bond strength in the presence of water determine the stability of such composite interfaces. Thus, DFT calculations were performed in the presence of dissociated water molecules and molecular water layers on oxide surfaces to evaluate the competitive bond strengths of selected molecules and water. The results of the DFT simulations and experimental investigations have shown a very good agreement, leading to a profound description of studied interfaces.

Project Description

Since decades complex alloys are governing the material selection in automobile, appliance and manufacturing industries. The most common alloys include iron, aluminium, zinc and magnesium as base metal and contain minute amounts of other metals to achieve improved properties like hardness, elasticity or corrosion resistance depending on the target applications. The surfaces of these alloys are covered with a mix-oxide layer of the respective metals. In the further steps of the production, these surfaces are also coated with organic layers like lacquer or paint.

The stability of this layered system in different corrosive environments is strongly dependent on the properties of the oxide layer and the strength of interaction at the metal oxide-polymer interface. Many methods have been developed to passivate the metal surfaces to achieve a successful corrosion protection and to improve the adhesion of the polymers to the surface. Recently the introduction of organic adhesion promoters offered a more sophisticated method to functionalize the metal

oxide surfaces with desired properties [1-2]. Bi-functional molecules can not only serve as linkers between the oxide and polymer layers, but can also offer interesting properties like ultra-hydrophobicity and biocompatibility.

The aim of this project is to investigate the surface stability of metal oxide surfaces (Al_2O_3, ZnO, MgO) and study the binding mechanisms of organic adhesion promoters (carboxylic acids, organothiols, organosilanes, organophosphonates, etc.) to these systems. Calculations were performed using density functional theory with the generalized-gradient approximation (GGA) and utilizing the exchange-correlation potential developed by Perdew, Burke and Ernzerhof (PBE) [3]. The SIESTA [4] code was employed with its localized atomic orbital basis sets and pseudopotential representation of the core states. The SIESTA pseudopotentials (PP) are generated using the program ATOM supplied as part of the SIESTA program package. For the PP generation the PBE functional was used to comply with the main SIESTA calculations [3, 4]. Relativistic Troullier–Martins pseudopotentials [5] with non-linear core corrections [6] were implemented in their fully non-local form [7-8].

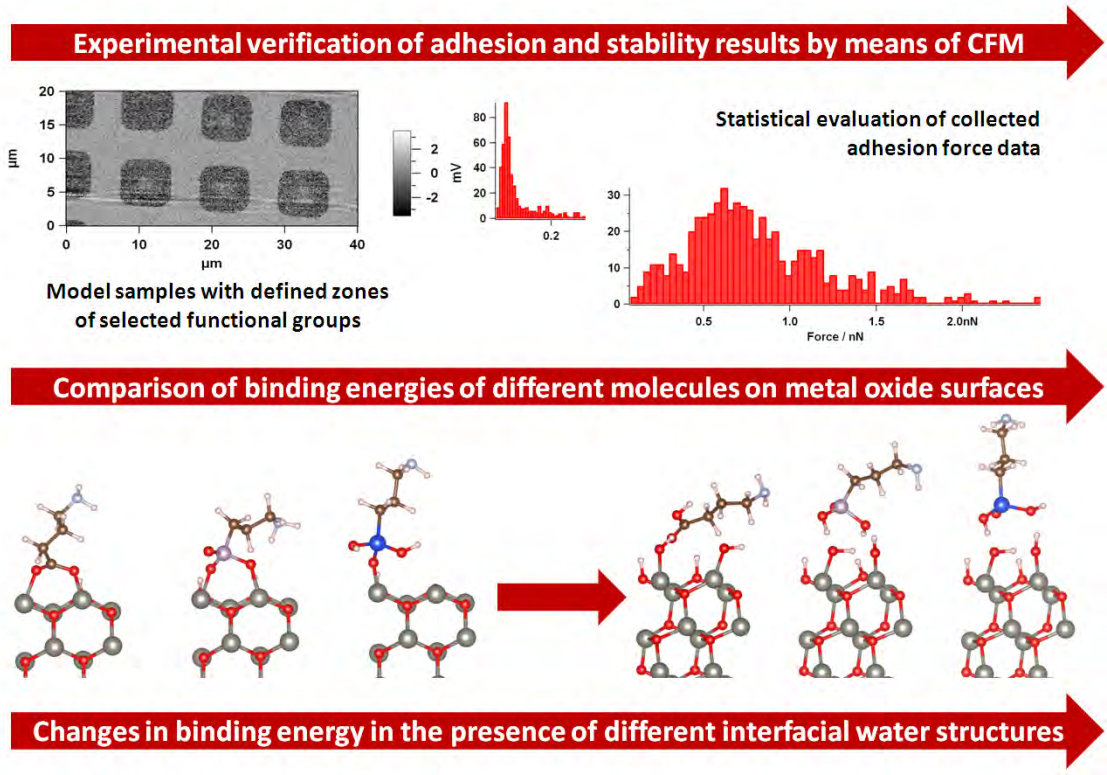

Fig. 1: Summary of the approach followed within this project

The calculations yielded a successful ranking of the adhesion promoting molecules in terms of binding energy and interfacial stability, which was in excellent aggreement with the experimental verification studies by means of Chemical Force Microscopy (CFM). A significant coverage dependency of binding energies was not observed. This may be explained with the short chain length of the chosen probe molecules, also not leading to a self assembly in experimental studies.

Current activities involve the generation of thin oxide films on metal surfaces by means of large scale molecular dynamics simulations by varying the water/oxygen ratio in the atmosphere in contact with the metallic surface. Such calculations shall provide new model metal oxide systems, which may bridge the results of the DFT calculations on perfectly single crystalline oxide surfaces and thin oxide films governing the surface chemistry of technical alloys.

SIESTA code is a very suitable code for the calculation of large systems since the computation time scales almost linearly with the system size and the parallelization is achieved efficiently. This is very important for our surface calculations, since the realistic simulation of surface defects, reconstructions as well as adsorbed species on these surfaces requires large cell sizes and thus high number of atoms to be considered.

References

[1] Ulman, A.: Chem. Rev. 96 (1996) 1533.
[2] Lim, M.S.; Feng, K.; Chen, X.; Wu, N.; Raman, A.; Nightingale, J.; Gawalt, E.S; Hornak, L.A. and Timperman, A.T.: Langmuir 23 (2007) 2444.
[3] Perdew, J.P.; Burke, K. and Ernzerhof, M.: Phys. Rev. Lett., 77 (1996) 3865.
[4] Soler, J.M.; Artacho, E.; Gale, J.D.; García, A.; Junquera, J.; Ordejón, P. and Sánchez-Portal, D.: J. Phys.: Condens. Matter, 14 (2002) 2745.
[5] Troullier, N. and Martins, J.L.: Phys. Rev. B, 43 (1991) 1993.
[6] Louie, S.G.; Froyen, S. and Cohen, M.L.: Phys. Rev. B, 26 (1982) 1738.
[7] Kleinman, L. and Bylander, D.M.: Phys. Rev. Lett., 48 (1982) 1425.
[8] Coquet, R.; Hutchings, G.J.; Taylor, S.H. and Willock, D.J. and Mater, J.: Chem., 16 (2006) 1978.

5.1.3 Theoretical studies on polyfunctional S-N donor complexes

Supervisor:	Prof. Dr. Gerald Henkel, University of Paderborn
Members:	Alexander Oppermann, University of Paderborn
Supported by:	DFG (FOR 1405)

Abstract

Our research topic is the synthesis of copper complexes with sulfur and nitrogen containing ligands, which can serve as models for biological centers such as the Cu_A site in cytochrome-c-oxidase and N_2O reductase. Exceedingly important is the Cu_A center that represents - due to its essential importance for many organisms – one of the most exciting research areas within biological systems. Herein we report about new polyfunctional S-N donor complexes and theoretical calculations based on the density functional theory. We present here a dinuclear copper complex $[Cu_2^{II}(Gua_{ph}S)_2Cl_2]$ in its *syn* conformation that exhibits some features of the target molecule Cu_A. But more important is the mixed valence *anti* conformer that is more stable than the *syn* form based on our calculations and that fits even better in a role as a model for this biological center. Furthermore, we constructed a theoretical model complex $[Cu_2(Gua_{ph}S_{et}S)_2]$ that looks very promising based on our DFT calculations. In a Cu-Cu coordinate scan we found a minimum at about 2.6 Å that is in good agreement with the Cu_A center. These complexes are expected to mimic structural and electrochemical properties of Cu_A but require further improvement to approach our target within the protein as close as possible. This task will be supported by theoretical studies aimed at finding alternative trajectories for our chemical protocols not accessible by experiment.

Project Description

The biomimetic chemistry of copper complexes with polyfunctional N donor ligands is one of the most interesting research fields in bioinorganic chemistry. This interest derives from the occurrence of a large number of metallo-biomolecules, from which the molecules with a dinuclear copper center have been in our focus for many years. A distinct type within this category contains the Cu_A center (fig.1) that can be found in cytochrome-c oxidases (CcO) and N_2O reductases (N_2OR).[1,2]. Within respiration, Cco is responsible for the reduction of molecular oxygen to water. The transfer of electrons from cytochrome-c to oxygen proceeds via Cu_A and results in the conversion of an electro-chemical redox potential into a chemical proton potential. The mechanism of this electron transfer is not yet fully enlightened. Cu_A contains the unique cyclic planar Cu_2S_2 core with bridging cysteine residues and two terminally bonded histidine residues attached to copper in an equatorial fashion. The copper coordination within the mixed-valence fully delocalized site (mean oxidation state +1.5) is completed by secondary copper-chalcogen bonds resulting in distorted tetrahedral environments.[3,4]

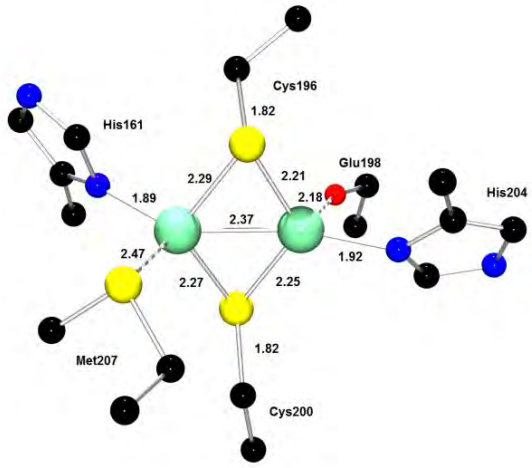

Fig. 1: Structure of Cu_A from bovine heart mitochondria (bond distances in Å)[4a]

Our focus lies on the synthesis and characterization of model complexes for the biological Cu_A center that help us to understand Cu_A–assisted electron transfer within cytochrome-c oxidases in more detail. An excellent tool for modelling electronic structures of complexes is the DFT (density functional theory) which allows for calculating optical and electronic spectra. Based on insights that we can receive from theory, novel aspects emerge as guides for chemical protocols helping us to construct synthetic copper complexes approaching higher levels of biological relevance.

For our theoretical studies we chose the hybrid density functional B3LYP in combination with the 6-31G(d) and 6-311G+(d) basis sets. This combination shows a good overall performance in accordance with a good agreement of the experimental data in our benchmarking. All complexes are optimized in the gas phase.

In our research group we developed a dinuclear copper(II) complex containing the cyclic Cu_2S_2 core with bridging sulfur atoms that bears key characteristics of the Cu_A center but cannot be reduced to the biological relevant mixed valence state. This could be due to a non-planar Cu_2S_2 unit (fig. 2) which – in contrast to the biological archetype – is folded along its S…S vector. Ground state calculations were performed on this molecule confirming π stacking effects observed in the crystal structure. Absorption spectra were calculated taking molecular orbital compositions as well as a charge density analysis (CDA) into account. It allowed us to assign orbital transitions to the observed spectral features and revealed LMCT (Ligand Metal Charge Transfer) transitions from the sulfur ligands (preferred) and the chloride ligands to the metal atoms.

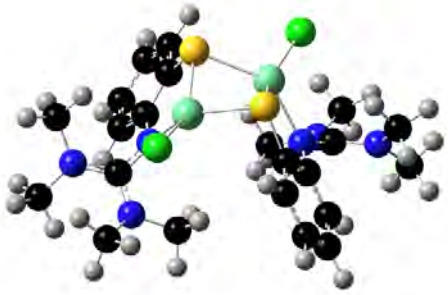

Fig. 2: Crystal structure of the dinuclear copper(II) complex $[Cu_2^{II}(Gua_{ph}S)_2Cl_2]$ (*syn* form)

Based on these results, the centrosymmetric anti-form of the dinuclear copper(II) complex $[Cu_2(Gua_{ph}S)_2Cl_2]$ was constructed and optimized with DFT methods (fig. 3). This conformer is slightly less stable (about 2 kJ/mol) than the *syn* form. The Cu_2S_2 core is planar after ground state optimization – in accordance with the requirements of the Cu_A center. With this further information in mind, our target is now to synthesize this conformer following tailored reaction pathways. If we compare the geometries of both isomers in their mixed-valence states, the *anti* form is about 3 kJ/mol more stable. Its UV/Vis spectrum was calculated showing some interesting features and proofs us right to keep track on the synthesis of this other conformer in the mixed valence state.

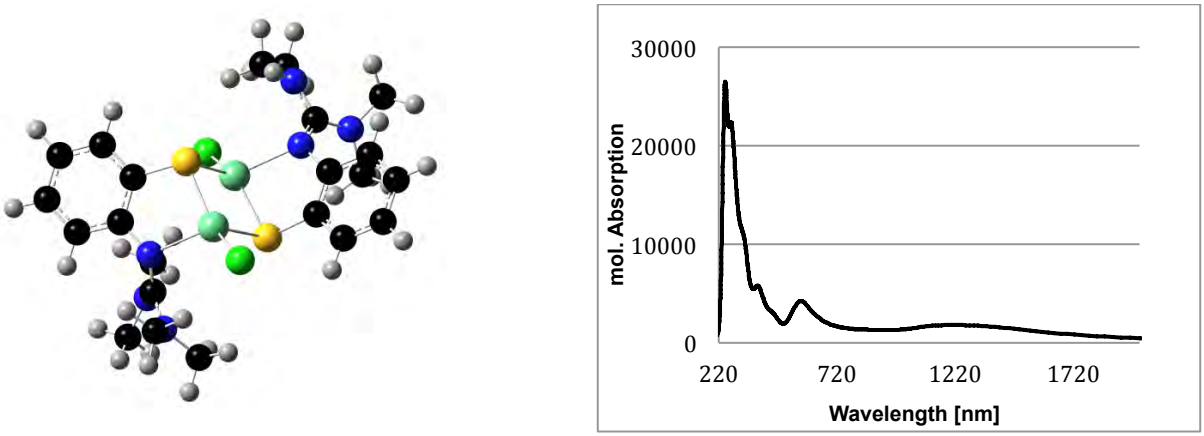

Fig. 3: The proposed mixed-valence dinuclear copper(I/II) complex *anti*-$[Cu_2(Gua_{ph}S)_2Cl_2]$: DFT model (left) and calculated absorption spectrum (right)

In a parallel approach, ligands containing biomimetic NSS donor sets perfectly suited to stabilize copper complexes mimicking structural and electrochemical properties of Cu_A have been developed. As an example, the structure of $[Cu_2(Gua_{ph}S_{et}S)_2]^+$ (fig. 4) has been optimized by DFT methods. Cu-Cu distance scans show two minima, a short one at 2.6 and a longer one at 2.9 Å. The short bond length can be stabilized by allowing the – axial - thioether functionality to leave the first coordination shell and the guanidine donor function to approach the copper in the equatorial direction. This property of the ligand is unprecedented in biomimetic Cu_A chemistry.[5,6]

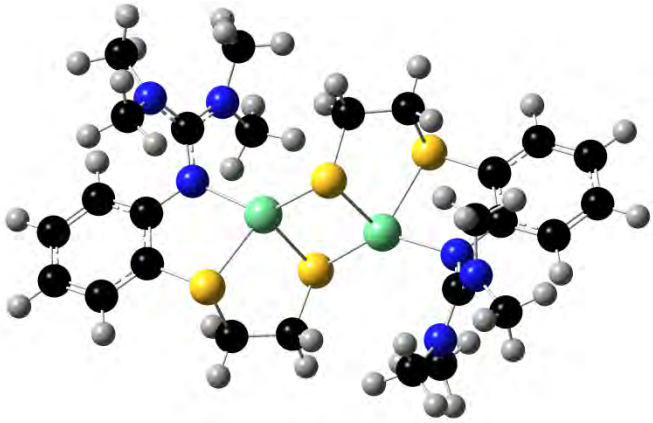

Fig. 4: DFT model of a new mixed valence dinuclear copper complex ion $[Cu_2(Gua_{ph}S_{et}S)_2]^+$

Beside examples resulting from research directed towards Cu_A model complexes, metal-sulfur complexes obtained from reactions directed towards other scientific goals deserve DFT attention as well, so that novel insights into unprecedented electronic states can be expected to emerge from suitable calculations. Examples of a plethora of new complexes are given in figs. 5 and 6 depicting molecular structures of the novel Ni-S cluster complexes $[Ni_8(\mu_6\text{-}S)(\mu\text{-}S\textit{t}Bu)_9]$ and of $[Ni_{20}(\mu_5\text{-}S)_2(\mu_4\text{-}S)_{10}(\mu\text{-}S\textit{t}But)_{10}]^{2-}$ which contain nickel in unusual low metal oxidation states.[7]

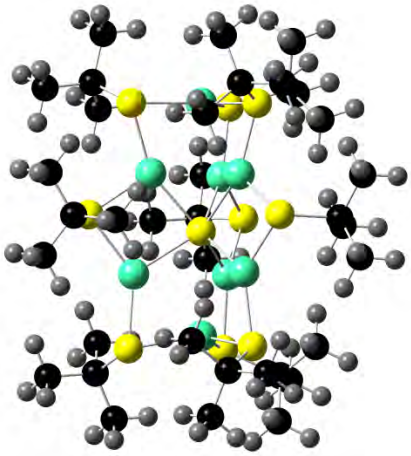

Fig. 5: Optimized DFT structure of the complex $Ni_8\mu_6\text{-}S(\mu\text{-}S\textit{t}But)_9$

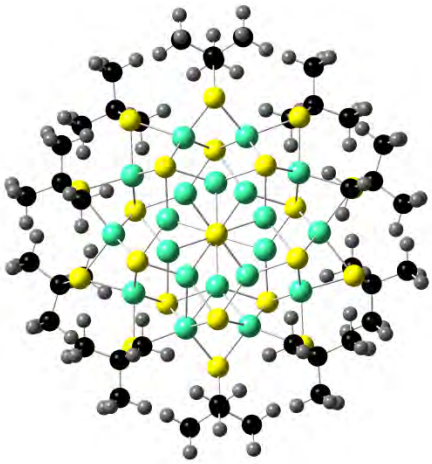

Fig. 6: Structure of the complex anion $[Ni_{20}(\mu_5\text{-}S)_2(\mu_4\text{-}S)_{10}(\mu\text{-}S\textit{t}But)_{10}]^{2-}$

All calculations were performed on the OCULUS and the ARMINIUS clusters using the Gaussian09 software package. Quantum chemical calculations require an enormous amount of computing power and therefore a lot of calculation time. Especially time-dependent density functional theory, frequency analyses (infrared, Raman etc.) and the calculation of transition states require a lot of memory, too. The OCULUS cluster with its excellent RAM configuration and its 16 cores within one node is especially well suited for these kinds of calculations.

References

[1] Neuba, A.: *PhD thesis*, Paderborn, **2009**

[2a] Neuba, A.; Flörke, U.; Meyer-Klaucke, W.; Salomone-Stagni, M.; Bill, E.; Bothe, E.; Höfer, P. and Henkel, G: *Angew. Chem.* **2011**, *123*, 4596-4600; *Angew. Chem. Int. Ed.* **2011**, *50*, 4503-4507;

[2b] Neuba, A.; Haase, R.; Meyer-Klaucke, W.; Flörke, U.; Henkel, G.: *Angew. Chem.* **2012**, *124*, 1746-1750; *Angew. Chem. Int. Ed.* **2012**, *51*, 1714-1718.

[3] Henkel, G.; Müller, A.; Weißgräber,S .; Buse, G.; Soulimane, T.; Steffens, G.C.M. and Nolting, H.F.: *Angew. Chem.* **1995**, *107*, 1615-1619; *Angew. Chem. Int. Ed. Engl.* **1995**, *34*, 1488-1492.

[4a] Tsukihara, T.; Aoyama, H.; Yamashita, E.; Tomizaki, T.; Yamaguchi, H.; Shinzawa-Itoh, K.; Nakashima, R.; Yaono, R. and Yoshikawa, S.: Crystall structure of Cu_A. *Science* **1995**, *269*, 1069-1074,

[4b] Iwata, S.; Ostermeier, C.; Ludwig, B. and Michel, H.: *Nature* **1995**, *376*, 660-669,

[4c] Wilmanns, M.; Lappalainen, P.; Kelly, M. and Sauer-Eriksson, E.: *Proc. Natl. Acad. Sci. USA* **1995**, *92*, 11955-11959.

[5] Gennari, M.; Pécaut, J.; DeBeer, S.; Neese, F.; Collomb, M.N. and Duboc, C.: *Angew. Chem.* **2011**, *123*, 5780-5784; *Angew. Chem. Int. Ed.* **2011**, *50*, 5662-5666.

[6] Houser, R.P.; Young Jr., V.G. and Tolman, W.B.: *J. Am. Chem. Soc.* **1996**, *118*, 2101-2102.

[7] Özer, M. *PhD thesis*, Paderborn, **2009**

5.1.4 Tyrosinase Models as efficient oxidation catalysts

Supervisor:	Sonja Herres-Pawlis, Ludwig-Maximilians-Universität München
Members:	Alexander Hoffmann, Ludwig-Maximilians-Universität München
Supported by:	DFG (FOR1405)

Abstract

Inspection of enzymatic reactions often provides chemists strategic direction to approach difficult molecular transformations. Paramount to efficiency is the mechanistic route, so attempting duplication of an enzymatic mechanism, while challenging, is a rational method of catalyst design. Tyrosinase, found in nearly all species of Life, catalyzes the aerobic oxidation of phenols to catechols through the intermediacy of a dioxygen-derived, side-on bonded peroxide coordinated to two copper centers. Within the last decades, huge efforts have been undertaken to mimic tyrosinase´s hydroxylation of phenols selectively in ortho-position. Numerous structural models have been presented but mostly, these models are only stable at low temperatures. Rare examples with room temperature stability did not exhibit any hydroxylation activity. Within the group of low-temperature structural models, some exhibited hydroxylation activity but only in the stoichiometric mode. Only three models display catalytic activity strongly limited to few substrates. In 2013 we presented a tyrosinase mimic capable of regioselective hydroxylation of a wide range of phenols, including substrates incompatible with the enzyme, in both stoichiometric and catalytic modes. This is the first example of catalytic phenol oxidation with evidence that the reaction proceeds through the enzymatic mechanism. Theoretical understanding of this species is crucial for directing the reactivity towards suited substrates.

A. Hoffmann, S. Herres-Pawlis, Hiking on the potential energy surface of a functional tyrosinase model – implications of singlet, broken-symmetry and triplet description, Chem. Commun. 2014, 50, 403 - 405.

Project Description

Tyrosinase is a ubiquitous copper enzyme that catalyses the hydroxylation of phenols to catechols and the subsequent oxidation of catechols to quinones by activating dioxygen in the form of a side-on-bonded peroxide dicopper(II) species (P core).[1] With regard to the unique and impressive catalytic oxidation chemistry of tyrosinases, decades of effort have been directed to reproduce their reversible dioxygen binding and oxidative reactivity in small synthetic complexes.[2,3] Besides the biological occurring side-on-bonded peroxide, the isomeric bis(μ-oxo) dicopper(III) core (O core) has often been found in model complexes.[3,4] The most accepted mechanism, based on both theory and experimental data, proposes that a P core species performs the hydroxylation reaction through an electrophilic aromatic

substitution reaction and that the cleavage of the O-O bond occurs either concerted with or after the C-O bond formation.[5] However, radical mechanisms have been proposed[6] and several examples of highly active pure O core complexes kept the discussion about the truly hydroxylating species in tyrosinase alife.[7] To complicate matter, the isomeric equilibrium (Fig. 1) between O and P core can be shifted by the choice of the ligands, temperature and counteranions.[3] Moreover this equilibrium is theoretically regarded as torture track for computational chemistry,[8,9] since the amount of exact exchange heavily influences the predicted energies for the O/P equilibrium.[9] Several studies with multi-reference (MR) calculations based on a wave functional theory (WFT) method such as CASPT2,[10] MRCI + Q,[11] DMRG,[12] RASPT2[13] have been carried out with ammonia ligands as a substitution of histidine residues. However, the small model does not reproduce experimental Cu–Cu and O–O distances of "real" peroxo complexes. Further DFT studies focused on real-life systems,[7,14] but still "cutting" of the ligands or substrates yielded deviating results. In a very recent study utilising DFT and the full complex system, Liu and Blomberg gave an explanation for the early cleavage of the O-O bond with subsequent phenolate cordination.[15] These results fit excellently with the experimental data by Stack et al.[16] and emphasize the importance of the O core for substrate activation. Moreover, they point out the importance to simulate "full" systems without simplifications.

In spite of decades of effort, only four complexes achieve significant catalytic phenol hydroxylation using dioxygen: a dinucleating, polydentate imine complex reported by Réglier,[17] another dinuleating benzimidazole system with 1.2 turnovers reported by Casella[18] and with the first mononucleating analogues, Tuczek et al. found systems capable of 30 turnovers at maximum in the presence of triethylamine.[19] They propose the P core species as active species. Recently, we presented a new catalytic tyrosinase model based on bis(pyrazolyl)pyridyl-methane ligands.[20] The model complex $[Cu_2O_2(HC(3\text{-}tBuPz)_2(Py))_2]^{2+}$ could be unambiguously identified as P core by spectroscopic methods such as UV/Vis, Raman, X-ray absorption spectroscopy (XAS) and mass spectrometry. For the theoretical description, geometrical data from XAS and optical data from UV/Vis spectroscopy have been used for benchmarking purposes. The hybrid functional TPSSh[21] has been found to treat this 108 atom-system reasonably in combination with the 6-31g(d) basis set (see SI). To shed light on the PES, a 64-point grid was used by equidistant variation of the Cu-Cu and O-O distance, setting the chosen value as constant and full relaxation of the rest of the molecule.

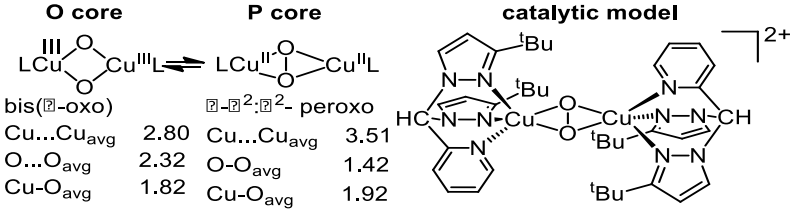

Fig. 1: Equilibrium between O and P core species, catalytic model[20] $[Cu_2O_2(HC(3\text{-}tBuPz)_2(Py))_2]^{2+}$

The distances have been varied between 2.89 – 3.79 Å for the Cu…Cu vector and 1.36 – 2.15 Å for the O…O vector. Since the P core is not adequately described by a pure closed-shell singlet,[8,9,15,22] we have calculated the full broken-symmetry PES. Figure 2 depicts the closed-shell and open-shell singlet PES. The effect of spin contamination was found to be negligible (0.5 kcal/mol). Both PES represent a remarkably narrow valley with steep sides. The O core lies in a shallow high valley whereas the P core lies in a deep immersion. The pass between both species seems not to be unsurmountable with 8.0 kcal/mol from the P side. Applying the broken symmetry approach changes this picture: the P core gains 3.3 kcal/mol stabilisation yielding a difference of electronic energies of 9.3 kcal/mol and a barrier height of 11.2 kcal/mol. With regard to the two-determinant description of the P species, the triplet state has been studied by single-point calculations up to now and was found to be close in energy in some cases.[8,9,22] We provide with a fully relaxed triplet PES (Figure 3) and find that this PES is not so steep as the singlet PES (as was expected for an excited state) and lies app. 10 –20 kcal/mol above the BS PES.

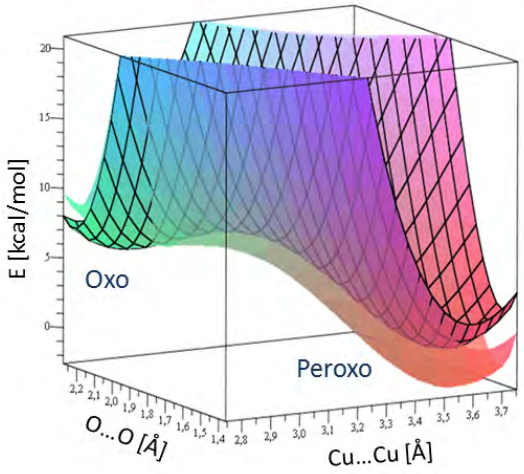

Fig. 2: Potential energy surfaces of the catalytic model system; with grid: singlet PES; transparent: open-shell singlet PES (singlet P set as zero)

It is highly noteworthy that the triplet P minimum is only 3.7 kcal/mol higher than the singlet P species and 7.0 kcal/mol higher than the BS P species The triplet P minimum is shifted towards a slightly shorter Cu…Cu distance (3.51 Å in comparison to 3.56 Å for the closed-shell singlet).

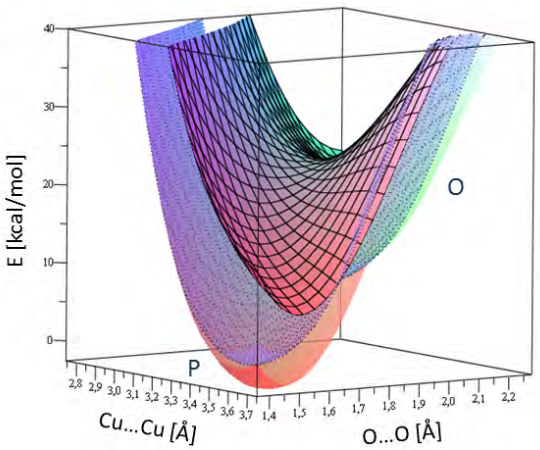

Fig. 3: Potential energy surfaces of the catalytic model system; with light grid: singlet PES; transparent: open-shell singlet PES, with dark grid: triplet PES (singlet P set as zero)

After inspection of the three PES, we focused on the minimum path between O and P core by varying the O…O distance and keeping it at fixed values between 1.36 – 2.15 Å. In order to proof the functional and basis set influence, we relaxated the complex molecules with fixed O…O distances (Figure 4A). Remarkably, the mimimum profile does not change significantly when using hybrid or pure functionals or applying a PCM solvent model. When using Ahlrichs triple-zeta basis set, the O state cannot be found as local minimum at all. For the singlet minimum path, we were able to obtain the O→P transition state TS with a transition normal mode of 185 cm^{-1} in form of a Cu_2O_2 core deformation vibration. Inspection of the minimum path towards the energies of the closed-shell singlet, open-shell singlet (broken-symmetry) and triplet states (Figure 4B) gives a similar surprising picture as the PES: the BS P species is stabilised by 3.3 kcal/mol, the triplet P just lying 3.7 kcal/mol over the singlet P.

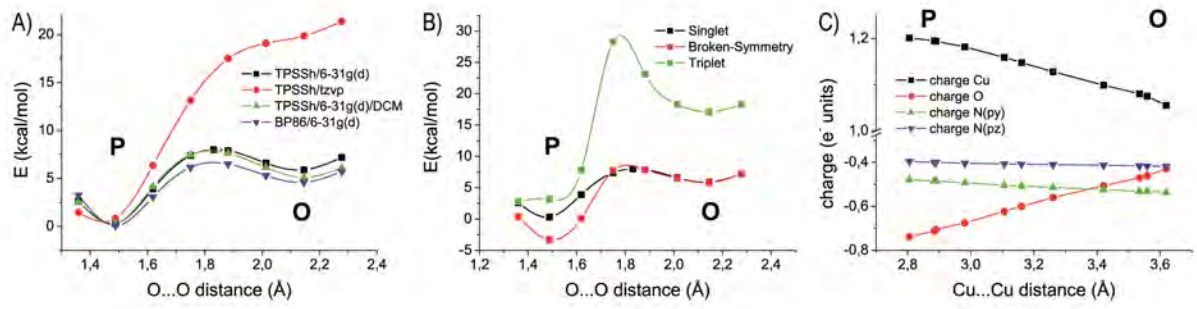

Fig. 4: A) Singlet minimum path for functional/basis set combinations (P with TPSSh/6-31g(d) set as zero); B) minimum path (TPSSh/6-31g(d)) for the three states (singlet P set as zero); C) NBO charges for the O/P transition

Hence, the great relevance of triplet states for the activity of tyrosinase and its models has to be underscored since such an excited state can be easily attained by optical excitation into the $p_v^* \rightarrow d_{xy}$ transition. On the O side, the triplet is 11.0

kcal/mol higher in energy. This can be explained by the d^8 configuration of the Cu atoms which try to avoid the triplet state.

In order to understand the electronic situation of the P core, we performed NBO analysis[23] (Figure 4C) and charge decomposition analysis (CDA, Figure 5).[24] The HOMO of the P core is the bonding interaction between peroxide σ* and Cu d_{xy} orbitals whereas the LUMO is the antibonding combination of p_s* and Cu d_{xy}.[3,25] When the P core is transformed to the O core, these electrons are shifted more into the s* orbital of the peroxide moiety yielding the oxido bridges but the resulting HOMO is still a bonding combination of oxygen σ* and Cu d_{xy} orbitals with more oxygen contribution.[25] The NBO charges in Figure 4C illustrate that the charge on the copper atoms changes only by 0.12 e-units whereas the oxygen charge changes by 0.24 e-units during this transition. The overall charge is then compensated by the pyrazolyl and pyridine donors. The CDA analysis allows a detailed insight into (back)bonding of the P, TS and O species. The backbonding of the Cu to the unoccupied s* orbital is thus very small in the P species with 1.7% and grows to a contribution of 40.4% in the O core, since here, this orbital is now formally filled and represents the HOMO (mainly consisting of the filled s*). The increasing charge on the oxygen atoms is also reflected in the increase in back-donation of peroxide p* to Cu on the P→O pathway. The marginal s* population in the P species is a hallmark for an enhanced electrophilic hydroxylation activity which is found experimentally.[20]

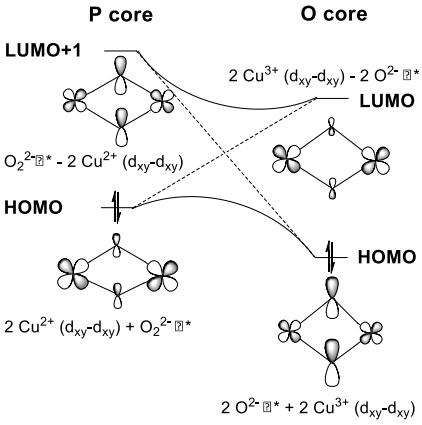

Fragment CDA analysis of using Mulliken populations and **P**-type fragmentation

	P	TS	O
π*(Cu->O_2^{2-})[a]	1.7	20.7	40.4
π*(O_2^{2-}->Cu)[b]	41.8	41.5	45.9

[a]Summation of the unoccupied π* O_2^{2-} fragment orbital in the occupied MOs. [b]Summation of the occupied π_β* and π_v* O_2^{2-} fragment orbitals in the unoccupied MOs.

Fig. 5: P→O correlation diagram[25] and CDA analysis results

In summary, we present the first full PES analysis of a P/O core equilibrium for the three important states. Moreover, this complete analysis has been accomplished for a real-life catalytic tyrosinase model. We could show that the P core lies in a deep global minimum with additional broken-symmetry stabilisation. With regard to the simple optical excitation by visible light, the low-lying triplet P state appears as viable alternative for induction of biological hydroxylation activity. In this context, we plan further studies with regard to excited states which are relevant in the catalytic cycle.

Hardware/Software: Arminius and Oculus/ Gaussian09 and Turbomole

References

[1] Matoba, Y.; Kumagai, T.; Yamamoto, A.; Yoshitsu, H. and Sugiyama, M.: J. Biol. Chem., 2006, 281, 8981.

[2] Solomon, E. I.; Sundaram, U.M. and Machonkin, T.E.: Chem. Rev., 1996, 96, 2563; Rolff, M.; Schottenheim, J.; Decker, H. and Tuczek, F.: Chem. Soc. Rev., 2011, 40, 4077; Itoh, S. and Fukuzumi, S.: Acc. Chem. Res., 2007, 40, 592; Karlin, K.D.; Itoh, S. and Rokita, S.: (Eds.) in Copper-Oxygen Chemistry, John Wiley & Sons, Inc., Hoboken, New Jersey, 2011T. D. P. Stack, Dalton Trans., 2003, 10, 1881; W. B. Tolman, Acc. Chem. Res. 1997, 30, 227; P. L. Holland, W. B. Tolman, Coord. Chem. Rev. 1999, 192, 855. S. Schindler, Eur. J. Inorg. Chem. 2000, 2311; L. Q. Hatcher, K. D. Karlin, Adv. Inorg. Chem. 2006, 58, 131.

[3] Mirica, L. M. and Ottenwaelder, X.: T. D. P. Stack, Chem. Rev. 2004, 104, 1013.

[4] Halfen, J. A.; Mahapatra, S.; Wilkinson, E.C.; Kaderli, S.; Young, V.G.; Que, L.; Zuberbühler, A.D. and Tolman, W:B.: Science 1996, 271, 1397.

[5] Que, L.; Tolman, Jr., W. B.: Nature, 2008, 455, 333; Mahadevan, V.; Gebbink, R. J. M.; Stack, T. D. P. : Curr. Op. Chem. Biol., 2000, 4, 228.

[6] Inoue, T.; Shiota, Y. and Yoshizawa, K.: J. Am. Chem. Soc., 2008, 130, 16890.

[7] Company, A.; Palavicini, S.; Garcia-Bosch, I.; Mas-Balleste, R.; Que, L.; Rybak-Akimova, E. V.; Casella, L.; Ribas, X. and Costas, M.: Chem. Eur. J., 2008, 14, 3535; Herres-Pawlis, S.; Verma, P.; Haase, R.; Kang, P.; Lyons, C.T.; Wasinger, E.C.; Flörke, U.; Henkel, G. and Stack, T. D. P.: J. Am. Chem. Soc., 2009, 131, 1154.

[8] Cramer, C. J.; Wloch, M.; Pieruch, P.; Puzzarini, C. and Gagliardi, L.: J. Phys. Chem. A, 2006, 110, 1991; P. E. M. Siegbahn, J. Biol. Inorg. Chem., 2006, 11, 695; Lewin, J.L., Heppner, D.E. and Cramer C.J.: J. Biol. Inorg. Chem., 2007, 12, 1221; Poater, A. and Cavallo, L.: Inorg. Chem., 2009, 48, 4062; Saito, T.; Kataoka, Y.; Nakanishi, Y., Matsui, T.; Kitagawa, Y., Kawakami, T.; Okumura, M. and Yamaguchi, K.: Int. J. Quantum Chem. 2009, 109, 3649.

[9] Gherman, B. F.; Cramer, C.J.: Coord. Chem. Rev. 2009, 253, 723.

[10] Flock, M. and Pierloot, K.: J. Phys. Chem. A, 1999, 103, 95.

[11] Rode, M.F. and Werner, H.-J.: Theor. Chem. Acc., 2005, 114, 309.

[12] Marti, K. H.; Ondík, I. M.; Moritz, G. and Reiher, M.: J. Chem. Phys., 2008, 128, 014104.

[13] Malmqvist, P. Å.; Pierloot, K.; Shahi, A. R. M.; Cramer, C. J. and Gagliardi, L.: J. Chem. Phys., 2008, 128, 204109.

[14] Op't Holt, B. T.; Vance, M. A.; Mirica, L. M.; Heppner, D. E.; Stack, T. D. P. and Solomon, E.I.: J. Am. Chem. Soc., 2009, 131, 6421.

[15] Liu, Y. F.; Yu, J. G.; Siegbahn, P. E. M. and Blomberg, M. R. A.; Chem. Eur. J. 2013, 19, 1942.

[16] Mirica, L. M.; Vance, M.; Rudd, D.J.; Hedman, B.; Hodgson, K.O.; Solomon, E.I. and Stack, T. D. P.: Science, 2005, 308, 1890.
[17] Réglier, M.; Jorand, C. and Waegell, B.: J. Chem. Soc., Chem. Commun., 1990, 1752.
[18] Palavicini, S., Granata, A.; Monzani, E. and Casella, L.: J. Am. Chem. Soc. 2005, 127, 18031; Casella, L.; Gullotti, M.; Radaelli, R. and Di Gennaro, P.: J. Chem. Soc., Chem. Commun., 1991, 1611.
[19] Rolff, M.; Schottenheim, J.; Peters, G. and Tuczek, F.: Angew. Chem. 2010, 122, 6583; Angew. Chem., Int. Ed. 2010, 49, 6438; J. Schottenheim, N. Fateeva, W. Thimm, J. Krahmer, F. Tuczek, Z. Anorg. Allg. Chem., 2013, 639, 1491.
[20] Hoffmann, A.; Citek, C.; Binder, S.; Goos, A.; Rübhausen, M., Troeppner, O.I. Ivanović-Burmazović, E. C. Wasinger, T. D. P. Stack, S. Herres-Pawlis, Angew. Chem. 2013, 125, 5508; Angew. Chem. Int. Ed. 2013, 52, 5398.
[21] V. N. Staroverov, G. E. Scuseria, J. Tao, J. P. Perdew, J. Chem. Phys. 2003, 119, 12129.
[22] Poater, A.; L. Cavallo, Theor. Chem. Acc., 2013, 132, 1336.
[23] F. Weinhold, C. Landis, Valency and Bonding – A Natural Bond Orbital Donor-Acceptor Perspective, Cambridge University Press, New York, 2005.
[24] S. Dapprich, G. Frenking, J. Phys. Chem., 1995, 99, 9352.
[25] G. Y. Park, M. F. Qayyum, J. Woertink, K. O. Hodgson, B. Hedman, A. A. N. Sarjeant, E. I. Solomon, J. Am. Chem. Soc., 2012, 134, 8513.

5.1.5 Theoretical study on Stereoselective Lactide polymerisations

Supervisor:	Sonja Herres-Pawlis, Ludwig-Maximilians-Universität München
Members:	Ines dos Santos Vieira, Technische Universität Dortmund
	Britta Glowacki, Ludwig-Maximilians-Universität München
Supported by:	DFG (FOR1405)

Abstract

In the 21st Century the need for sustainable and environmentally benign polymers has never been more urgent.[1] This is due to dwindling supplies of the fossil fuel starting material, used in the majority of commercial polymers, and the desire from companies and consumers to be "greener".[2] To this end there are many green processes being championed in the literature – without question one of the main success stories is that of polylactide (PLA).[3] Its sustainable building block is lactic acid, which can be obtained from the fermentation of corn starch, using well established procedures.[4] Lactic acid can then be converted to the cyclic monomer, lactide, which in-turn is polymerised (typically in a ring opening polymerisation[3b]) to produce PLA.[5] This process is not only an academic curiosity but PLA is produced on an industrial scale in Europe, Asia and in the United States.[2] Lactide can be used in either its stereo-pure form (L- or D-lactide, LA) or as a racemic mixture, rac-LA. Using rac-LA it is possible to produce heterotactic, atactic or isotactic stereoblock PLA, with the properties of the polymer (e.g. Tm and degradation rates) being intrinsically linked to the polymer's microstructure.[6] Consequently, in recent years there has been an exigent desire to develop new initiators for the stereoselective production of PLA.[7] Stereoselective catalysis is a major drive for organic chemistry, with many stereoselective mechanisms being well understood and predictable.[8] This is by no means the case in the area of stereoselective polymerisation of rac-LA, with it being almost impossible to predict the stereochemical outcome of a polymerisation beforehand.[9] For example, it has been shown that a Zr(IV) C3-symmetric amine(trisphenolate) complex produces near perfect heterotactic PLA;[10] whereas when one of the methylene bridges and a tBu group are removed atactic PLA is formed.[11-13]

I. dos Santos Vieira, E. L. Whitelaw, M. D. Jones. S. Herres-Pawlis, Synergistic Empirical and Theoretical Study on the Stereoselective Mechanism for the Aluminium Salalen Complex mediated Polymerisation of rac-Lactide, Chem. Eur. J. 2013, 19, 4712 - 4716.

Project Description

One of the main breakthroughs in the understanding of stereoselectivity in small molecular catalysis is the synergy of experimental results with computational studies.[14] This marriage of computer-with-experiment is in its early days in the ROP of rac-LA although there are pioneering studies by Rzepa and co-workers, where they successfully illustrated that DFT calculations can be applied to the ROP of LA.[15] They demonstrated that this precedes via two transition states (TS) with the highest energy TS governing the stereochemistry of the monomer insertion for β-diketiminate magnesium systems yielding heterotactic PLA.[15] We have also shown that DFT calculations can be coupled with empirical data with great effect using zinc guanidine complexes.[16] Other examples of the coupling of DFT calculations with cyclic ester polymerisation are rare.[17-19]

One of the most significant classes of initiators is based on Al(III) centres. To the best of our knowledge there have been no reported DFT studies on the polymerisation of rac-LA initiated with Al(III) centres at all. However, Svensson has used DFT to investigate the ROP of glycolide and DXO (1,5-dioxepan-2-one) with Me2AlOMe.[20] Recently, we have shown that Al(III)-salalen complexes can produce PLA with strong stereoselective bias.[12] The exact role the ligand plays in inducing stereoselectivity in the polymer is not understood. Therefore, in this paper we wish to present the further use of these Al-salalen complexes for the polymerisation coupled with the use of DFT calculations to analyse and understand the empirical data. The salalen ligands used in this study are shown in figure 1. The para tBu groups are present for ease of synthesis and are omitted in the DFT study to reduce the computational time required, as the presence of these has no effect upon the steric demands of the ligand once coordinated. The aluminium complexes are prepared by the addition of 1 eq. of AlMe3 to the ligand. To generate the active alkoxide 1 eq. of benzyl alcohol is added to the aluminium-methyl species prior to the polymerisation.[12] The complexes have C1 symmetry in the solid-state. It must be noted that upon complexation the tertiary amine becomes chiral and due to the chelation of the ligand the metal centre is also chiral giving potentially a pair of enantiomers.

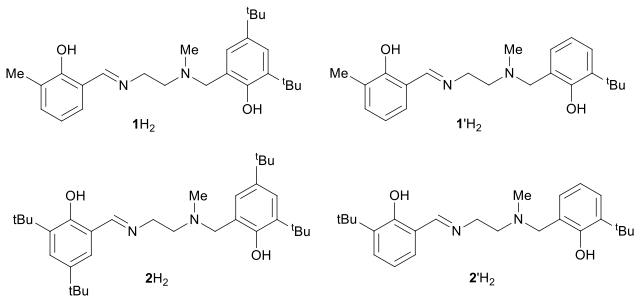

Fig.1: Ligands used in this study, those labelled with a ‘ are the ligands used in the computational study, with the para *t*Bu groups omitted.

As the complexes crystallise in centrosymmetric space groups both enantiomers are present.

When these ligands are complexed to octahedral metal centres (e.g. group 4) the β-cis confirmation is observed in the solid-state with the salan fragment fac and the salen mer.[21] Significantly, as the ortho substituent is changed from a Me to a tBu there is a sharp decrease in the probability of racemic enchainment in the final polymer, with the PLA having a Pr = 0.75 for Al(1)Me and Al(2)Me produces PLA with a slight isotactic bias (Pr = 0.4).[12] We have now investigated this change in selectivity in more detail.

The kinetics for the polymerisation with (S,S)- and rac-LA have been investigated with both initiators and the results are presented in Table 1. The process was shown to be first order with respect to lactide with a linear plot of ln[LA] vs. time. These kinetic results are in agreement with our previously published study;[12] Al(1)Me produces heterotactic PLA, with the polymerisation of rac-LA being approximately twice as fast as the homochiral (S,S) form. The isotactic enchainment is not pronounced for Al(2)Me and hence there is little difference in the rate of insertion of an (S,S)-LA compared to rac-LA.

	Rate Constant[a]/mins-1	
Monomer	Al(1)Me	Al(2)Me
(S,S)-LA	7.1 × 10-5	34.0 × 10-5
rac-LA	13.8 × 10-5	33.5 × 10-5

Table 1: Kinetic results for the polymerisation of (S,S)/rac-LA monomer. [a]These were determined, on an NMR scale, at 80 ºC in C6D5CD3 (0.6 ml) using lactide (0.05 g) and a 1:1:100 ratio of Initiator:BzOH: monomer.

The initiating species for the polymerisation is the -OCH2Ph residue. The model complexes were designed by substitution of the Me group attached to the Al with a OBz residue from the crystal structures of Al(1)Me or Al(2)Me. A (R,R)- or (S,S)-lactide has been inserted as LA1 into the Al–OBz bond and the geometry optimised. For the chain propagation four different sequences of lactide insertion were considered as the inserted lactide LA1 and the inserting lactide LA2 can both be either (R,R) or (S,S). For these four combinations the mechanistic intermediates have been calculated using density functional theory (DFT) with the B3LYP functional and the economical 6-31G(d) basis set implemented in the Gaussian03 suite of programs.[22] This rather simple protocol has been chosen due to robustness of the functional and massive transition state search efforts for overall eight lactide combinations within large aluminium

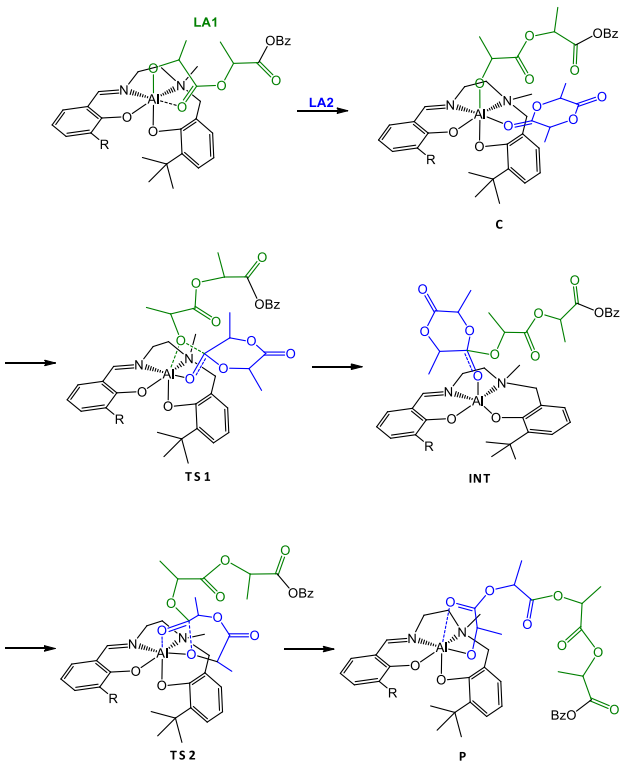

Scheme 1. Mechanism for the chain growth in the ROP of lactide with Al salalen complexes Al(**1'**) and Al(**2'**); (**C** = aluminium coordinated lactide, **TS** = transition state, **INT** = intermediate, **P** = propagating species).

complexes. Only one enantiomer of the complex was investigated via DFT as the converse sequences of lactide behave analogously with the other enantiomer of the complex.

ROP proceeds via a coordination-insertion mechanism[3] as depicted in Scheme 1. In the first step the lactide coordinates to the metal centre, which leads to the first intermediate C. The approach path of LA2 to the Al centre is predetermined by the ligand and the arrangement of LA1. The Me and tBu groups at the phenyl rings in Al(1') respectively the two tBu groups in Al(2') are in close proximity to the Al centre and direct the incoming LA moiety. The first transition state TS1 follows which corresponds to the nucleophilic attack of the alkoxide function of LA1 to the carbonyl C atom of the coordinating LA2. Thereby the carbonyl carbon atom undergoes a change of hybridisation from sp2 to sp3. After the C–O bond formation the intermediate INT is formed. In contrast to the mechanism we reported for zinc guanidine bis(chelate) complexes and previous studies with β-diketiminate magnesium systems, a geometry where the intracyclic oxygen of the (still closed) LA2 joins the coordination of the metal centre could not be found as an energetic minimum in a geometry optimisation.[15, 16] The next transition state TS2 is reached which corresponds to the ring opening in LA2 where the intracyclic C–O bond is broken. After the ring cleavage chain reorganisations occur and the insertion product P is formed. In the coordinated geometry C and the transition states TS1 and TS2 the aluminium centre possesses an octahedral environment (Figure 2). In these cases from all the possible isomers the β-cis conformation is formed with the salan moiety fac and the salen mer, as observed with octahedral group 4 complexes of such ligands.[21] The other geometries show a five-fold coordination of the Al in a trigonal bipyramidal manner.

For Al(1') (Scheme 1, Figure 3a) the coordination geometries C have similar energies indicating that in the coordination no one isomer is significantly preferred over another. The activation enthalpies ΔH≠ for the transition state TS1 are relatively low for the sequences (RR,RR), and (SS,RR) with values of 5.3 and 5.0 kcal·mol-1. The (RR,SS) sequence has a moderate first transition state with a ΔH≠ of 11.4 kcal·mol-1. For TS1 the highest ΔH≠ is observed for the (SS,SS) sequence with a value of 19.4 kcal·mol-1 causing the (SS,SS) sequence to be the least favoured.

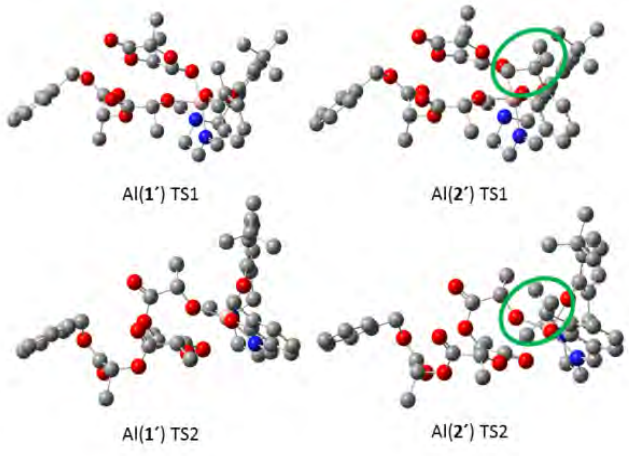

Fig. 2: Calculated transition states **TS1** and **TS2**for Al(**1'**) and Al(**2'**) [the green circle indicates the stereo-differentiating ^{t}Bu group].

Except for the (SS,SS) sequence the second transition state TS2 has a higher ΔH≠ than TS1. The (RR,RR) sequence shows the highest ΔH≠ at a value of 28.8 kcal·mol-1. The (RR,SS) sequence in comparison is energetically more favoured with 21.8 kcal·mol-1. The (SS,SS)

sequence has the lowest ΔH≠ to TS2 at 13.3 kcal·mol-1 but is though not favoured due to the high ΔH≠ to TS1. Taking both transitions states into account the (SS,RR) sequence is energetically most favoured due to its lowest ΔH≠ for TS1 (5.0 kcal·mol-1) and also a comparatively low ΔH≠ for TS2 at 18.5 kcal·mol-1. Furthermore, the (RR,SS) sequence is more favoured than the (RR,RR) sequence. Thus, statistically the (SS,RR) and (RR,SS) routes are taken more often which would lead to heterotactic PLA, which is observed experimentally.

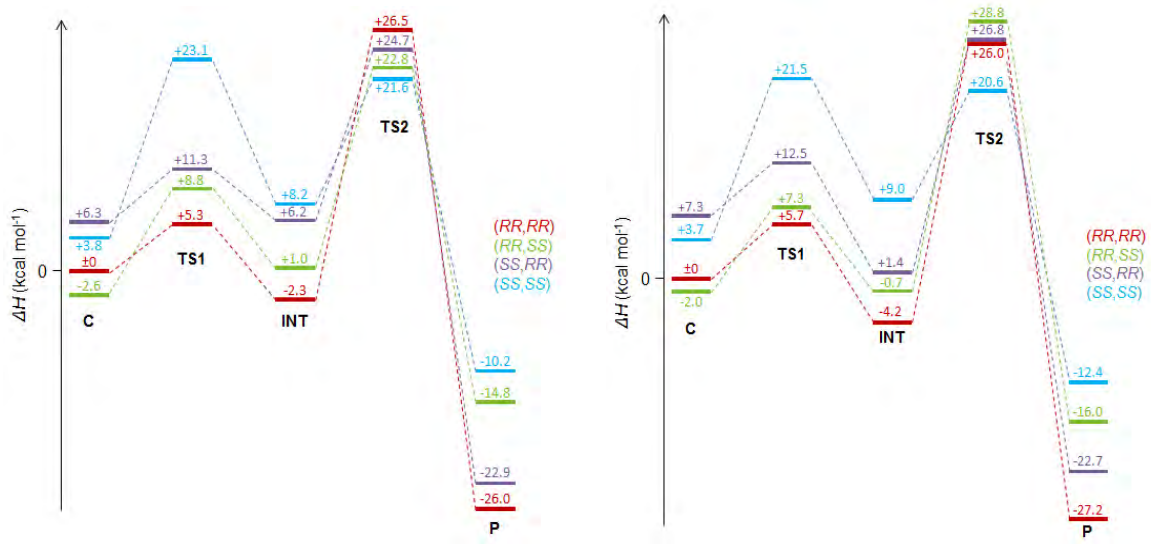

Fig 3.: **a)** left: Calculated enthalpies (kcal·mol-1) for the reaction coordinates of the chain propagation model with complex Al(1'); **b)** right: Calculated enthalpies (kcal·mol-1) for the reaction coordinates of the chain propagation model with complex Al(2') (C = aluminium coordinated lactide, TS = transition state, INT = intermediate, O = opened species, P = propagating species).

In Al(2') the aluminium centre is more shielded than in Al(1') due to the higher steric demand of the second tBu, as illustrated by the green circles in Figure 2. The impact on the enthalpies of the different mechanistic intermediates is depicted in Figure 3b. The influence on the coordinated states C and the first transition states TS1 is low when compared to Al(1') which leads to similar activation enthalpies to TS1. This means the steric demand of the tBu and therefore the smaller approach pathway for LA2 effects all the combinations to the same degree. Also in this case the (SS,SS) sequence has the highest ΔH≠ to TS1 with 17.8 kcal·mol-1 while for the other sequences this ΔH≠ is between 5.3 and 9.2 kcal·mol-1. However, for TS2 the ΔH≠ values differ significantly from Al(1'). For the (RR,RR) sequence the ΔH≠ is comparable to that of Al(1') at 30.2 kcal·mol-1 {cf. 28.8 kcal·mol-1 for Al(1')} while for the (RR,SS) sequence the value is much higher at 29.6 kcal·mol-1. Therefore the (RR,SS) sequence is no longer favoured over (RR,RR) as was the case with Al(1'). For the (SS,RR) sequence the ΔH≠ rises to 25.4 kcal·mol-1 compared to 18.5 kcal·mol-1 in Al(1'). This makes the (SS,SS) sequence with ΔH≠s of 17.8 and 11.6 kcal·mol-1 the most favoured pathway which supports the experimentally observed small isotactic enrichment. The calculations have employed the complexes with an

(S) chiral centre on the amine centre; therefore with the (R) enantiomer of the complex the (RR,RR) sequence would be preferred.
We have investigated the influence of the steric shielding of the aluminium centre for two aluminium salalen complexes, and we have shown that the polymerisation proceeds via a chain end controlled mechanism. Experimentally the substitution of one Me moiety close to the catalytically active metal centre with the sterically more demanding tBu group led to a significant switch from heterotactically enriched PLA to PLA with a small degree of isotactic enchainment. The experimentally observed polymer tacticities could be confirmed theoretically by comparing calculated activation enthalpies with different sequences of consecutive (R,R)- and (S,S)-lactide insertion. The subtle difference of having a second tBu in the active centre of Al(2') steers the tacticity of the growing chain towards isotactic enrichment by dissecting the incoming lactides for their "fit" into the reaction chamber. The ortho-substituent of the ligand is extremely critical for the positioning of the new incoming lactide which we could now prove theoretically. For other ligands, the influence can be evaluated computationally as well in order to design a suited catalytic pocket. This study enables now the targeted development of further catalysts with designated stereo-preference.

Hardware/Software: Arminius / Gaussian03 and Turbomole

References

[1] a) Auras, R.; Harte, B. and Selke, S.: Macromol. Biosci. 2004, 4, 835-864;
b) Edlund, U. and Albertsson, A.C.: Degradable Aliphatic Polyesters 2002, 157, 67-112;
c) Kataoka, C.; Harada, A. and Nagasaki, Y.: Adv. Drug Delivery Rev. 2001, 47, 113-131;
d) Lim, L.T.; Auras, R. and Rubino, M.: Prog. Polym. Sci. 2008, 33, 820-852;
e) Stridsberg, K.M.; Ryner, M. and Albertsson, A.C. in Degradable Aliphatic Polyesters, Vol. 157 (Ed.: A. C. Albertsson), 2002, pp. 41-65;
f) Williams, C.K.: Chem. Soc. Rev. 2007, 36, 1573-1580.

[2] Vink, E.T.H.; Rabago, K. R.; Glassner, D.A.; Springs,B.; O'Connor,R.P.; Kolstad,J. and Gruber,P.R.: Macromol. Biosci. 2004, 4, 551-564.

[3] a) Platel, R.H.; Hodgson, L.M. and Williams, C.K.: Polymer Reviews 2008, 48, 11-63;
b) Auras, L.-T. L. R.; Selke, S. E. M. and Tsuji, H.: in Poly(lactid acid) - Synthesis, Structures, Properties, Processing, and Applications, John Wiley & Sons, Inc, Hoboken, New Jersey 2010;
c) Thomas, C.M.: Chem. Soc. Rev 2010, 39, 165-173.

[4] a) Datta, R. and Henry, M.: J. Chem. Technol. Biotechnol. 2006, 81, 1119-1129;
b) Holm, M.S.; Saravanamurugan,S. and Taarning,E. Science 2010, 328, 602-605.

[5] O'Keefe, B.K.; Hillmyer, M.A. and Tolman, W.B.: J. Chem. Soc., Dalton Trans. 2001, 2215-2224.

[6] a) Albertsson, A.C.; and Varma, I.K.: Biomacromolecules 2003, 4, 1466-1486;
b) Stanford, M.J. and Dove, A.P.: Chem. Soc. Rev. 2010, 39, 486-494.

[7] a) Amgoune, A.; Thomas, C.M.; Roisnel, T. and Carpentier, J.F.: Chem. Eur. J. 2006, 12, 169-179;
b) Bonnet, F.; Cowley, A.R.; and Mountford, R.: Inorg. Chem. 2005, 44, 9046-9055;
c) Chamberlain, B.M.; Cheng, M.; Moore, D.R.; Ovitt,T.M.; Lobkovsky,E.B. and Coates, G.W.; J. Am. Chem. Soc. 2001, 123, 3229-3238;
d) Cheng, M.; Attygalle, A.B.; Lobkovsky, E.B. and Coates, G.W.: J. Am. Chem. Soc. 1999, 121, 11583-11584;
e) M. H. Chisholm, J. C.M. H.; Gallucci, K.J. C. and Phomphrai,K.: Inorg. Chem. 2004, 43, 6717-6725;
f) Gendler, A.; Segal, S.; Goldberg, I.; Goldschmidt, Z. and Kol, M.: Inorg. Chem. 2006, 45, 4783-4790;
g) Hormnirun, P.; Marshall, E.L.; Gibson, V.C.; White, A.J.P. and Williams, D.J.: J. Am. Chem. Soc. 2004, 126, 2688-2689;
h) Kim, Y.; Jnaneshwara, G.K. and Verkade, J.G.: Inorg. Chem. 2003, 42, 1437-1447;
i) Lohmeijer, B.G.G.; Pratt, R.C.; Leibfarth,F.; Logan,J.W.; Long,D.A.; Dove,D.A.; Nederberg,F.; Choi,J.; Wade,C.; Waymouth,R.M. and Hedrick,J.L.: Macromolecules 2006, 39, 8574-8583;
j) Nomura, N.; Ishii, R.; Akakura, M. and Aoi, K.: J. Am. Chem. Soc. 2002, 124, 5938-5939;
k) Zhong, Z. Y.; Dijkstra, P. J. and Feijen,J.: Angew. Chem., Int. Ed. Engl. 2002, 41, 4510-4513;
l) Zhong, Z. Y.; Dijkstra, P.J. and Feijen,J.: J. Am. Chem. Soc. 2003, 125, 11291-11298.

[8] a) Abdur-Rashid, K.; Clapham, S. E.; Hadzovic, A.; Harvey,J.N.; Lough,A.J.; Morris, R.H.: J. Am. Chem. Soc. 2002, 124, 15104-15118;
b) Noyori, R.; Yamakawa, M. and Hashiguchi, S.: J. Org. Chem. 2001, 66, 7931-7944;
c) Sandoval, C.A.; Ohkuma, T.; Muniz, K. and Noyori, R.: J. Am. Chem. Soc. 2003, 125, 13490-13503.

[9] Chisholm, M. H.; Gallucci, J. C.; Quisenberry, K. T.; Zhou, Z. P.: Inorg. Chem. 2008, 47, 2613-2624.

[10] Chmura, A. J.; Davidson, M. G.; Frankis, C. J.; Jones, M. D. and Lunn, M. D.: Chem. Commun. 2008, 1293-1295.

[11] Whitelaw, E. L.; Jones, M. D.; Mahon, M. F. and Kociok-Kohn, G.: Dalton Trans. 2009, 9020-9025.

[12] Whitelaw, E. L.; Loraine, G.; Mahon, M. F. and Jones, M. D.: Dalton Trans. 2011, 40, 11469-11473.

[13] Stopper, A.; Okuda, J. and Kol, M.: Macromolecules 2012, 45, 698-704.

[14] a) Fraile, J. M.; Garcia, J. I.; Martinez-Merino, V.; Mayoral, J. A. and Salvatella, L.: J. Am. Chem. Soc. 2001, 123, 7616-7625;
b) Guest, M. F.; Bush, I. J.; Van Dam, H. J. J.; Sherwood, P.; Thomas, J. M. H.; Van Lenthe, J. H.; Havenith, R. W. A. and Kendrick, J.: Mol. Phys. 2005, 103, 719-747;
c) Shi, F. Q.; Li, X.; Xia, Y.; Zhang, L.;. and Yu, Z. X.: J. Am. Chem. Soc. 2007, 129, 15503-15512.

[15] Marshall, E. L.; Gibson, V. C. and Rzepa, H. S.: J. Am. Chem. Soc. 2005, 127, 6048-6051.

[16] Börner, J.; dos Santos Vieira, I.; Pawlis,A.; Doring,A.; Kuckling,D. and Herres-Pawlis,S.: Chem. Eur. J. 2011, 17, 4507-4512.

[17] Barros, N.; Mountford, P.; Guillaume, S.M. and Maron, L.: Chem. Eur. J. 2008, 14, 5507-5518.

[18] Dyer, H. E.; Huijser, S.; Susperregui, N.; Bonnet, F.; Schwarz, A. D.; Duchateau, R.; Maron, L. and Mountford, P.: Organometallics 2010, 29, 3602-3621.

[19] Sarazin, Y.; Liu, B.; Roisnel, T.; Maron, L. and Carpentier, J.F.: J. Am. Chem. Soc. 2011, 133, 9069-9087.

[20] von Schenck, H.; Ryner, M.; Albertsson, A.C.;. and Svensson,M.: Macromolecules 2002, 35, 1556-1562.

[21] Whitelaw, E. L.; Jones, M. D. and Mahon, M. F.: Inorg. Chem. 2010, 49, 7176-7181.

[22] Gaussian 03, Frisch, M. J.; Trucks, G.W.; Schlegel, H.B.; Scuseria, G.E.; Robb, M.A.; Cheeseman, J. R.; Montgomery, Jr., J.A.; Vreven, T.; Kudin, K.N.; Burant, J.C.; Millam, J.M.; Iyengar, S.S.; Tomasi, J.; Barone, V.; Mennucci, B.; Cossi, M.; Scalmani, G.; Rega, N.; Petersson, G.A.; Nakatsuji, H.; Hada, M.; Ehara, M.; Toyota, K.; Fukuda, R.; Hasegawa, J.; Ishida, M.; Nakajima, T.; Honda, Y.; Kitao, O.; Nakai, H.; Klene, M.; Li, X.; Knox, J.E.; Hratchian, H.P., Cross, J.B.; Bakken, V.; Adamo, C.; Jaramillo, J.; Gomperts, R.; Stratmann, R.E.; Yazyev, O.; Austin, A.J.; Cammi, R.; Pomelli, C., Ochterski, J.W.; Ayala, P.Y.; Morokuma, K.; Voth, G.A.; Salvador, P., Dannenberg, J.J.; Zakrzewski, V.G.; Dapprich, S., Daniels, A.D.; Strain, M.C.; Farkas, O.; Malick, D.K.; Rabuck, A.D.; Raghavachari, K.; Foresman, J. B.; Ortiz, J.V.; Cui, Q.; Baboul, A.G.; Clifford, S.; Cioslowski, J.; Stefanov, B.B.; Liu, G.; Liashenko, A.; Piskorz, P.; Komaromi, I.; Martin, R.L.; Fox, D.J.; Keith, T.; Al-Laham, M.A.; Peng, C.Y.; Nanayakkara, A.; Challacombe, M.; Gill, P. M. W.; Johnson, B.; Chen, W.; Wong, M.W.; Gonzalez, C. and Pople, J.A.: Gaussian, Inc., Wallingford CT, 2004.

5.1.6 Detailed quantum dynamics study of the H + CH_4 → H_2 + CH_3 reaction on a new potential energy surface

Supervisor:	Ralph Welsch, University of Bielefeld
Members:	Robert Wodraszka, University of Bielefeld
	Roman Ellerbrock, University of Bielefeld

Supported by:	DFG

Abstract

The project studies the quantum state-specific dynamics of polyatomic reactions. While a fully quantum state resolved level of understanding has been achieved for triatomic and selected tetratomic reactions, extending this level of understanding towards reactions involving a larger number of atoms is a challenge. The reactions of methane with atoms as H, Cl, F, or O are important processes in atmospheric and combustion chemistry as well as prototypical reactions
extensively studied by fundamental research focusing on the detailed understanding of chemical reactivity. Impressive progress was achieved in experimental studies of these systems. However, accurate full-dimensional quantum dynamics simulations of the fully state-resolved reaction dynamics have not yet been published for any reaction consisting of more than four atoms. Our project focuses on the reaction of methane with hydrogen using a novel, yet unpublished potential energy surface (PES). This PES is constructed using a neural network and thus is evaluated efficiently. Thermal rate constants, initial state-selected and state-to-state reaction probabilities of the H + CH_4 → H_2 + CH_3 (J=0) reaction will be calculated.

Project Description

The understanding of chemical reactivity on the most detailed level of quantum state resolution is a central aim of fundamental research in chemistry. This level of understanding can nowadays routinely be achieved for triatomic reactions. Excellent agreement between theory and experiment for quantum state-resolved differential cross sections has recently also been achieved for a tetratomic reaction [1]. Recent research in this area focuses on polyatomic reactions studying the reactions of methane with different atoms as prototypical examples. See Refs. [2–8] for prominently published experimental studies.

The theoretical description of the state-specific dynamics of reactions of methane with H, Cl, F, or O is a very challenging subject. The last decade has seen tremendous progress in the construction of multi-dimensional potential energy surfaces (PESs) required by accurate reaction dynamics calculations. Based on the permutationally invariant polynomial approach developed by Braams, Bowman, and coworkers [9], full-dimensional PESs have been constructed for these reactions [10–

15]. A global PES for the $H+CH_4 \rightarrow H_2+CH_3$ reaction has also been developed based on the Shepard interpolation approach [16] and using neural networks (NN) [17].
In contrast to the progress in the development of accurate PESs, full-dimensional quantummechanical calculations studying the reaction dynamics on these PES on the level of quantum state-resolution have not yet been published. The only detailed quantum-mechanical description of the methane reactions is provided by reduced-dimensional wave packet dynamics calculations which explicitly include six to eight coordinates in the dynamical treatment [8, 16–24]. While these calculations provide a reliable description of reaction of partially deuterium-substituted methane, $X+CHD_3 \rightarrow HX+CD_3$, it fails to describe the four hydrogens in CH_4 symmetrically and to account for the degeneracy in the vibrational modes of CH_4.
Full-dimensional quantum dynamics calculations for $X + CH_4 \rightarrow HX + CH_3$ reactions have only been published by our research group [25–34]. These calculations require the (multi-layer) multi-configurational time-dependent Hartree ((ml-)MCTDH) [35, 36] approach to accurately and efficiently simulate the high-dimensional wave-packet dynamics and flux-correlation functions [37–39] to obtain the desired observables. The approach employs a rigorous quantum transition state concept [40, 41] and has originally been designed to accurately calculate reaction rates [42]. Thermal rate constants and cumulative reaction probabilities for vanishing total angular momentum (J=0) of different methane reactions [29–33,43,44] and initial state-selected (J=0) reaction probabilities for the $H+CH_4 \rightarrow H_2+CH_3$ reaction [27, 28] have been computed. However, due to the numerical effort involved, the latter calculation could only employ an inaccurate semi-empirical PES [45] which could be evaluated with little computational effort. This severely limited the overall accuracy of the results obtained.
Utilizing these developments, we are presently performing accurate quantum dynamics calculations studying the state-selected reaction probabilities for the $H+CH_4 \rightarrow H_2+CH_3$ reaction. These calculation will not only result in initial state-selected reaction probabilities but can be extended to provide fully state-resolved scattering matrix elements and reaction probabilities. Here a newly developed theoretical approach [46, 47] which extends the flux-correlation function formalism and the quantum transition state concept to the calculation of state-to-state observables is used.
So far thermal rate constants were computed using the NN-PES. They agree with former accurate rate constant calculations [25] and show the accuracy of the NN-PES around the transition state. Furthermore, most of the quantum dynamics calculations propagating towards the reactant asymptotic region are finished, but for most of these calculations the analysis is not yet finished. For the smallest basis set the results are within the error margin of the calculation using the accurate Shepard PES indicating the accuracy of the NN-PES also for the reactant channel. The calculations propagating towards the product channel are still running and will take one to four more months. The analysis of the calculations and obtaining state-to-state reaction probabilities will take further two to three months.

References

[1] Xiaoc, C.: et al., Science **333**, 440 (2011).
[2] Lin, J.; Zhou, J.; Shiu, W. and Liu, K.: Science **300**, 966 (2003).
[3] Shiu, W.; Lin, J. and Liu, K.: Phys. Rev. Lett. **92**, 103201 (2004).
[4] Zhang, W.; Kawamata, H. and Liu, K.: Science **325**, 303 (2009).
[5] Yan, S.: et al., Science **316**, 1723 (2007).
[6] Yan, S.: et al., PNAS **105**, 12667 (2008).
[7] Wang, F.; Lin, J.S. and Liu, K.: Science **331**, 900 (2011).
[8] Zhang, W.: et al., PNAS **107**, 12782 (2010).
[9] Braams, B. J. and Bowman, J.M.: Int. Rev. Phys. Chem. **28**, 577 (2009).
[10] Zhang, X.; Braams, B.J. and Bowman, J.M.: J. Chem. Phys. **124**, 021104 (2006).
[11] Zie, Z.; Bowman, J.M. and Zhang, X.: J. Chem. Phys. **125**, 133120 (2006).
[12] Czak´o, G.; Shepler, B.C.; Braams, B.J. and Bowman, J.M.: J. Chem. Phys. **130**, 084301 (2009).
[13] Czako, G. and Bowman, J.M.: Sciene **334**, 343 (2012).
[14] Czako, G. and Bowman, J.M.: J. Chem. Phys. **136**, 044307 (2000).
[15] Czako, G. and Bowman, J.M.: PNAS **109**, 7997 (2012).
[16] Zhou, Y.: et al., J. Chem. Phys. **134**, 064323 (2011).
[17] Liu, S.; Chen, J.; Zhang, Z. and Zhang, D.H.: J. Chem. Phys. **138**, 011101 (2013).
[18] Yang, M.; Zhang, D.H. and Lee, S.Y.: J. Chem. Phys. **117**, 9539 (2002).
[19] Zhang, L.; Lu, Y.; Zhang, D.H. and Lee, S.Y.: J. Chem. Phys. **127**, 234313 (2007).
[20] Liu, R.; Xiong, H. and Yang, M.: J. Chem. Phys. **137**, 174113 (2012).
[21] Zhou, Y.; Wang, C. and Zhang, D.H.: J. Chem. Phys. **135**, 024313 (2011).
[22] Zhang, Z: et al., J. Phys. Chem. Lett. **3**, 3416 (2012).
[23] Yang, M.; Lee, S.Y. and Zhang, D.H.: J. Chem. Phys. **126**, 064303 (2007).
[24] Liu, R.: et al., J. Phys. Chem. Lett. **3**, 3776 (2012).
[25] Welsch, R. and Manthe, U.: J. Chem. Phys. **138**, 164118 (2013).
[26] Welsch, R. and Manthe, U.: J. Chem. Phys. **137**, 244106 (2012).
[27] Schiffel, G. and Manthe, U.: Chem. Phys. **374**, 118 (2010).
[28] Schiffel, G. and Manthe, U.: J. Chem. Phys. **132**, 191101 (2010).
[29] Wu, T.; Werner, H.J. and Manthe, U.: Science **306**, 2227 (2004).
[30] Huarte-Larrañaga, F. and Manthe, U.: J. Chem. Phys. **113**, 5115 (2000).
[31] Huarte-Larrañaga, F. and Manthe, U.: J. Chem. Phys. **116**, 2863 (2002).
[32] Wu, T.; Werner, H.J. and Manthe, U.: J. Chem. Phys. **124**, 164307 (2006).
[33] Huarte-Larrañaga, F. and Manthe, U.: J. Chem. Phys. **117**, 4635 (2002).
[34] Schiffel, G. and Manthe, U.: J. Chem. Phys. **132**, 084103 (2010).
[35] Meyer, H.D.; Manthe, U. and Cederbaum, L.S.: Chem. Phys. Lett. **165**, 73 (1990).
[36] Meyer, H.D.; Manthe, U. and Cederbaum, L.S.: J. Chem. Phys. **97**, 3199 (1992).
[37] Yamamoto, T.: J. Chem. Phys. **33**, 281 (1960).
[38] Miller, W.H.: J. Chem. Phys. **61**, 1823 (1974).

[39] Miller, W:H.; Schwartz, S.D. and Tromp, J.W.: J. Chem. Phys. **79**, 4889 (1983).
[40] Manthe, U. and Miller, W.H.: J. Chem. Phys. **99**, 3411 (1993).
[41] Manthe, U.: Mol. Phys. 109, 1415 (2011).
[42] Matzkies, F. and Manthe, U.: J. Chem. Phys. **108**, 4828 (1998).
[43] van Harrevelt, R.; Nyman, G. and Manthe, U.: J. Chem. Phys. **126**, 084303 (2007).
[44] Nyman, G.; van Harrevelt, R. and Manthe, U.: J. Phys. Chem. A **111**, 10331 (2007).
[45] Jordan, M. and Gilbert, R.: J. Chem. Phys. **102**, 5669 (1995).
[46] Welsch, R.; Huarte-Larrañaga, F. and Manthe, U.: J. Chem. Phys. **136**, 064117 (2012).
[47] Welsch, R. and Manthe, U.: Mol. Phys. **110**, 703 (2012).

5.1.7 Quantum-Chemical Investigation of Bixbyite-Type Vanadium Sesquioxide

Supervisor:	Thomas Bredow, University of Bonn
Members:	Christoph Reimann, University of Bonn
	Eike Caldeweyer, University of Bonn
Supported by:	DFG, SPP1415

Abstract

Vanadium sesquioxide V_2O_3 has received a lot of attention in the past as model system for a Mott-Hubbard transition: At low temperatures, it is an antiferromagnetic insulator with a monoclinic crystal structure (M1), while above ~160 K it turns into a paramagnetic conductor with a rhombohedral corundum-type structure. [1] The metal-insulator transition is a consequence of the complicated nature of the localized vanadium *d* electrons.

Some years ago a new metastable polymorph has been synthesized that crystallizes in the bixbyite-type structure (Fig. 1). [2] Performing periodic quantum-chemical calculations at density functional theory (DFT) level we determined that V_2O_3 with bixbyite structure is approximately 9 kJ/mol less stable than the thermodynamically stable phases. [2] Using PBE+*U* or hybrid Hartree-Fock(HF)/DFT approaches, further properties like the fundamental band gap and the preferred magnetic ordering have been obtained. [3] Furthermore the thermodynamics of oxygen incorporation into bixbyite-type V_2O_3 was discussed in detail. [4] In all cases close agreement between theoretical results and experimental findings was obtained.

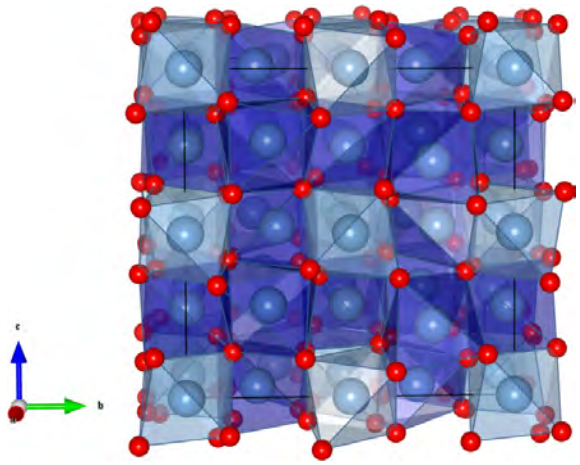

Fig. 1: V_2O_3 with bixbyite-type structure (large blue spheres: V, small red spheres: O). Vanadium atoms are coordinated by distorted octahedral of oxygen ions.

Lately, we used the pure HF method to study the electronic structure of V_2O_3. Thereby we found that the initial *d* orbital occupuation has a large impact onto the unrestricted HF wave function of the bixbyite phase. Using the results of accurate Quantum Monte Carlo (QMC) calculations we will demonstrate that this interesting effect is a consequence of the neglect of electron correlation in the HF approach

Project Description

In earlier work we performed structure relaxations at DFT (PBE and PW91) and PBE+*U* level for several V_2O_3 polymorphs (Fig. 2). [5] As vanadium sesquioxide is a member of the family of strongly correlated materials, we used complementary

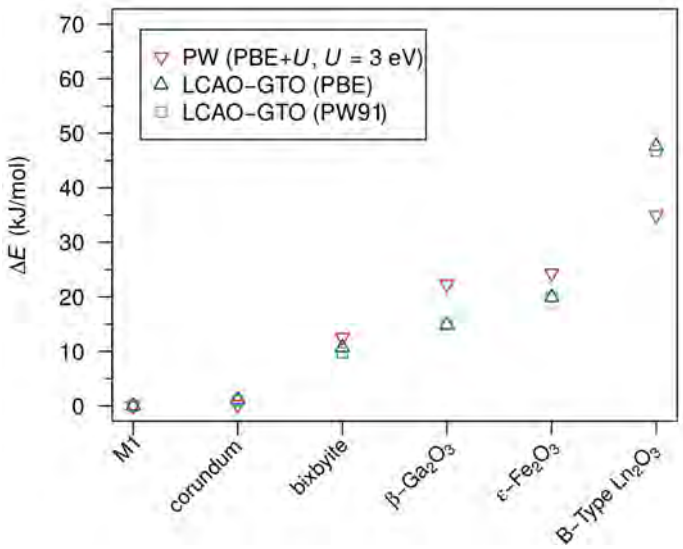

Fig. 2: Relative energies of the six most stable V_2O_3 polymorphs obtained with complementary methods (1. plane waves (PW) and PBE+*U*, 2. atom-centered Gaussian functions (LCAO-GTO) and two GGA (PBE, PW91) functionals*).*

methods by employing different kinds of basis functions (either plane waves or atom-centered Bloch functions). The results did not depend strongly on the underlying computational approach, yielding only small variations in the obtained relative energies. However, when repeating the structure relaxations employing a DFT/HF hybrid method like PBE0 or PW1PW, a significant overstabilization of the bixbyite-type phase with respect to monoclinic V_2O_3 (M1) was observed if the symmetry of the phases was not conserved during optimization.

d_{z^2}	d_{xz}	d_{yz}	$d_{x^2-y^2}$	d_{xy}	*ΔE*
↑	↑				*-8.7*
↑		↑			*-52.5*
↑			↑		*-52.5*
↑				↑	*199.5*
	↑	↑			*199.5*
	↑		↑		*10.9*
	↑			↑	-
		↑	↑		*155.6*
		↑		↑	*199.5*
			↑	↑	*217.8*

Table 1: Effect of the initial *d* orbital occupation onto the total energy in single point calculations with the UHF method. The energy differences $\Delta E=E^{bixbyite}-E^{M1}$ *(kJ/mol) were calculated with respect to one formula unit of* V_2O_3 *(*E^{M1} *shows no dependence on the initial configuration of the 3d electrons).*

In order to analyze this behavior in greater detail, we performed single point calculations with the unrestricted HF method using the experimental structures. It turned out that the initial occupation of the *d* orbitals has a pronounced effect onto

the UHF wave function of V_2O_3 with bixbyite structure, which is best elucidated by means of the corresponding relative SCF energies (Tab. 1).
In all cases an atomic d^2 configuration was assumed for vanadium so that the unpaired spins at one V atom are aligned parallel to each other. The distribution of the spins across different *d* orbitals lead to large energy differences in the case of vanadium sesquioxide with bixbyite structure, while no such effect occurred in the case of the M1 or corundum-type phase. Especially important are the configurations (d_{z^2}, d_{yz}) and $(d_{z^2}, d_{x^2-y^2})$ that lead a stabilization of the bixbyite-type polymorph of more than 50 kJ/mol with respect to the M1 phase.
Due to the variational nature of the HF method these calculated energies are always higher than the exact ground state energy, so that only the lowest values correspond to the HF ground state. Thus the bixbyite-phase is indeed falsely predicted to be most stable at the HF level which is not in accordance with experimental findings. This result does not change if another basis set or spin structure is employed. With pure GGA functional, the SCF energy does not depend on the *d* orbital occupation, so that the stabilization of the M1 phase with respect to bixbyite-type V_2O_3 is a consequence of the inclusion of electron correlation in the calculation.
It is possible to take correlation effects into account explicitly in solid state calculations by using a computationally expensive QMC approach. The most often employed techniques for chemical systems are the Variational Monte Carlo (VMC) and the Diffusion Monte Carlo (DMC) method. The VMC method is commonly applied to optimize a Jastrow factor that accounts for the electron correlation as it contains the distances between electrons as an explicit parameter. The DMC method uses this optimized wave function and can in principle yield a numerically exact solution of the electronic Schrödinger equation.
In order to calculate the energy difference between the M1 and the bixbyite phase of V_2O_3 considering the electron correlation explicitly, we used a $V_{32}O_{48}$ supercell in order to minimize finite-size effects and optimized a Jastrow factor for both systems independently. After 10,000 steps during the DMC statistics accumulation we obtained a standard error of less than 25 kJ/mol. The M1 V32O48 supercell is more stable than the bixybiyte-type supercell by 139.6 kJ/mol, which corresponds to a net energy difference of 8.7 kJ/mol per formula unit V_2O_3. This demonstrates the importance of correlation effects in the monoclinic low-temperature phase of vanadium sesquioxide.

Computational Details

The periodic quantum-chemical calculations employing atom-centered Gaussian basis sets were conducted with the CRYSTAL09 program package, [6,7] while for the plane wave calculations our collaborators (C. Wessel and R. Dronskowski, RWTH Aachen) used the VASP code. [8] The Gaussian basis sets employed in this study are based on the Stuttgart-Dresden effective core potentials and have been optimized explicitly for the use in solid-state calculations [9]. All QMC calculations have been carried out with the CASINO code [10].

References

[1] Morin, F.: Phys. Rev. Lett. 3, 34 (1959).
[2] Weber, D.; Stork, A.; Nakhal, S.; Wessel, C.; Reimann, C.; Hermes, W.; Müller, A.; Ressler, T.; Pöttgen, R.; Bredow, T.; Dronskowski, R. and Lerch, M.: Inorg. Chem. 50, 6762 (2011).
[3] Wessel, C.; Reimann, C.; Müller, A.; Weber, D.; Lerch, M.; Ressler, T.; Bredow, T. and Dronskowski, R.: J. Comput. Chem. 33, 2102 (2012).
[4] Reimann, C.; Weber, D.; Lerch, M. and Bredow, T.: J. Phys. Chem. C 117, 20164 (2013).
[5] Wessel, C.; Dronskowski, R.; Reimann, C.; Bredow, T., Weber, D.; Stork, A. and Lerch, M.: Z. Anorg. Allg. Chem. 636, 2056 (2010).
[6] Dovesi, R.; Orlando, R.; Civalleri, B.; Roetti, C., Saunders, V. and Zicovich-Wilson, C.: Z. Kristallogr. 220, 571 (2005).
[7] Dovesi, R.: *et al.* CRYSTAL09 User's Manual. University of Torino: Torino, 2009.
[8] Kresse, G. and Furthmüller, J.: Comput. Mater. Sci. 6, 15 (1996).
[9] Reimann, C.: Script for basis set optimization with CRYSTAL09, http://github.com/chrr/Pcrystal09_bsopt, 2012.
[10] Needs, R.J.; Towler, M.D.; Drummond, N.D. and López Ríos, P.: J. Phys.: Condensed Matter 22, 023201 (2010).

5.1.8 High Performance Molecular Dynamics Simulations

Supervisor:	Dr. Jens Krüger, Applied Bioinformatics Group, University of Tübingen
Members:	1 plus students
Supported by:	EU project SCI-BUS (RI 283481)

Abstract

Molecular Dynamics Simulations have become an invaluable tool when studying the dynamics behavior of proteins, lipids and other biomolecules. These simulations require a considerable amount of compute resources to be accomplished in reasonable time. Popular simulation applications such as the GROMACS package offer the possibility to make the most out of these resources. Anyhow its usage requires a steep learning curve, making it difficult for novice user to obtain scientifically meaningful results. To overcome these issues the MoSGrid portal was created, currently maintained through the EU-project SCI-BUS. It offers easy access to compute resources while ensuring high scientific standards through the implementation of high-level protocols as workflows.At the same time the users desire to solve bigger and more complex molecular simulations systems, which raise the need for not only fast, but also smarter simulation techniques. CUDA based GPU computing with GROMACS represents a viable solution.

Project Description

The MoSGrid portal was started in 2009 by multiple German partners from academia and industry involving also the PC², aiming at facilitating molecular simulations [1]. The project was funded by the BMBF and is currently maintained via the EU project SCI-BUS with support from partners from the EU project ER-Flow. The portal itself is based on Liferay and gUSE/WS-PGrade technology taking advantage of the middleware UNICORE. A key focus of our work is to enable access to modern simulation techniques such as GROMACS based molecular dynamics (MD) simulations. On the one hand the implementation of scientifically meaningful simulation protocols as workflows has been done (see Figure 1). There are a couple of typical steps a user always has to

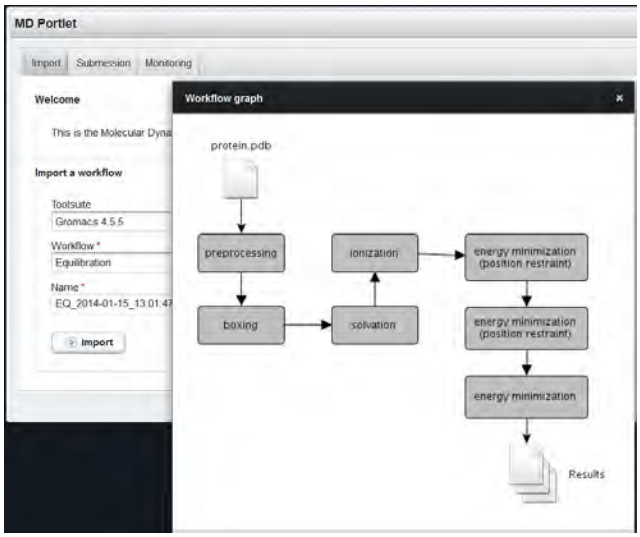

Fig. 1: The workflow selection for the molecular dynamics portlet of the MoSGrid portal is shown. A simplified workflow description is highlighted, to guide the user's selection

carry out when starting a MD simulation. The molecule of interest, e.g. a protein needs to be processed to generate a molecular topology. The molecule has to be placed into a periodic box and solvated, adding a suitable amount of counter ions. Finally a stepwise energy minimization followed by multiple equilibration steps is performed. All these typical tasks are covered by corresponding workflows accessible through portlets of the MoSGrid portal.

On the other hand performance and efficiency of the calculations themselves are of large interest. Each of the individual tasks of a workflow has different computational resource requirements. While most preparation and analysis tools of GROMACS demand only a small amount of resources, in the sense of CPU hours, memory and GPU access, the main application `mdrun` represents a special case. It offers hardware specific routines, e.g. taking advantage of SSE to speed up calculation.

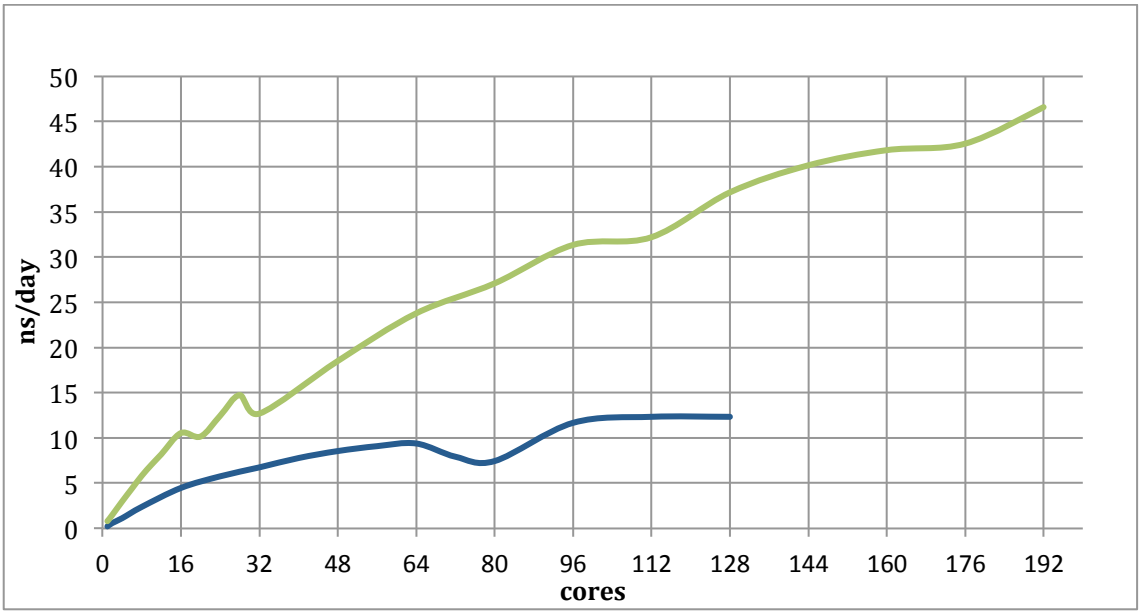

Fig. 2: The performance of GROMACS for the new OCuLUS system (green) is shown as function of cores, compared to older data from the ARMINIUS system (blue). The scaling improved not only comparing the different hardware generations of the compute clusters, but also regarding the algorithmic development of GROMACS

Furthermore it is fully MPI enabled and allows threading on multicore CPU's. With the latest versions (4.5+) GROMACS routinely supports CUDA based GPU computing. All these features offer a plentitude of possibilities to not only carry out a MD simulation, but to do it fast and efficient. Normally users are mainly interested in how many nanoseconds of simulated molecules they can achieve in how much real time. As shown in Figure 2 the current version of GROMACS scales well up to hundreds of cores, just using standard settings. For this benchmark not even an optimization of the parameters of the molecular system or its simulation settings were made.

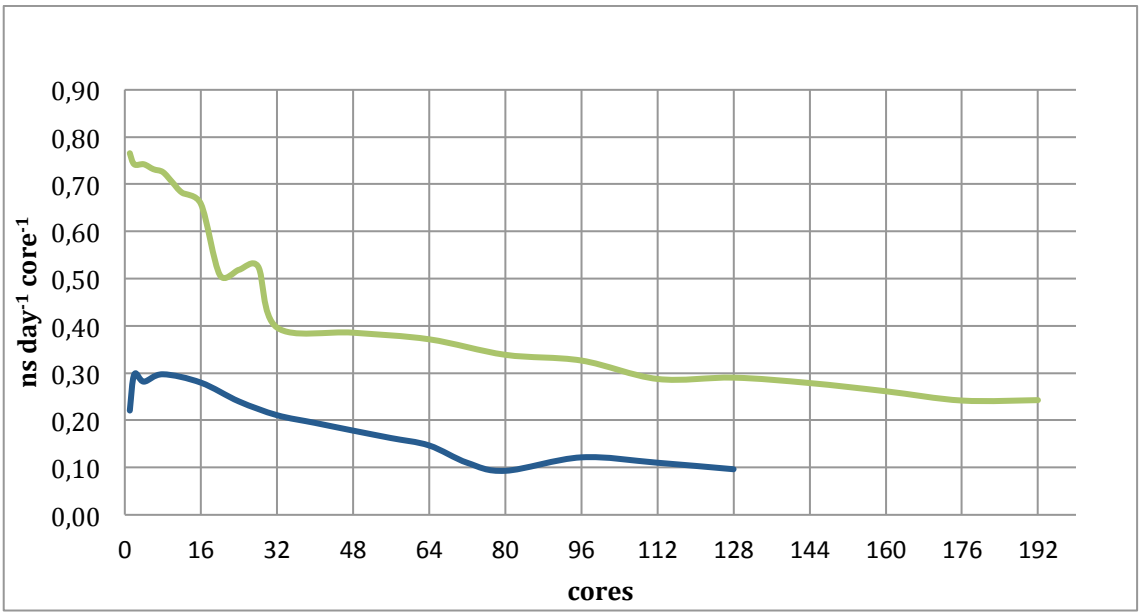

Fig. 3: A relative representation of the performance per core was chosen, to illustrate the efficiency of the simulation. The green curve corresponds to data from OCuLUS and the blue curve to older data from Arminius. For typical use cases with several similar simulations the usage of a small number of cores (1 to 16) is more efficient

Typically a further performance gain of 30 % can be expected. The little deviations from a perfect curvature e.g. around 16 and 32 cores can be contributed to the overhead of inter-CPU and inter-node communication.

Use cases from scientists daily routines can be typically split into two categories: 1. Finish the single or small set of simulation(s) as fast as possible. In this situation the usage of a high number of compute cores is advisable. 2. Create a full dataset for given scientific problem including repetitions and replicas in order to obtain proper statistics. In this case multiple very similar simulations have to be carried out. As depicted in Figure 3 it is much more efficient to use only a small number of cores per simulation as soon as several nearly identical simulations have to be made.

We are yet in the middle of evaluating GPU computing with GROMACS. Preliminary data indicates that a further performance boost in the range of 10 to 30 % can be achieved. As this kind of simulation technique requires a different simulation parameter setup, we are currently working on the reproducibility and comparability of the simulation results.

The scientific focus of our work lies on ion channels, membrane systems and protein aggregation gratefully taking advantage of the HPC resources the PC2² offers. Insight into these complex biological systems helps to generate a better understanding of diseases such as Alzheimer's dementia, achromatopsia and cancer to name only a few.

References

[1] Gesing, S., Grunzke, R., Krüger, J., Birkenheuer, G., Wewior, M., Schäfer, P., Schuller, B., Schuster, J., Herres-Pawlis, S., Breuers, S., Balasko, A., Kozlovszky, M., Szikszay Fabri, A., Packschies, L., Kacsuk, P., Blunk, D., Steinke, T., Brinkmann, A., Fels, G., Müller-Pfefferkorn, R., Jäkel, R., and Kohlbacher, O. (2012) *A Single Sign-On Infrastructure for Science Gateways on a Use Case for Structural Bioinformatics,* Journal of Grid Computing, 10(4):769-790.

[2] Grunzke, R., Breuers, S., Gesing, S., Herres-Pawlis, S., Kruse, M., Blunk, D., de la Garza, L., Packschies, L., Schäfer, P., Schärfe, C., Schlemmer, T., Steinke, T., Schuller, B., Müller-Pfefferkorn, R., Nagel, W., Atkinson, M., Krüger, J. (2013) *Standards-based Metadata Management for Molecular Simulations,* Concurrency and Computation: Practice and Experience, DOI: 10.1002/cpe.3116

5.2 Mathematics

5.2.1 Solution of inverse electromagnetic scattering problems via shape optimization

Supervisor:	Prof. Dr. Andrea Walther, University of Paderborn
Members:	Dipl. Math. Maria Schütte, University of Paderborn
Supported by:	BMBF-Project HPC-FLiS

Abstract

This project focuses on the identification of unknown objects in a predefined computational domain [1]. The non-invasive identification of hidden structures is a typical task in fields like material testing, medical diagnostics, ...
Common strategies like direct methods cannot be applied to this kind of problem due to geometric and physical reasons. Therefore radar measurements leading to an inverse scattering problem are used as possible alternative. While common strategies like FDTD (Finite Difference in Time Domain)-methods have serious problems in dealing with complex geometries, a DG (Discontinuous Galerkin)-method is applied here. In former work, we reconstructed the permittivity in each grid cell of partitioned domain. This led to a huge amount of data and we did not exploit our prior knowledge of the approximate position of the geometric object. This is the point where shape optimization comes into play. Here, the dependencies on the discretization of the domain vanishes. We derive no longer with respect to material variables but with respect to the shape of the obstacle. One ingredient is here the consideration and solution of the adjoint equations. Another one is the shape gradient, which has to be derived from the Maxwell's equations. For the computation of the numerical results, FEniCS, a tool for the solution of pdes, is used.

Project Description

The propagation of the electromagnetic fields through the computational domain is governed by the 3D time-dependent Maxwell’s equations. The whole formulation of our optimization problem is the following

$$\min_{\Gamma_{obstacle}} J(H,E,\Omega) = \frac{1}{2}\int_{t_0}^{t_f}\int_{\Gamma_{in/out}} \left\| -\alpha\sqrt{\frac{\mu}{\epsilon}}\,(n\times H) - n\times(E\times n) - F_{meas} \right\|^2 dS\,dt$$

s.t.

$$\mu\frac{\partial H}{\partial t} = -\operatorname{curl} E \qquad \text{in } \Omega$$

$$\epsilon\frac{\partial E}{\partial t} = \operatorname{curl} H - \sigma E \qquad \text{in } \Omega$$

$$n\times(H\times n) + \sqrt{\frac{\epsilon}{\mu}}\,(n\times E) = g_h\sqrt{\mu\epsilon} \qquad \text{on } \Gamma_{in/out}$$

$$n\times(H\times n) + \sqrt{\frac{\epsilon}{\mu}}\,(n\times E) = 0 \qquad \text{on } \Gamma_{non\_reflect}$$

$$n\times H = 0 \qquad \text{on } \Gamma_{obstacle}$$

where *H* describes the magnetic flux, *E* the electric flux, F_{meas} the measured data, *n* the normal vector, μ the permeability, ϵ the permittivity and σ the conductivity. The material variables may vary over the domain for different obstacles. The incoming flux is denoted by g_h. Γ_* reflect different boundaries. Depending on the factor $\alpha \in \{0,1\}$ the reflected fields E and H are taken into account or just the reflected E-field.

Especially for complex geometries the use of FDTD-methods turned out to be unsuitable [2]. One alternative is the use of a DG scheme here. DG-methods combine features of the Finite Element und Finite Volume method. One component is the element-based discretization of the domain. Since these are local methods, the Maxwell's equations in a weak formulation are required. For combining all local elementwise solutions into a global solution, an upwind flux is used. Upwind fluxes are of the form

$$(au)^* = \frac{au^- + au^+}{2} + |a|\frac{1}{2}(\hat{n}^-u^- + \hat{n}^+u^+)$$

Where *a* is a constant, *u* the flux, u^- the flux which comes from the left-hand side, and u^+ the flux from the right-hand side of the interface. For the realization on the PC, the DG-method is already provided by the Software Tool FEniCS, but the upwind fluxes as well as the behavior of the fluxes at different kind of boundaries have to be implemented.

The FEniCS project ([3],[4]) is a collection of free software and can be used as a standalone solver for partial differential equations (pde). It is a tool for development and implementation of new methods. Since it is quite near to mathematical notation, it is very user-friendly. With the extension *dolfin_adjoint*, *libadjoint* one can automatically generate and solve adjoint equations. In case of high memory requirement, checkpointing strategies are provided as well.
Our test scenario is the following: We want to reconstruct the location of a sphere, which is in this case in the middle of the computational domain (see Illustration 1).

For better illustration one part of the cube is cut off. The yellow and red arrows in Illustration 1 and 2 represent the electric resp. magnetic field.

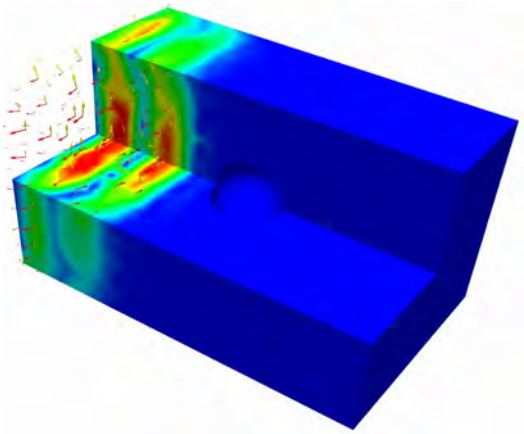

Illustration 1: Start of simulation

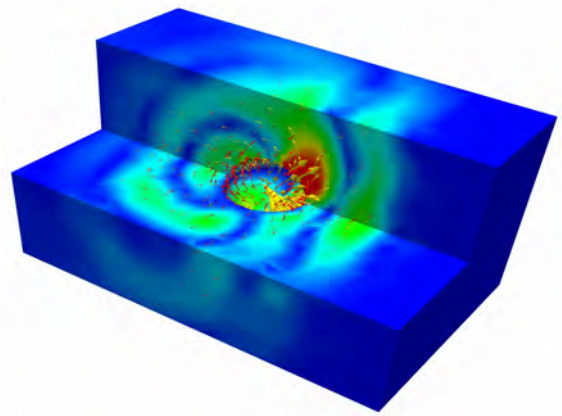

Illustration 2: Reflection at obstacle

So far the simulation as well as the adjoint computation is validated.
For the solution of the Maxwell's equations, a DG-method with test and basis functions of degree 1 is used. In Illustration 1 one can see how a sinusoidal pulse enters the domain and how it propagates in the direction of the obstacle. In Illustration 2 the reflection at the surface of the sphere is displayed. Having this simulated data und the data from the adjoint calculation, the shape gradient has to be computed. Despite having an explicit form of the gradient, several challenges in computing occur. Finding solutions to these problems are part of our current work. Having overcome these difficulties, gradient-based methods for the optimization part can be applied.

This is joint work with Stephan Schmidt from the Imperial College London.

The numerics for this kind of problems cannot be computed on an average personal computer due to their high memory requirement. A fine discretization of the inner obstacle requires a very fine mesh, which leads to a very high computational effort.

References

[1] Landmann, D.; Plettemeier, D.; Statz, C.; Hoffeins, F.; Markwardt, U.; Nagel, W.; Walther, A.; Herique, A. and Kofman, W.: Three-dimensional reconstruction of comet nucleus by optimal control of Maxwell's equations: A contribution to the experiment CONSERT onboard space mission ROSETTA. Proceedings IEEE International Radar Conference 2010, pp.1392-1396 (2010)

[2] Hesthaven, J.S. and Warburton, T.: Nodal Discontinuous Galerkin Methods: Algorithms, Analysis, and Applications, Springer (2008)

[3] http://fenicsproject.org

[4] Logg, A.; Wells, G.N. and Hake, J.: *DOLFIN: a C++/Python Finite Element Library*, Automated Solution of Differential Equations by the Finite Element Method, Volume 84 of Lecture Notes in Computational Science and Engineering, Springer, Chapter 10 (2012)

5.2.2 Performance of sparsity exploiting Algorithmic Differentiation on Multicore Architecture

Supervisor: Andrea Walther, Institute for Mathematics, University of Paderborn
Members: Kshitij Kulshreshtha, Institute for Mathematics, University of Paderborn,
Benjamin Letschert, Institute for Mathematics, University of Paderborn,
Duc Nguyen Chi, Dept. of Computer Science, Purdue University,
Assefaw Gebremedhin, Dept. of Computer Science, Pudue University,
Alex Pothen, Dept. of Computer Science, Purdue University

Abstract
Physical, engineering and industrial applications involving optimization of nonlinear functions or solution of nonlinear systems of equations require the computation of derivatives from computer programs. Over the last several decades, research and development in the field of Algorithmic Differentiation (AD) has made much progress and these techniques are now used in various software tools. However most of the work has been largely focused on differentiating functions implemented as serial codes. With increasing ubiquity of parallel computing especially multicore machines in desktop computing, there is a great need for developing AD techniques for parallel codes. Due to the structure of the applications in physics and engineering the Jacobian and Hessian matrices in these applications tend to be sparse. The subject of our work is on AD capabilities for multithreaded functions and the focus is on techniques for exploiting the sparsity available in the Jacobian and Hessian matrices using operator overloading efficiently for both runtime and memory. Using nonlinear optimization problems as test cases, we show that the algorithms involved in various steps can be adapted to multithreaded computations.

Project Description
Algorithmic Differentiation (AD) techniques are classified by the two approaches for computing derivatives of computer programs, i.e., source transformation and operator overloading [2]. Derivative calculation via AD for parallel codes has been considered previously [4-9], but the focus has largely been on source transformation techniques. This is mainly because having a compiler at hand during the source transformation makes it relatively easy to detect parallel regions using either MPI function calls or OpenMP directives. Detecting parallel sections of code for an operator overloading tool such as ADOL-C [3] is much harder since the corresponding parallelization function calls or directives are difficult or even impossible to detect at runtime. For that reason, the operator overloading tool ADOL-C uses its own wrapper functions for handling functions that are parallelized with MPI. For parallel function evaluations using OpenMP, ADOL-C uses the concept of nested taping to take advantage of the parallelization provided by the simulation for

the derivative calculation as well. Now we extend this approach to exploit sparsity in parallel as well in [1].

By exploiting sparsity we mean avoiding computing with zeroes in order to reduce the runtime and memory costs, often drastically. We exploit sparsity for both Jacobian and Hessian computations. In the serial setting there is and established scheme for efficient computation of Jacobians and Hessians involving four major steps, namely automatic sparsity detection, seed matrix determination using graph coloring, compressed matrix computation and recovery.

Here we shall assume that the user provides a parallel program using OpenMP as sketched in Fig.1. Here after an initialization phase, calculations are performed in parallel followed by a possible finalization phase performed by a single dedicated thread. The way ADOL-C currently differentiates such a parallel code using OpenMP is sketched in Fig. 2. Here the *tracing* part represents essentially the parallel function evaluation provided by the user using ADOL-C's wrapper data types and function calls. Then ADOL-C performs a parallel derivative calculation using the same OpenMP strategy. In order to compute sparse derivatives efficiently we incorporate the four steps mentioned above with this parallelization strategy. This is sketched in Fig. 3.

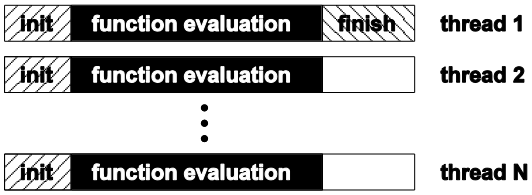

Fig. 1: Function evaluation of an OpenMP parallel code

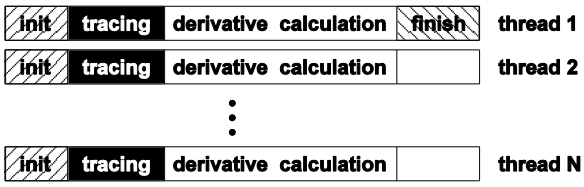

Fig 2: Derivative calculation with ADOL-C for an OpenMP parallel code

We performed numerical experiments for the runtime using a scalable PDE constrained optimization problem from [10] that has been implemented in C++ serially. This discrete problem has n variables and m constraints. For a given grid-size $\tilde{n}$ the number of variables is $n = \tilde{n}^2 + (\tilde{n}+2)^2$ and the number of constraints is $m = \tilde{n}^2$.

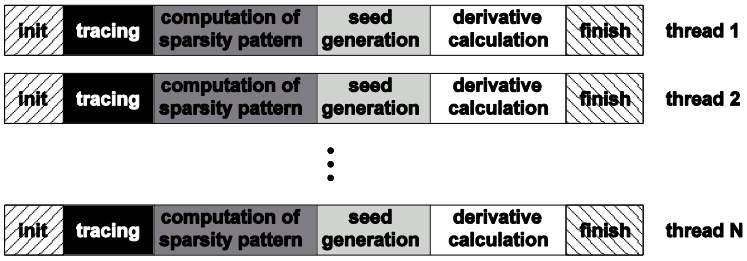

Fig 3: Derivative calculation with ADOL-C for an OpenMP parallel code exploiting sparsity

$\tilde{n}$	m	n	$n+m$	nnz (∇c)	nnz $(\nabla^2 L)$
600	360 000	722 404	1 082 404	2 160 000	2 880 000
800	640 000	1 283 204	1 923 204	3 840 000	5 120 000
1 000	1 000 000	2 004 004	3 004 004	6 000 000	8 000 000

Table 1: Summary of problem sizes used in the experiments

The problem sizes are summarized in Table 1. The number of non-zeroes in the Jacobian and Hessian is considerably less than the full dense size of these matrices $m \times n$ and $n \times n$ respectively. We chose a straightforward parallelization strategy of distributing the computation of the single target function and m constraints equally on the available threads.

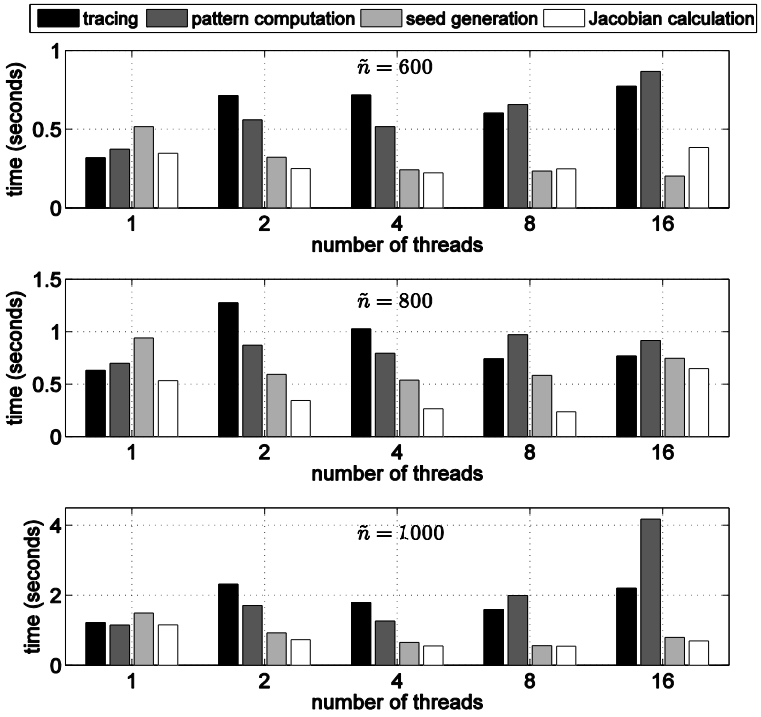

Fig 4: Timing results for multithreaded Jacobian computations

Runtimes were measured using GCC version 4.4 compiler and its OpenMP implementation on the PC^2 ARMINIUS system. Fig. 4 shows the runtimes for the multithreaded Jacobian computation exploiting sparsity and Fig. 5 shows the runtimes for the multithreaded hessian computation exploiting sparsity. The figures show each of the four steps involved separately.

A few observations on the trend in Fig. 4 and 5 are summarized below.

- *Tracing:* This phase scales poorly with the number of threads and this is significant especially for the Jacobian case. A likely reason is that this is memory intensive. For the Hessian case this is a small fraction of the total runtime and thus less important.
- *Sparsity pattern detection:* In the Jacobian case this does not scale well, however for the Hessian case it scales fairly well. A plausible reason for poor scalability in the Jacobian case is that the runtime is too short to be impacted by the use of more threads.

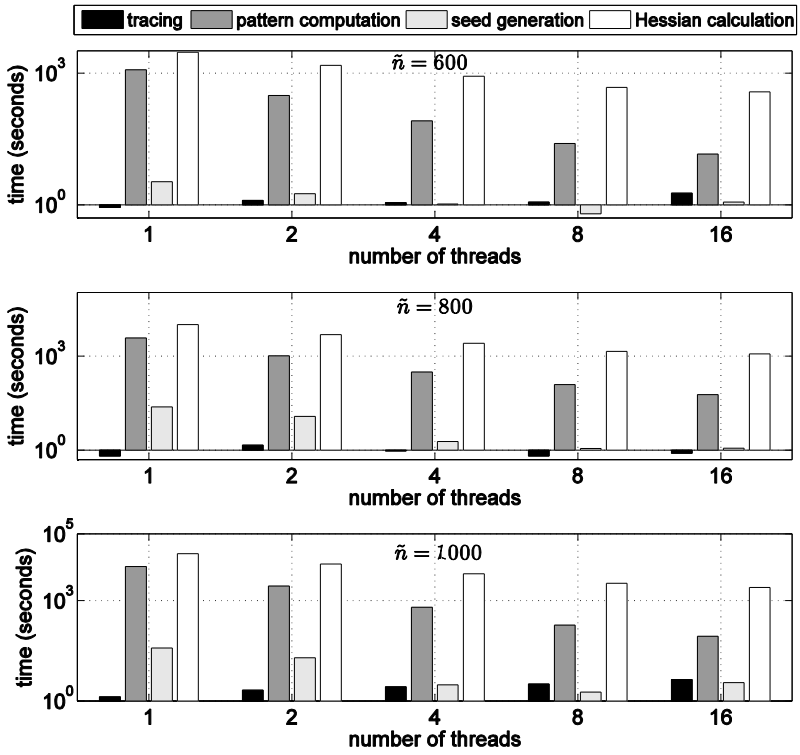

Fig 5: Timing results for multithreaded Hessian computation

- *Seed generation:* This includes the time for graph coloring and seed matrix construction. This phase scales relatively well. Further the number of colors used by the coloring heuristic turned out to be optimal or nearly optimal.
- *Derivative computation:* This phase scales modestly for both Jacobian and Hessian computation.
- *Comparison with dense computation:* Runtimes for the Jacobian computation without exploiting sparsity are 3 to 4 orders of magnitude slower, requiring hours instead of seconds. For large problem sizes the dense computation fails due to excessive memory requirements.

Future work will require an exploration for ways to improve scalability. In particular, more investigation is needed to improve the scalability of the sparsity pattern detection algorithm and the tracing phase. Another direction of future work is the

development of a parallel optimizer that could take advantage of the distributed function and derivative evaluation.

References

[1] Letschert, B.; Kulshreshtha, K.; Walther, A.; Nguyen, D.; Gebremedhin, A. and Pothen, A.: Exploiting sparsity in automatic differentiation on multicore architectures. In S. Forth, P. Hovland, E. Phipps, J. Utke, and A. Walther, editors, Recent Advances in Algorithmic Differentiation, volume 87 of Lecture Notes in Computational Science and Engineering, pages 151–162. Springer, 2012. Proceedings of the 6th International Conference on Automatic Differentiation, Fort Collins, CO, USA.

[2] Walther, A. and Griewank, A.: Evaluating Derivatives: Principles and Techniques of Algorithmic Differentiation, Second Edition, SIAM (2008).

[3] Walther. A. and Griewank, A.: Getting started with ADOL-C. In: U. Naumann, O. Schenk (eds.) Combinatorial Scientific Computing. Chapman-Hall (2012). See also http://www.coin-or.org/projects/ADOL-C.xml

[4] Conforti, D.; Luca, L.D.; Grandinetti, L. and Musmanno, R.: A parallel implementation of automatic differentiation for partially separable functions using PVM. Parallel Computing 22, 643–656 (1996).

[5] Fischer, H.: Automatic differentiation: Parallel computation of function, gradient and Hessian matrix. Parallel Computing 13, 101–110 (1990).

[6] Maurer, H. and Mittelmann, H.: Optimization techniques for solving elliptic control problems with control and state constraints. II: Distributed control. Comput. Optim. Appl. **18**(2), 141–160 (2001).

[7] Bücker, H.M.; Rasch, A. and Vehreschild, A.: Automatic generation of parallel code for Hessian computations. In: M.S. Mueller, B.M. Chapman, B.R. de Supinski, A.D. Malony, M. Voss (eds.) OpenMP Shared Memory Parallel Programming, Proceedings of the International Workshops IWOMP 2005 and IWOMP 2006, Eugene, OR, USA, June 1–4, 2005, and Reims, France, June 12–15, 2006, *Lecture Notes in Computer Science*, vol. 4315, pp. 372–381. Springer, Berlin / Heidelberg (2008). DOI 10.1007/978-3-540-68555-5_30.

[8] Bücker, H.M.; Rasch, A. and Wolf, A.: A class of OpenMP applications involving nested parallelism. In: Proceedings of the 19th ACM Symposium on Applied Computing, Nicosia, Cyprus, March 14–17, 2004, vol. 1, pp. 220–224. ACM Press, New York (2004). DOI 10.1145/967900.967948. URL http://doi.acm.org/10.1145/967900.967948.

[9] Utke, J.; Hascoët, L.; Heimbach, P.; Hill, C.; Hovland, P. and Naumann, U.: Toward adjoinable MPI. In: Proceedings of the 10th IEEE International Workshop on Parallel and Distributed Scientific and Engineering, PDSEC-09 (2009). DOI http://doi.ieeecomputersociety.org/10.1109/IPDPS.2009.5161165.

5.3 Mechanical Engineering

5.3.1 Marangoni convection at deformable single rising droplets – a numerical investigation of fluid dynamics and mass transfer

Supervisor:	Prof. Dr.-Ing. habil. Eugeny Kenig, University of Paderborn
Members:	Dipl.-Ing. Roland Engberg, University of Paderborn

Abstract

Concentration gradients due to mass transfer at rising droplets can lead to a variation of the interfacial tension and induce Marangoni convection. As a result, mass transfer is intensified and the rise behavior of the droplet is affected. To investigate these phenomena, a CFD-code was developed and implemented in the CFD-toolbox OpenFOAM®. The code can handle the inherently three-dimensional Marangoni convection. Moreover, it takes the coupling of momentum and mass transfer as well as interface deformation into account. In this project, full three-dimensional simulations were performed and validated.

Project Description

The Liquid/liquid extraction is one of the most important unit operations in chemical engineering. For the design of such processes, an exact knowledge of fluid dynamics and mass transfer characteristics of rising droplets are essential. In particular, the complex interaction of various transport phenomena has to be taken into account. Mass transfer, for instance, can lead to a tangential variation of interfacial tension which may cause Marangoni convection. This effect can affect the fluid dynamics of rising droplets considerably; in general, the rise velocity is reduced (cf. Wegener et al. [1]).

In addition to experimental investigations, numerical simulations contribute to the understanding of the complex transport phenomena at moving boundaries to an increasing degree. In this work, the impact of Marangoni convection on mass transfer and fluid dynamics of single droplets in liquid-liquid-systems was studied with CFD simulations. For this purpose, we developed a CFD code which employs the classical level set method to capture the moving interface. A typical problem of this method is volume (or mass) conservation – usually, the droplet loses volume in the course of a simulation. Therefore, two recently published methods [2,3] were implemented which ensure an exact conservation of the initial droplet volume. The code was completed with a concentration dependent interfacial tension and a model for mass transfer which takes the concentration jump at the interface into account. It was implemented in the open source CFD toolbox OpenFOAM®.

To the best of our knowledge, no *three-dimensional* simulations of mass transfer with Marangoni convection at *deformable* droplets in liquid-liquid-systems have been published before. Wang et al. [4] performed axially symmetric two-dimensional simulations of deformable droplets which fall short of the inherent three-dimensional character of Marangoni convection. In contrast, Wegener et al. [1] investigated Marangoni convection with three-dimensional simulations of rigid spherical droplets.
In this work, full three-dimensional simulations of deformable toluene droplets with an initial diameter of 2 mm rising in water were performed. The concentration of the transferred component acetone was varied.

Fig. 1 illustrates the effect of Marangoni convection qualitatively with slices through the center of the droplet parallel to the rise path. In both figures, the streamlines and the concentration profile are shown for simulations with an initial acetone concentration of 3.7 g/L. In the simulation shown on the left, a constant interfacial tension was assumed, while on the right side, Marangoni effects were taken into account. The streamlines of the left figure depict the internal ciculations observed in droplets without Marangoni convection. Accordingly, the concentration profiles have characteristic toroidal shape. In contrast, the streamlines of the figure on the right are extremely irregular. Reflecting the chaotic nature of Marangoni convection, the strong internal mixing due to Marangoni effects is evident in the concentration profile.

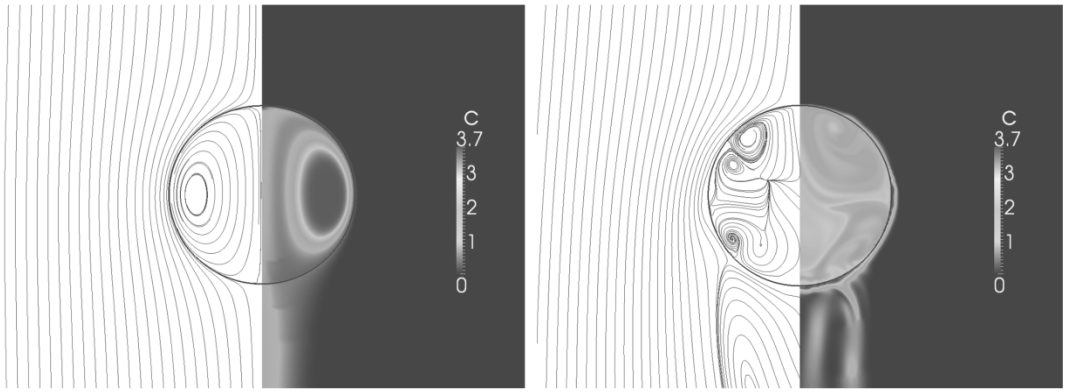

Fig 1: Streamlines (left) and concentration profiles of a simulation without (left) and with Marangoni convection (right) after a rise time of 0.45 s. The initial concentration of acetone was 3.7 g/L in both cases

Furthermore, the results for the transient rise velocity, mass transfer and droplet trajectories are in good qualitative, and in many cases also quantitative, agreement with the experimental data of Wegener et al. [1].

The results of this project have been presented at national [5,6] and international conferences [7]. Moreover, a German paper was recently accepted [8] and an English paper was submitted to the International Journal of Heat and Mass Transfer.
Future work will be focused on phenomena with stronger deformation, e.g. larger droplets and coalescence of two droplets. These phenomena require even more computational power than the small droplets currently investigated.

Resource Usage

CFD simulations of moving interfaces require significant computational power. Simulations are run on several cores (typically 12 to 48) and usually take several weeks or even month. Consequently, we use the OCULUS cluster every day which is, therefore, an essential basis to our work. We use the open source CFD-code OpenFOAM and, for different projects, the commercial CFD-code Star-CCM.

References

[1] Wegener, M.; Grüning, J.; Stüber, J.; Paschedag, A.R. and Kraume, M.: Transient rise velocity and mass transfer of a single drop with interfacial instabilities-experimental investigations. Chem. Eng. Sci. 62 (2007), 2967-2978.

[2] Groß, S.: Numerical methods for three-dimensional incompressible two-phase flow problems. Dissertation, RWTH Aachen, 2008.

[3] Hartmann, D.; Meinke, M. and Schröder, W.: The constrained reinitialization equation for level set methods. J. Comput. Phys. 229 (2010), 1514-1535.

[4] Wang, J.F.; Wang, Z.H.; Lu, P.; Yang, C. and Mao, Z.S.: Numerical simulation of the Marangoni effect on transient mass transfer from single moving deformable drops. AIChE Journal 57 (2011), 2670-2683.

[5] Engberg, R.F. and Kenig, E.Y.: Modellierung und Simulation von Stofftransport und Marangonikonvektion an verformbaren Einzeltropfen. In: ProcessNet-Jahrestreffen der Fachgruppen Agglomerations- und Schüttguttechnik und Computational Fluid Dynamics, Weimar, 2013.

[6] Engberg, R.F. and Kenig, E.Y.: Marangonikonvektion an Einzeltropfen - eine numerische Untersuchung zu Fluiddynamik und Stofftransport. In: Jahrestreffen der Fachgemeinschaft Fluiddynamik und Trenntechnik, Würzburg, 2013. Chemie Ingenieur Technik 85, (2013), 1389

[7] Engberg, R.F. and Kenig, E.Y.: Marangoni convection at deformable single rising droplets - a numerical investigation of fluid dynamics and mass transfer. In: 2012 AIChE Annual Meeting, Pittsburgh, 2012.

[8] Engberg, R.F.; Wegener, M. and Kenig, E.Y.: Numerische Simulation der konzentrationsinduzierten Marangonikonvektion an Einzeltropfen mit verformbarer Phasengrenze. Chem. Ing. Tech. 86 (2014),1-11.

5.3.2 Numerical Simulation of Fully-Filled Conveying Elements

Supervisor:	Prof. Dr.-Ing. V. Schöppner, University of Paderborn
Members:	Dipl.-Wirt.-Ing. T. Herken, University of Paderborn
	Dipl.-Inform. N. Kretzschmar, University of Paderborn
Supported by:	Verein zur Förderung der Kunststofftechnologie e.V.

Abstract

The current project aims to simulate the different processing stages of a co-rotating twin screw extruder in a fast and precise manner. In that way the efforts of costly test series can be minimized. SIGMA [1], a software that was initiated by the University of Paderborn in 1992, is able to quickly map important process values, e.g. temperature development of a thermoplastic, based on analytical equations. In order to simulate more accurately, a spatially resolved consideration of the process is required. For this purpose, the Black Box module Extrud3D was developed and combined with SIGMA.

The module basically uses FeatFlow [2], a scientific code that resolves the Navier–Stokes equations in a robust, quick and exact manner. The numerical calculation of screw elements requires an extremely high computing performance because each sub-process has to be considered spatially and temporally resolved. For the efficient use and further development of this system, high-performance computing (HPC) is indispensable.

Project Description

SIGMA is a special simulation software that simulates different process stages of the extrusion and processing of plastics. SIGMA mainly uses one-dimensional balance equations. Therefore it can compute the relevant process values efficiently and, above all, quickly. However, from the SIGMA user's perspective a closer look at the process values is desirable. This can be the case when, for example, trying to estimate local overheating of the material.

For this reason the current project aims to enable the user to regard a sub-process spatially and temporally resolved, starting with fully-filled conveying elements. Calculations of this kind can be made with CFD (Computational Fluid Dynamics, flow simulation). IANUS Simulation GmbH will join KTP for the integration into SIGMA. IANUS is a spinoff of the TU Dortmund and works exclusively with the FeatFlow software package (developed by workgroup of Prof. Turek, Institute for applied Mathematics and Numerics, TU Dortmund).

FeatFlow basically solves the Navier–Stokes equations (first and second equation; torque balance and incompressibility constraint) extended by energy conservation (third equation). The complete, fully coupled model for velocity u, pressure p, temperature Q and stress tensor t reads as follows:

$$\rho\frac{\partial \mathbf{u}}{\partial t} + \rho(\nabla \mathbf{u})\mathbf{u} = -\nabla p + 2\eta_s \Delta \mathbf{u} + \frac{\eta_p}{\Lambda}\nabla \cdot \boldsymbol{\tau}$$

$$\nabla \cdot \mathbf{u} = 0$$

$$\frac{\partial \Theta}{\partial t} + (\nabla \Theta)\mathbf{u} = k\ \nabla^2 \Theta + \boldsymbol{\tau} : \mathbf{D}$$

The central mathematical methods for the numerical treatment of flow problems are based on LBB-stable finite element methods (Q2/P1 approach with quadratic velocity and linear pressure elements). To further reduce computing performance, the calculations were parallelized.

FeatFlow has been in scientific and industrial use for many years (via IANUS) and is considered a reliable software package. In comparison to other commercial codes (CFX, Fluent, Polyflow, etc.) the cooperation between KTP and IANUS offers the opportunity to integrate both codes, SIGMA and FeatFlow, in a way that will lead to a faster and more user-friendly package. Figure 1 is a schematic illustration of the proposed integration.

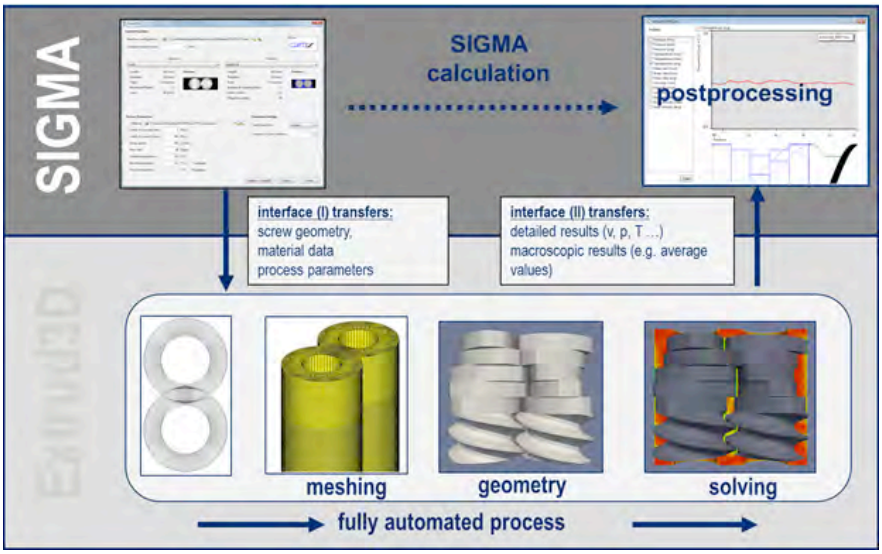

Fig.1: Schematical depiction of the planned integration of Extrud3D in SIGMA

The coupling 1D-3D will gradually be realized:

1. Transfer of geometry, material data and process parameters from SIGMA to Extrud3D
2. Extrud3D automatically processes a 2D coarse mesh and a 3D fine mesh. It also compiles a mathematical description of moving geometry parts
3. Numerical solution to the time-dependent 3D problems
4. Transfer of the detailed results (e.g. as sectional representations of velocity, pressure and temperature results) or in compact form

After the successful simulation the results (see Figure 2) will be returned to SIGMA as a 1D result. The post-processing tool Paraview supports the user to examine the results in 3D.

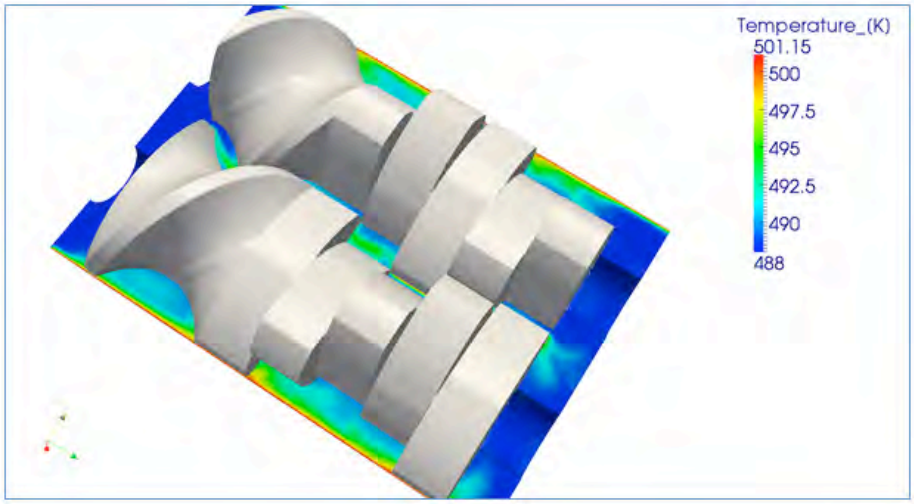

Fig. 2: Numerically calculated conveying elements

In the last 2 years the Extrud3D software has been successfully upgraded with new program features.
Because of this, there is now the possibility, to simulate double- and triple-flighted kneading elements, aside from the conveying elements. These can be simulated with conveying, reconveying and neutral characters. By the interlinking of two different elements, the transition of the flow can be visualized and calculated within the simulation. Furthermore, an RTD (residence time distribution) module was integrated in the numeric calculation process of Extrud3D. This results in the possibility of a visualization of the flow procedures within the kneading and conveying elements. On the other hand, the spreading of the tracer can be used as a basis for the calculation of average dwell times and dwell time distribution. As a result of this, the mixture of the separate elements can be characterized. Apart from this, the implementation of new geometries, that excel the complexity of the Erdmenger-Elements, is in the planning stage. Specifically Zahn Misch-, Screw Mixing Element, Shouldered Kneading Block should be integrated. Implicated equations for the surface geometry can be used for the mathematical description, these can be developed in combination with the KTP. Furthermore the import of additional special elements is prepared. The possibility is tested, e.g. to process geometry-triangulations, for the case, that a mathematical description is not possible using simple implicit or explicit equations. Additionally, the possibility of simulations with three conjoined elements should be given. Also, the implemented function for the calculation of residence time distribution (RTD) will be developed further in the next step of the project. This way, the examination of mixtures can be improved. The user will be able to choose from two speed-zones from which the spreading of the tracer particles can be calculated. The mix-RTD function continuously monitors and records the position of the particles. In the following, statistic methods are used to calculate the local and global mixing

quality of the elements. For the user there is the possibility, to graphically depict the mixing quality using different colored particles.

Resource Usage

The FEM software package FeatFlow was developed for Linux systems and needs at least three processor cores for simulation. Therefore its use on a conventional workstation computer, which can run SIGMA, is hard to realize. In this case KTP utilizes the services of the PC², more specifically of the Arminius Cluster. By using 1 or 2 nodes (12 or 24 CPU cores with 36 or 72 GB RAM) the user can expect results after 14 hours of computing time. The use of the Computer Center Software (CCS) brings further benefits. It enables a more convenient resource reservation within the Arminius Cluster. The shortened computing time, achieved by parallelization, as well as the quick implementation into our system lead to an effective further development of the software.

References

[1] Potente, H. and Thümen, A.: Method for the Optimisation of Screw Elements for Tightly Intermeshing, Co-rotating Twin Screw Extruders, International Polymer Processing (February 2006), pp. 149-154.

[2] Turek, S.: Efficient Solvers for Incompressible Flow Problems: An Algorithmic and Computational Approach.

5.3.3 *Thermodynamics of Droplets*

Supervisor:	Stefan Eckelsbach, University of Paderborn
Members:	René Chatwell, University of Paderborn
	Gabriela Guevara-Carrión, University of Paderborn
	Matthias Heinen, University of Paderborn
	Marco Hülsmann, University of Paderborn
	Tatjana Janzen, University of Paderborn
	Andreas Köster, University of Paderborn
	Svetlana Miroshnichenko, University of Paderborn
	Gábor Rutkai, University of Paderborn
	Thorsten Windmann, University of Paderborn
Supported by:	Lehrstuhl für Thermodynamik und Energietechnik, University of Paderborn

Abstract

For the description of droplet dynamics, the knowledge of thermodynamic properties is crucial. Especially for mixtures and extreme ambient conditions the experimental database shows significant gaps. Molecular simulation is based on a sound physical foundation and is therefore well suited for the prediction of such properties. Also the simulation of binary or higher mixtures is conceptually straightforward, needing only one additional parameter per binary combination for the unlike dispersion to ensure a high precision. Nitrogen, oxygen, acetone and their mixtures were studied with a focus on the extended critical region in association with the Sonderforschungsbereich-Transregio 75.

A new force field model for acetone was developed and parameterized on the basis of quantum chemical calculations and experimental data for the saturated liquid density as well as the vapor pressure. This model was combined with molecular models for nitrogen and oxygen from preceding work of our group [1]. The unlike dispersive interaction parameter were adjusted for both pairs with acetone. Two different molecular simulation codes [2, 3] were used to determine various thermodynamic properties in the homogeneous fluid region, transport data and interfacial properties. The simulation results were compared with experimental data and equation of states, where these were available. In general, a good agreement was achieved.

Project Description

Droplets play a crucial role in many fields of nature and technology. A fundamental understanding of droplet dynamics is essential for the optimization of technical systems or the better prediction of natural phenomena. Particularly in energy technology, many of these processes occur under extreme conditions of temperature

or pressure. Such processes are actively used by the industry, although striking gaps remain in their essential understanding of droplet dynamics. Even for its description, the knowledge of thermodynamic properties is crucial. At the same time, thermodynamic data for most technically interesting systems are still scarce or even unavailable despite the immense experimental effort that was invested over the last century. This especially applies for mixtures of two or more components and systems under extreme conditions.

In contrast to phenomenological methods, molecular simulation is based on a sound physical foundation and is therefore well suited for the prediction of such properties under extreme ambient conditions. The aim of this project is to close the gap for the three substances nitrogen, oxygen, acetone and their mixtures, using the excellent predictive power of molecular modelling and simulation. Thereby, the simulations were focused on high temperatures close to the critical point of acetone which was considered as a model fuel.

The vapor-liquid equilibrium (VLE) of the binary mixture nitrogen + acetone was studied by molecular simulation with a focus on the extended critical region. For this purpose the simulation tool *ms*2 [2] was used. First, a force field model for acetone was developed and parameterized on the basis of quantum chemical calculations and experimental data for the saturated liquid density as well as the vapor pressure. Compared with molecular models from the literature, the new model is significantly superior. The present acetone model was extensively validated with the fundamental equation of state (EOS) by Lemmon and Span [4] and with experimental pure fluid data from the literature with respect to the heat of vaporization, various properties in the homogeneous fluid region (density, isobaric heat capacity, enthalpy, speed of sound), second virial coefficient, self-diffusion coefficient, shear viscosity and thermal conductivity.

Combining this acetone model with molecular models for nitrogen and for oxygen from prior work [1], the unlike dispersive interaction between nitrogen and acetone as well as oxygen and acetone was adjusted. Based on these mixture models, the VLE of nitrogen + acetone and oxygen + acetone was determined by molecular simulation using the Grand Equilibrium method [5] and assessed with experimental data that was partly measured in our own lab at the University of Paderborn [6].

Due to the scarcity of experimental data at high pressures in the literature, simulations with the molecular models discussed before were carried out for nitrogen + acetone for the three isotherms 400, 450 and 480 K. The data points at 450 K are shown in Fig. 1 as an example. It can be seen that the simulation data and the data from experiment agree well in the region of small mole nitrogen fractions x_{N2}. However, with rising x_{N2}, particularly in the near critical region, the molecular model overestimates the vapor pressure of the mixture. Additional results were presented by Windmann et al. [6].

Based on the previously described VLE simulations, a closer look was taken at the interfacial region, especially with respect to the surface tension. For this purpose, the highly parallel molecular dynamics simulation tool *ls*1 [3] was used. Simulations were carried out considering the pure substances as well as the mixtures nitrogen + oxygen and nitrogen + acetone. Oxygen + acetone will be studied in the near future.

The systems were set up with a liquid phase surrounded by a vapor phase. The two-phase system thus forms two interfaces, where a direct calculation of the surface tension can be done. After an initial equilibration period, the density profile over the length of the simulation volume remained constant, indicating an equilibrated system.

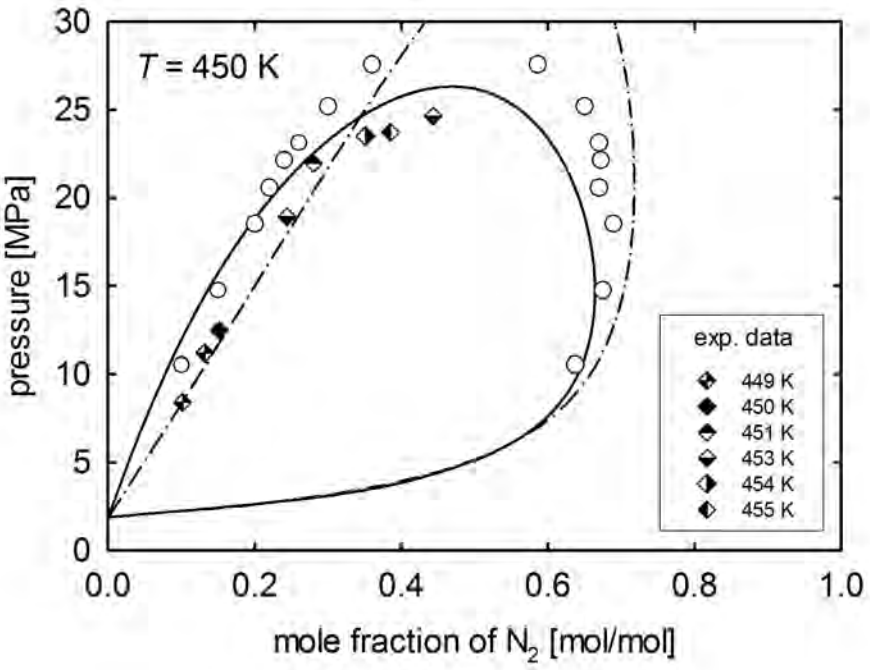

Fig. 1: Vapor-liquid equilibrium of nitrogen + acetone at around 450 K: ○ simulation data; ◊ experimental data; Peng-Robinson EOS with different mixing rules: --- Huron-Vidal (l_{ij} = -369.9, l_{ji} = 2200), -·- quadratic (k_{ij} = 0.0670)

Due to the inhomogeneity of the simulated systems, the long range correction of Janeček [7] was adapted [8]. The surface tension was calculated following the virial approach according to Irving and Kirkwood [9]

$$\gamma = \frac{1}{2A}\left(2\Pi_{zz} - \left(\Pi_{xx} + \Pi_{yy}\right)\right),$$

where *A* is the area of the interface and Π is the virial tensor, which is defined as

$$\Pi_{\alpha\beta} = \left\langle \frac{1}{2}\sum_{i=1}^{N}\sum_{j=1}^{N} r_{ij}^{\alpha} f_{ij}^{\beta} \right\rangle .$$

The upper indices α and β represent the x-, y- or z-directions of the distance vector rij and the force vector fij between the molecules i and j.

For the pure substances nitrogen and oxygen and their mixture, the surface tension is plotted in Fig. 2. The simulations show an excellent agreement with the experimental data and data calculated from an accurate equation of state [10].

In the future, further research will be carried out regarding the surface tension of the system oxygen + acetone and the ternary mixture of the considered components.

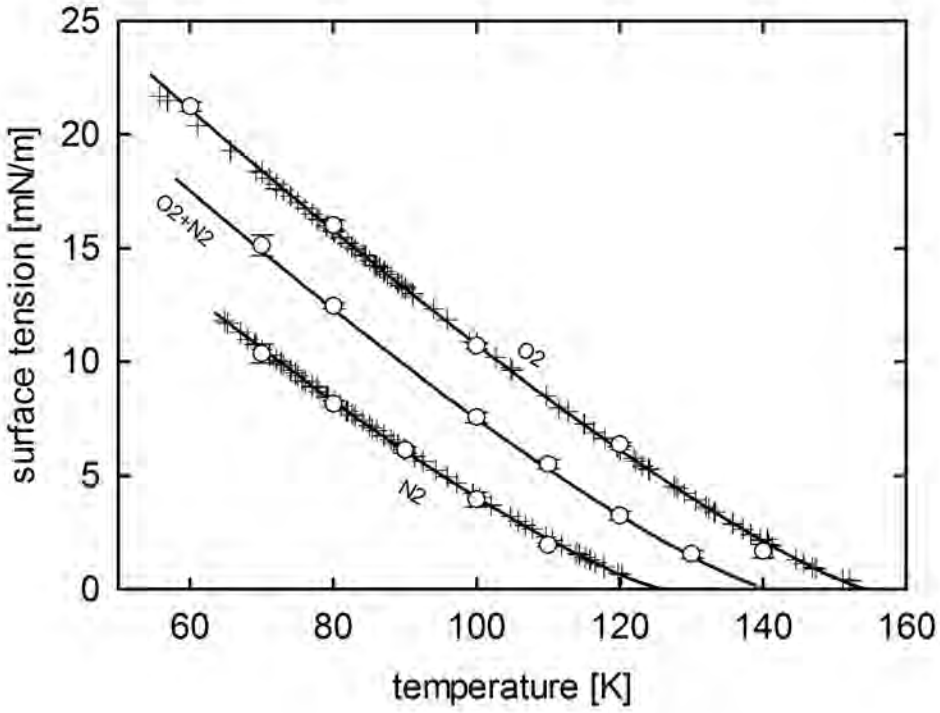

Fig. 2: Surface tension of nitrogen and oxygen and their mixture:○ simulation data; + experimental data; — equation of state [10]

References

[1] Vrabec, J.; Stoll, J.; Hasse, H.: *J. Phys. Chem. B* 105, 12126-12133 (2001).

[2] Deublein, S.; Eckl, B.; Stoll, J.; Lishchuk, S. V.; Guevara-Carrion, G.; Glass, C. W.; Merker, T.; Bernreuther, M.; Hasse, H. and Vrabec, J.: *Comp. Phys. Commun.* 182: 2350-2367 (2011).

[3] Buchholz, M.; Bungartz, H.-J. and Vrabec, J.: *J. Comp. Sci.* 2: 124-129 (2011).

[4] Lemmon, E. W. and Span, R. *J. Chem. Eng. Data* 51: 785-850 (2006).

[5] Vrabec, J. and Hasse, H.: *Mol. Phys.* 100: 3375-3383 (2002).

[6] Windmann, T.; Linnemann, M. and Vrabec, J. *J. Chem. Eng. Data* 59: 28-38 (2014).

[7] Janeček, J.: *J. Phys. Chem. B* 110: 6264-6269 (2006).

[8] Werth, S.; Rutkai, G.; Vrabec, J.; Horsch, M. and Hasse, H.: *Molecular Physics* (2013), DOI: 10.1080/00268976.2013.861086.

[9] Irving, J. H. and Kirkwood, J. G. *J. Chem. Phys.* 18: 817-829 (1950).

[10] Lemmon, E. W.; Penoncello, S. G.: *Adv. Cryo. Eng.* 39: 1927-1934 (1994).

5.3.4 Crack growth in functionally graded materials and structures

Supervisor:	Prof. Dr. rer. nat. Maria Specovius-Neugebauer, University of Kassel
	Prof. Dr.-Ing. Hans Albert Richard, University of Paderborn
Members:	Dr. rer. nat. Martin Steigemann, University of Kassel
	Dipl.-Ing. Britta Schramm, University of Paderborn
Supported by:	Sonderforschungsbereich TR/TRR30, DFG

Abstract

This work is part of the project “Crack growth in functionally graded materials and structures” within the collaborate research center SFB TR/TRR 30 kindly supported by the DFG. The main purpose of the project is the prediction and simulation of crack propagation processes especially in inhomogeneous materials.

Cracks in structures and components do not only limit the lifetime but may also cause catastrophic failures harming men as well as environment. In the last decades, many efforts have been taken to understand crack growth and its predictability. But the precise simulation of crack growth is still quite a hard problem. Defects or cracks in structural components can be formed by many different influences and even at the production process already. Especially for aspects of safety an essential question is, can a crack be detected and if not, how will this crack grow till the next service? Moreover, can it become critical? New developments in material sciences and the growing application of anisotropic and also functionally graded materials in order to fulfill the more and more specialized demands on structural components in modern engineering has given an impulse to the study of fracture mechanics in such structures.

From a physical point of view the energy principle, already formulated by Griffith in 1921, can be used for the prediction of quasi-static crack propagation also in anisotropic and inhomogeneous materials: A crack can only grow, if there is enough energy to break the material and form a new crack front [3].

Based on the combined approach of mathematical modeling of the energy principle, experimental investigations and numerical simulations the main focus of this project is to get a deeper understanding of fracture processes in inhomogeneous (functionally graded) materials (FGMs).

Project Description

The point of departure for modeling crack propagation in this project was a mathematical asymptotic representation for the change of energy [1]: if a crack in a plane two-dimensional linear elastic structure grows along a small elongation of length h directed at an angle ϑ the change of total energy can be calculated to

$$\Delta\Pi = \Delta\mathbf{S} + \Delta\mathbf{U} = 2\gamma(\vartheta)h - \frac{1}{2}\left(\sum_{i,j=1}^{2} K_i M_{i,j}(\vartheta) K_j\right) h + \dots$$

Here, $\mathrm{K_i}$ are the stress intensity factors (SIFs) arising from the asymptotic representation of the displacement field near the crack tip, and $\mathrm{M_{i,j}}(\vartheta)$ are so-called local characteristics, depending on the material properties and the angle of the crack elongation. The term $\Delta\mathbf{S} = 2\gamma(\vartheta)\mathrm{h}$ represents the surface energy or fracture toughness in direction ϑ. Following the energy principle, a crack can only grow, if the potential energy $\Delta\mathbf{U}$ can overcome the fracture toughness and the change of total energy is negative for some angle ϑ. The crack will grow to the direction of maximal energy release. As part of this project, this representation was generalized to inhomogeneous (functionally graded) materials [5][7]. With a formula for the energy release rate at hand, propagation of a crack can be simulated step-wise [6][10]. In each simulation step, the direction of the crack can be determined, if all the SIFs $\mathrm{K_i}$ and the quantities $\mathrm{M_{i,j}}(\vartheta)$ can be computed numerically. For this reason, a framework for the numerical simulation of crack growth was developed, called “MCrack2D”. MCrack2D is a pure research code based on finite elements with the intention to realize an exact-as-possible transfer of analytical models to numerics in order to test and improve theoretical ideas and make them finally applicable to real-world problems.

For high-accurate simulations MCrack2D uses goal-oriented adaptive mesh refinement schemes based on error estimators. For example, the quantities $\mathrm{K_i}$ can be presented as functionals in terms of the displacement field, see e.g. [6]. The error of such functional values can be estimated by the dual-weighted-residual method developed mainly by Rannacher and co-workers [4]. The result is a cell-based error estimator in terms of residuals of the displacement field and a solution of a dual problem, the so-called weight, which can be used for estimating the overall error of the functional, but also to refine only the parts of the mesh, which really contributes to the error. The drawback of this approach is, that the dual solution also has to be calculated with finite elements and this makes computations expensive. But nevertheless, the resulting adaptive strategy is more efficient as for example global refinement and the main point is the precise error control. Especially in the context of crack propagation inaccurate numerical results can have catastrophic effects, which surely justify the higher complexity of this method. Similar methods can be used for the computation of local integral characteristics and for more details we refer to [7] and [10].

For solving the linear elasticity equations, MCrack2D uses the open-source library deal.II (www.dealii.org) based on Galerkin finite elements [2] coupled with the p4est package (www.p4est.org). Especially p4est realizes algorithms for the distribution of triangulations over (nearly) arbitrary numbers of nodes based on MPI. Using additional libraries such as PETSc (www.mcs.anl.gov/petsc) coupled with the Hypre

preconditioner (www.acts.nersc.gov/hypre) or Trilinos (trilinos.sandia.gov) for solving distributed linear systems numerical computations in MCrack2D are truly parallel. The Arminius cluster with the InfiniBand connect is predestinated for our computations and we use up to 10 nodes (120 cores) for computing quantities such as SIFs.

Various numerical results for plane problems were obtained in the last period of the project on the Arminius cluster, see e.g. [7][10]. A simulation of a crack path, for example in a CTS-specimen as shown in Fig. 1 for an isotropic (left) and a functionally graded material (right), needs about 50 simulation steps. In each step, the energy release rate has to be calculated, which at least needs the computation of two SIFs and three local characteristics $M_{i,j}(\vartheta)$ for different kink angles ϑ. Each computation of a SIF needs up to six, of a local characteristic up to twelve mesh refinement steps, where in any refinement step two finite element solutions have to be computed. For homogeneous materials the local characteristics must be computed only once, but have to be recalculated in each simulation step, if the crack reaches inhomogeneous parts of the specimen. Overall a high-accurate crack path simulation needs at least assembling and solving 50 x 2 x 6 x 2 = 1.200 linear systems with 16.000 up to 1.600.000 degrees of freedom (DoF) plus the computation of 3 local integral characteristics for up to 19 different kink angles with also at least assembling and solving 12 x 2 linear systems with 500 up to 1.890.000 DoF, plus additional computations in inhomogeneous regions of the specimen. This huge amount of numerical computations makes it absolutely necessary to use parallel solvers.

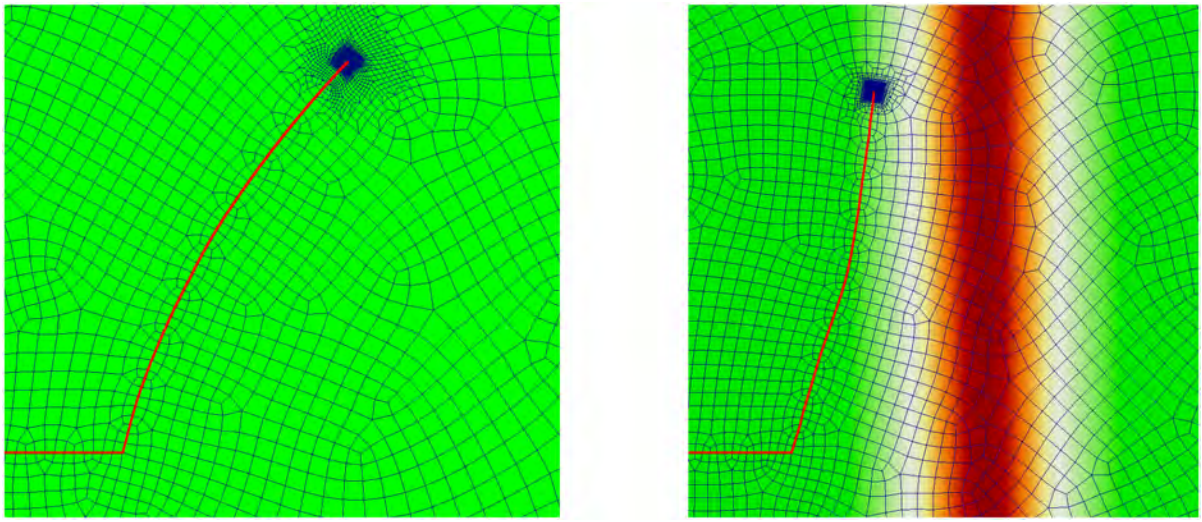

Fig. 1: Simulated crack paths in a CTS-specimen, Mode-II loading, isotropic Aluminium Alloy (left), and the same scenario with a local anisotropic inhomogeneity (right), see [10]

For a demonstration, the next table shows the calculation of a SIF in a CTS-specimen with 6 mesh refinement steps. Together with the estimated error, the number of DoF in the primal and dual problems plus the number of cells are shown. The grid is distributed over 120 cores and the number of cells hold on the first core is

printed in the first column. The last two columns show the total CPU time (in seconds) and the wallclock time. In all refinement steps the algorithm scales nicely to the number of processors.

Cells Core1/Total	DoF Primal	DoF Dual	Value SIF	Error	Total time (sec)	Wallclock time (sec)
66/7.933	16.618	64.978	284,05	17,01	2.210	18,5
119/14.305	30.846	121.712	285,29	7,76	2.730	22,7
223/26.833	58.462	231.796	285,96	3,81	3.660	30,5
423/50.854	110.562	439.486	286,22	1,90	5.270	43,9
805/96.670	209.166	832.994	286,38	0,96	7.880	65,7
1.533/184.015	392.764	1.565.890	286,44	0,48	12.800	107,1

On the way to the simulation of fully three-dimensional crack propagation in real-world problems the first barrier was a strategy, how the energy release can be calculated in such a scenario. Presented in [8] and [9], the change of potential energy caused by a small elongation of a smooth crack surface can be calculated to

$$\Delta \mathbf{U} = -\frac{1}{2} t \int_{\Gamma} h(s) \left(\sum_{i,j=1}^{3} K_i(s) M_{i,j}\big(\vartheta(s), s\big) K_j(s) \right) ds + \dots$$

Here, Γ is the crack front and s is the arc length. The length of the crack elongation in the normal plane at arc length s to direction $\vartheta(s)$ is $th(s)$, where t is a global time-like parameter and $h(s) \geq 0$ is a smooth function along the crack front.
The SIFs $K_i(s)$ depend on the displacement field of the solid and can be computed precisely at arc length s using a special sub-model technique and additional solutions of linear elastic problems depending on two space dimensions only, but with three vector components. Local characteristics $M_{i,j}(\vartheta(s), s)$ can be computed also from solving a linear elastic problem on a two-dimensional domain with three vector components, but depend highly on the material properties transformed to local curvilinear coordinates in the normal plane of the crack front at arc length s. A similar adaptive mesh refinement scheme based on error estimators as in two dimensions can be used to obtain high-accurate numerical results.
While the approach is very similar, the main difference to the simulation of two-dimensional problems is the astronomically large amount of computational work in three dimensions. As we have seen, in a plane crack scenario we had to solve at least 6 x 2 x 2 = 24 linear systems to obtain SIFs K_i accurately at the crack tip. Now, we have to compute at least three SIFs along the crack front in each step. Depending on the geometry of the structure and the crack front, this can mean that we have to solve about 6 x 2 x 3 = 36 linear systems at maybe some dozens of points along the crack front to obtain a reliable simulation.

Actual activities in this period of the project concern exactly these problems. The first aspect is, that we have to solve linear systems as fast as possible. Besides the optimization of solvers from external packages, like the Trilinos algebraic multigrid solver, the implementation of a matrix-free geometric multigrid solver tailored to these special linear elasticity problems is work in progress. A second aspect is, that the single problems to solve along the crack front are not too large itself, but there are many of them and ideal to parallelize. Together with a matrix-free solver the use of GPUs is a direction of actual and future work.

References

[1] Argatov, I. and Nazarov, S.: Energy release caused by the kinking of a crack in a plane anisotropic solid. *J. Appl. Maths. Mechs.* 2002; 66:491-503.

[2] Bangerth, W.; Hartmann, R. and Kanschat, G.: deal.II – a general-purpose object-oriented finite element library. *ACM Trans. Math. Softw.* 2007; 33(4):4.

[3] Griffith, A.: The phenomena of rupture and flow in solids. *Philos. Trans. Roy. Soc. London* 1921; 221:163-198.

[4] Rannacher, R.: Adaptive Galerkin finite element methods for partial differential equations. *J. Comput. Appl. Math.* 2001; 128:205-233.

[5] Specovius-Neugebauer, M.; Steigemann, M.; Nazarov, S. and Richard, H.A.: Energy release rates near the interface between two anisotropic solids. *Eng. Fract. Mech*. 2013; 108:162-169.

[6] Steigemann, M.: Verallgemeinerte Eigenfunktionen und lokale Integral-charakteristiken bei quasi-statischer Rissausbreitung in anisotropen Materialien. *Berichte aus der Mathematik*, Shaker Verlag: Aachen, 2009.

[7] Steigemann, M.: Simulation of quasi-static crack propagation in functionally graded materials. *Functionally Graded Materials*, Reynolds N (ed.). Nova Science Publishers, Inc. 2011.

[8] Steigemann, M.; Specovius-Neugebauer, M.; Schramm, B. and Richard, H.A.: On the calculation of crack paths in 3-dimensional anisotropic solids. *Proceedings of the 2012 Int. Conference on Crack Paths*, ISBN 978-88-95940-44-1.

[9] Steigemann, M. and Specovius-Neugebauer, M.: Change of energy caused by crack propagation in 3-dimensional anisotropic solids. Equadiff13 Conference, Prague, Czech Republic, accepted to appear in: *Special issues of Mathematica Bohemica dedicated to Equadiff13*, 2014.

[10] Steigemann, M. and Schramm, B.: On the precise computation of stress intensity factors and certain integral characteristics in anisotropic inhomogeneous materials. *Int. J. Fract*. 2013; 182:67-91.

5.4 Physics

5.4.1 Understanding materials from massively parallel ab initio calculations

Supervisor:	Prof. Dr. Wolf Gero Schmidt, University of Paderborn
Members:	Dr. Uwe Gerstmann, University of Paderborn Dr. Eva Rauls, University of Paderborn Dr. Simone Sanna, University of Paderborn Dr. Yanlu Li, University of Paderborn Dr. Heinz-Jürgen Wagner, University of Paderborn Marc Landmann, MSc, University of Paderborn Dipl.-Phys. Arthur Riefer, University of Paderborn Martin Rohrmüller, MSc, University of Paderborn Nora Jenny Vollmers, MSc, University of Paderborn Matthias Witte, MSc, University of Paderborn Hazem Aldahhak, MSc, University of Paderborn Rebecca Hölscher, MSc, University of Paderborn Andreas Lücke, MSc, University of Paderborn Christian Braun, BSc, University of Paderborn Sergej Neufeld, BSc, University of Paderborn Achraf Jaadouni, University of Paderborn Kris Holtgrewe, University of Paderborn
Supported by:	DFG (SCHM 1361/12, SCHM 1361/16, FWF I958, GE 1260/5, FOR 1405, FOR 1700), Nachwuchsgruppe des NRW-MIWFT, Solar-Weaver GmbH, contract No 2011-SW-01

Abstract

We employ density-functional theory and Green function methods in order to predict and understand a wide range of materials properties. Thereby we are interested in atomic geometries, electronic and optical excitation spectra, phase transitions and electron transport properties. Solid surfaces, organic/inorganic interfaces, ferroelectric materials and biomimetic model complexes are the focus of our present research. In the reporting period particular attention was paid to the optical properties of lithium niobate. Precisely, the frequency-dependent dielectric function and the second-order polarizability tensor of ferroelectric $LiNbO_3$ were calculated from first principles. The calculations are based on the electronic structure obtained from density-functional theory. The subsequent application of the GW approximation to account for quasiparticle effects and the solution of the Bethe-Salpeter equation yield a dielectric function for the stoichiometric material that slightly overestimates the absorption onset and the oscillator strength in comparison with experimental measurements. Calculations at the level of the independent-particle approximation indicate that these deficiencies are, at least, partially related to the neglect of intrinsic defects typical for the congruent material.

Project Description

The electro-optic, photorefractive, and nonlinear optical properties of ferroelectric lithium niobate [$LiNbO_3$ (LN)] are exploited in a large number of devices, such as optical modulators, acousto-optic devices, optical switches for gigahertz frequencies, Pockels cells, optical parametric oscillators, or Q-switching devices. The vast majority of actual applications and measurements employ congruent crystals grown by the Czochralski method. In fact, LN crystals are, in general, not stoichiometric LN (SLN) but congruent LN (CLN), i.e., Li deficient. Many physical properties, such as the Curie temperature, depend strongly on the existence of point defects related to doping or the Li deficiency of the congruent material. There are also indications that the optical properties of SLN and CLN differ notably. However, prior to our work no first-principles studies of the linear and nonlinear optical properties of congruent crystals were performed.

Generally, the polarization **P** of a medium may be expressed as a power series of the incident field **E**(ω) of frequency ω. In components, it is given by

$$P_\alpha(\omega) = \sum_\beta \chi^{(1)}_{\alpha\beta}(-\omega,\omega)E_\beta(\omega) + \sum_{\beta\gamma} \chi^{(2)}_{\alpha\beta\gamma}(-\omega,\omega_1,\omega_2)E_\beta(\omega_1)E_\gamma(\omega_2) + \sum_{\beta\gamma\zeta} \chi^{(3)}_{\alpha\beta\gamma\zeta}(-\omega,\omega_1,\omega_2,\omega_3)E_\beta(\omega_1)E_\gamma(\omega_2)E_\zeta(\omega_3) + \cdots$$

where $\chi^{(n)}(\omega)$ is the nth-order frequency-dependent susceptibility. $\chi^{(1)}(\omega)$ is the linear susceptibility related to the usual dielectric tensor through

$$\varepsilon_{\alpha\beta}(\omega) = \delta_{\alpha\beta} + 4\pi\chi^{(1)}_{\alpha\beta}(-\omega,\omega).$$

$\chi(2)(\omega) := \chi(2)(-2\omega,\omega,\omega)$ is relevant for the second-harmonic generation (SHG), where 2ω is the frequency of the field generated by the polarization of the medium and ω is the frequency of the incident field. Our work [1-4] aims at a better understanding of the influence of nonstoichiometry on the LN optical response. Calculations for the ordinary and extraordinary dielectric functions as well as for the energy dependence of the four nonvanishing components of the second-order polarizability tensor are presented.

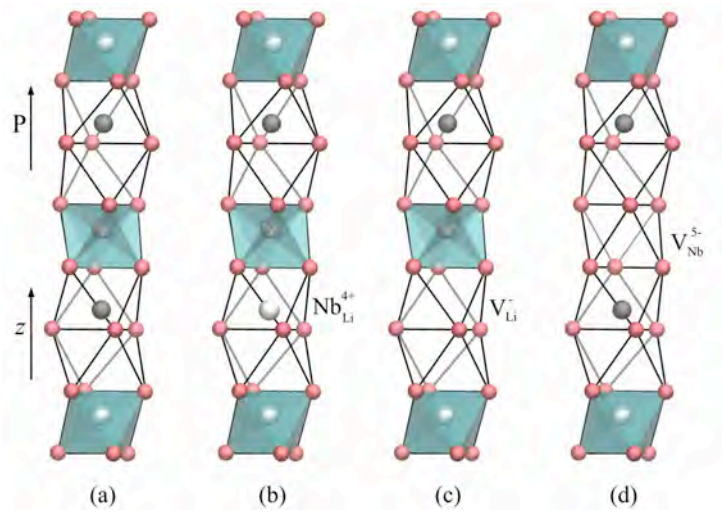

FIG. 1. Schematic of (a) bulk SLN and the defects considered in the CLN models: (b) Nb^{+4}_{Li} antisite, (c) lithium vacancy V^{-}_{Li}, and (d) niobium vacancy V^{-5}_{Nb}. Oxygen atoms are red, Li atoms are black, and Nb atoms are white. The Nb octahedra are shaded, the z axis and the polarization direction are indicated

CLN is strongly Li deficient and exhibits a [Li]/[Nb] ratio of 0.94. We simulate CLN by a charge-neutral supercell containing 360 atoms, which we construct by a 3×3×4 repetition of the primitive cell, with one Nb^{+4}_{Li} antisite and four Li vacancies V^{-}_{Li} (cf. Fig. 1). This corresponds a [Li]/[Nb] ratio of 0.92. For comparison, we also perform calculations within the Nb site vacancy model, denoted by CLN(Nb). In this case, a supercell of the same size containing five Nb^{+4}_{Li} antisites and four Nb vacancies V^{-5}_{Nb} is used, which again yields a [Li]/[Nb] ratio of 0.92

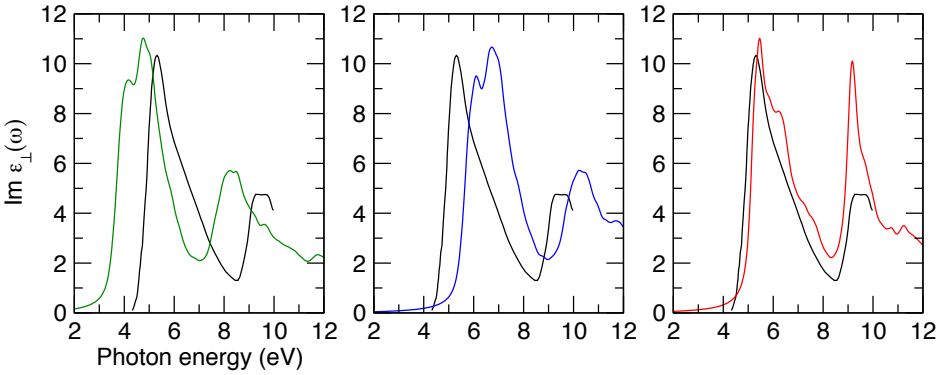

FIG. 2. Ordinary dielectric function of ferroelectric SLN. Calculated spectra on the DFT (green), GW (blue) and BSE (red) level of theory are compared with experiment (black)[7].

The calculation of the optical response proceeds [4-6] in three steps: First, we use density-functional theory (DFT) within the generalized gradient approximation to obtain the structural and ground-state electronic properties of ferroelectric SLN and CLN. Second, the quasiparticle band structure is calculated within the GW approximation (GWA) for the exchange-correlation self-energy. As usual, in practical applications of this scheme, we obtain the self-energy corrections to the electronic eigenvalue spectrum from a perturbative solution of the quasiparticle equation where the GGA exchange-correlation potential is replaced by the nonlocal and energy-dependent self-energy operator. We evaluate the latter in the standard non-self-consistent G_0W_0 approximation from the convolution of the single-particle propagator

G_0 and the dynamically screened Coulomb interaction W_0 in the random-phase approximation. Third, to obtain the linear dielectric function of SLN, we solve the Bethe-Salpeter equation (BSE) for coupled electron-hole excitations, which incorporates the screened electron-hole attraction as well as the unscreened electron-hole exchange. Here, we use the time-evolution method to obtain the polarizability. In Fig. 2, we show the calculated linear optical response of ferroelectric SLN according to the three levels of theory described above. While the inclusion of many-body effects such as electronic self-energy within the GWA and the electron-hole attraction via solving the BSE improves the agreement between experiment and

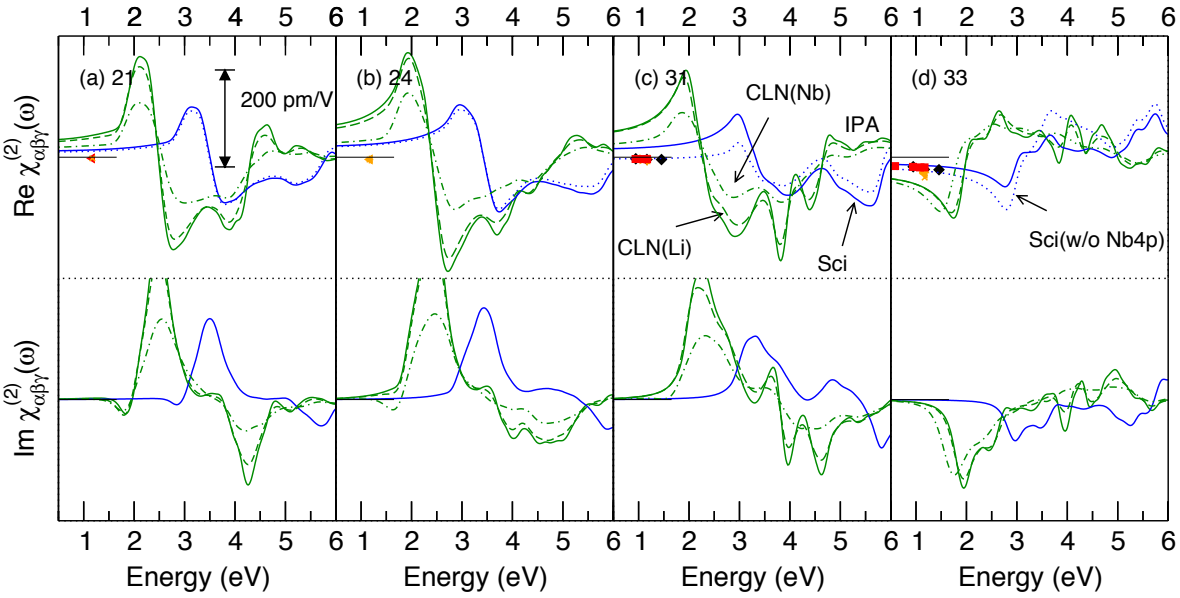

FIG. 3. Coefficients of the second-order polarizability tensor for SLN and CLN calculated within the DFT (green) and the GWA (blue), compared to experimental data [8].

theory considerably, there remain discrepancies. On the one hand, the calculations overestimate the onset of the optical absorption by about 0.2 eV. On the other hand, the double-peak structure of the first absorption maximum is far more pronounced in the calculations than observed experimentally. As we show in Ref. [1], part of these deviations arise from the neglect of point defects in the SLN calculations and are eliminated using the CLN models discussed above. Similar conclusions can be drawn for the nonlinear optical properties. In Fig. 3, we present the 21, 24, 31, and 33 components of the second-order polarizability tensor for ferroelectric LN calculated on the DFT and GW level of theory. Several experimental measurements of SHG data for LN have been reported in the literature, cf. discussion in [1]. The available data points are indicated by symbols in Fig. 3. The comparison with the calculated spectra at the DFT and GWA levels of theory shows that the former clearly overestimates the measured data, whereas, the calculations which include electronic self-energy effects, describe the optical nonlinearities better, especially the 33 component. Nevertheless, even the GWA calculations for SLN still yield stronger nonlinearities than observed experimentally. In this respect, it is interesting to note that the CLN results at the DFT level of theory indicate that the congruent material

gives rise to weaker SHG signals than predicted for SLN. This holds, in particular, for CLN(Nb). As for the linear response, the proper inclusion of defects in the congruent material, thus, also seems to improve the agreement between experiments and theory concerning $\chi(2)(\omega)$.

In summary, the linear and nonlinear optical responses calculated for the Li site vacancy model as well as the Nb site vacancy model are shown to be closer to the available experimental data than the spectra calculated for stoichiometric crystals: Compared to SLN, the CLN simulations lead to a redshift in the spectral features, wash out part of the fine structure, and reduce the nonlinearities. It is clear, however, that further work is required to fully understand the influence of crystal imperfections on the optical response of lithium niobate. On one hand, a variety of further defect configurations and defect complexes will have to be investigated. On the other hand, we expect many-body effects, which here were shown to have a strong impact on the optical response of SLN, to give rise to even stronger modifications of the CLN signal.

The Deutsche Forschungsgemeinschaft (DFG) is gratefully acknowledged for financial support. The calculations are performed within supercomputer time provided by the Paderborn Center for Parallel Computing PC^2 .

References

[1] Riefer, A.; Sanna, S.; Schindlmayr, A. and Schmidt, W.G.: Phys. Rev. B 87,195208 (2013).
[2] Riefer, A.; Sanna, S. and Schmidt, W.G.: Ferroelectrics 447, 78 (2013).
[3] Riefer, A.; Sanna, S.; Gavrilenko, A.V. and Schmidt, W.G.: IEEE Transactions on Ultrasonics, Ferro-electrics, and Frequency Control 59, 1929 (2012).
[4] Riefer, A.; Rohrmüller, M.; Landmann, M.; Sanna, S.; Rauls, E.; Gerstmann,U. and Schmidt,W.G.: High Performance Computing in Science and Engineering. '12, Springer-Verlag, Berlin, 17 (2013).
[5] Schmidt, W.G.; Albrecht, M.; Wippermann, S.; Blankenburg, S.; Rauls, E.; Fuchs, F.;Rödl,C.; Furthmüller,J. and Hermann,A.: Phys. Rev. B 77, 035106 (2008).
[6] Schmidt, W.G.; Glutsch, S.; Hahn, P.H. and Bechstedt, F. Phys. Rev. B 67, 085307 (2003).
[7] Wiesendanger, E. and Güntherodt, G.: Solid State Commun. 14, 303 (1974).
[8] Shoji, I.; Kondo, T.; Kitamoto, A.; Shirane, M. and Ito, R.: J. Opt. Soc. Am. B 14, 2268 (1997).

5.4.2 Lattice QCD on OCuLUS

Supervisor:	Olaf Kaczmarek, University of Bielefeld
	Mathias Wagner, Indiana University Bloomington
Members:	Florian Meyer, University of Bielefeld,
	Marcel Müller, University of Bielefeld
	Hiroshi Ono, University of Bielefeld
	Christian Schmidt, University of Bielefeld

Supported by:	BMBF under grant 05P12PBCTA
	DFG under grant GRK881
	EU unter grant 238353 (ITN STRONGnet)
	EU under grant 283286 (HadronPhysics3)

Abstract

We report on our research in high-energy physics. We investigate the properties of strongly interacting-matter, i.e. quarks and gluons under extreme conditions. The strong interaction is described by the theory of Quantum Chromodynamics (QCD). To approach QCD from first-principles Lattice QCD simulations are the method of choice. These simulations are computationally extremely demanding. Within our project we are continuing our efforts to obtain high-precision data for the fluctuations of conserved charges. One of the applications possible with these high-quality data is the determination of freeze-out conditions in heavy-ion collisions based on ratios of cumulants of net electric charge fluctuations. These ratios can reliably be calculated for a wide range of chemical potential values by using a next-to-leading order Taylor series expansion around the limit of vanishing baryon, electric charge and strangeness chemical potentials. A comparison of lattice QCD results for ratios of up to third order cumulants of electric charge fluctuations with experimental results allows us to extract the freeze-out baryon chemical potential and the freeze-out temperature. We have successfully applied this method to preliminary data of the STAR and PHENIX collaborations.

The necessary lattice simulations are very demanding and highly parallel. They consist of two parts, the generation of gauge field configurations and in the following a measurement of certain observables. Both parts are ideally suited to run on accelerator cards. We used the Nvidia Tesla K20X GPUs in the Oculus cluster to generate gauge configurations used as input for the measurement stage. We observed a 1.7x speedup on the Tesla K20X cards over a previous generation Tesla M2075. The obtained data – the measured fluctuations as well as the gauge configurations - are also the foundation for future projects.

Project Description

The exploration of the phase structure of strongly-interacting matter is one of the major goals of the experimental programs at the Relativistic Heavy-Ion Collider (RHIC) as well as for future experiments at the upcoming FAIR and NICA facilities. To interpret these explorations the measurement of observables that can be connected to first-principles theoretical investigations is favorable. The fluctuations of conserved charges, e.g., baryon number (B), electric charge (Q) and strangeness (S) have turned out to meet these criteria. The experimentally measured fluctuations stem from the time when hadrons reappeared and reflect the conditions at the chemical freeze-out. To reflect any signals of critical behavior the freeze-out must occur close to the QCD phase boundary. This phase boundary is quite reliably known for small chemical potential from first-principle Lattice QCD simulations [1,2,3]. The freeze-out temperature and chemical potential, however, are traditionally obtained from fits of the measured hadrons yields to statistical hadronization models [4]. Although this successful description suggests that these freeze-out conditions can indeed be characterized by a freeze-out temperature T^f and baryon chemical potential μ_B^f one would clearly prefer a determination of these important parameters based on first-principles.

Here we will discuss such an approach, which relies on the calculation of the fluctuations of the conserved charges from LQCD. These fluctuations are commonly discussed in terms of the generalized susceptibilities. For details of the Lattice simulations see [1,2,5,6].

To obtain the freeze-out parameters we now need to determine the two parameters, T^f and μ_B^f . Net electric charge fluctuations can be calculated from LQCD simulations and have – in contrast to baryon number fluctuations – also been measured in experiments at RHIC. To eliminate unknown explicit volume factors we will consider ratios of these fluctuations. At least two independent ratios are required to fix the freeze-out parameters.

We have chosen R_Q^{31} and R_Q^{12}:

In leading-order R_Q^{31} does not depend on the chemical potential and is therefore suitable as thermometer. Once the temperature has been determined the in leading-order linear μ_B^f -dependency of R_Q^{12} motivates its choice as baryometer.

To demonstrate the thermometer and baryometer we apply our method to preliminary data from STAR [7].

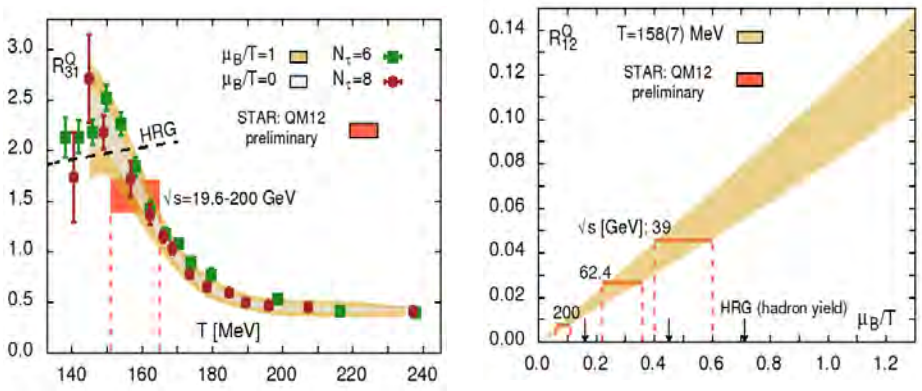

In the left figure we compare our data for R_Q^{31} with the corresponding preliminary data from the STAR experiment. From this we obtain T^f[8]
In the right figre we show the comparison for the ratio R_Q^{12}. For each collision energy the freeze-out chemical potential is obtained as the overlap of the experimental result with the LQCD data on the μ_B/T-axis. The black arrows indicate the freeze-out chemical potential obtained from the traditional statistical model fits [9].
This method is currently limited by the quality of the available experimental data. It is however preferable to have good control of the lattice data to reduce their contribution to the final error. Furthermore the use of various possible ratios and also fluctuations other than electric charge fluctuations is desirable to check the thermodynamic consistency of the approach.
The code used to generate the lattice data has been developed in Bielefeld. We started porting the measurement code to GPUs using CUDA back in 2009. Since 2012 we also ported the full rational hybrid Monte Carlo (RHMC) code used for the generation of gauge configurations to GPUs. To avoid performance impacts from copying data between the host system and the GPU we completely keep the data on the GPU and only rely on the CPU for control and I/O. Lattice QCD simulations are memory bandwidth-bound and require an optimized data layout and improved algorithms to avoid unnecessary memory access and saturate the available bandwidth. Details of the code have been presented in [10].
The Kepler architecture of the Tesla K20X cards feature several improvements which speedup lattice QCD simulations. Most of all the increased number of 255 registers per thread avoids the previously unavoidable spilling to cache or GPU main memory in some parts of the RHMC and the resulting performance impact. Furthermore the improved ECC implementation as well as the increased memory bandwidth allow for an increased performance. Compared to the previous generation Tesla M2075 cards we observed a speedup of about 1.7.
Currently we are porting our GPU program to the Xeon Phi architecture using the resources on OCuLUS to explore potential of those accelerators for future lattice QCD calculations.

In two other projects we are using CPU resources on OCuLUS in large MPI-parallelized calculations to determine transport properties of heavy quarks in the Quark Gluon Plasma phase. Using large quenched gauge field configurations, we obtained first results for the heavy quark momentum diffusion coefficient using a purely gluonic observable that require sophisticated noise reduction techniques [11] and for the heavy quark diffusion coefficient using hadronic correlation functions [12].

References

[1] Bazavov, A.: et al., Phys. Rev. Lett. 111, 082301 (2013).
[2] Bazavov, A.: et al., Phys. Rev. D 85, 054503 (2012).
[3] Kaczmarek, O. et al., Phys. Rev. D 83, 014504 (2011).
[4] Braun-Munzinger, P.; Redlich, K. and Stachel, J.: For a review see: In Hwa, R.C. (ed.) et al.: Quark gluon plasma 491-599, [nucl-th/0304013].
[5] Bazavov, A.: et al., Phys. Rev. Lett. 109, 192302 (2012).
[6] Bazavov, A.: et al., Phys. Rev. D 86, 034509 (2012).
[7] McDonald, D.: [STAR Collaboration], Nucl. Phys. A904-905 2013, 907c (2013).
[8] Mukherjee, S. and Wagner, M.: PoS CPOD 2013, 039 (2013).
[9] Cleymans, J.; Oeschler, H.; Redlich, K. and Wheaton, S.: Phys. Rev. C 73, 034905 (2006).
[10] Wagner, M.: GPU Technology Conference 2013, http://registration.gputechconf.com/quicklink/8S50xam
[11] Francis, A. and Kaczmarek, O.: et al., arXiv:1311.3759
[12] Ohno, H.: arXiv:1311.4565

5.4.3 Controlled motion of DNA-molecules through solid-state nanopores

Supervisor:	Peter Reimann, University of Bielefeld
Members:	Andreas Meyer, University of Bielefeld
	Thomas Töws, University of Bielefeld
Supported by:	DFG (SFB 613 and RE1344/8-1)

Abstract

We consider the translocation of short DNA fragments through a pore in a thin membrane with constant surface charge density. Membrane and particle (DNA) are surrounded by a container with electrolyte solution (i.e. potassium/sodium chloride), whose salt ions are screening the electric charges of particle and membrane. The particle is driven through the pore by thermal motion and an externally applied electrical field, which predominantly acts in the pore region. Our main objective is to theoretically analyze and tailor the translocation through the pore in order to control and slow down the motion of real DNA in experiments. From the electric current flowing through the pore one may, in principle, infer the DNA sequence because every DNA base-pair that is in the middle of the pore blocks it in an individual manner, resulting in different deviations from the empty pore current. Therefore, slowing down and controlling the DNA motion is required to achieve high resolution and sequence-related current signals. In one of our preliminary works, we explored a new separation mechanism for short and long nanorods in the presence of a pore. Based on the fact that, in the limit of small screening lengths, the net force on a particle inside the pore vanishes if its charge density is comparable to that of the membrane, we could explain the origin of the forces which lead to motion through the pore in opposite directions. Using a gate electrode, it is possible to tune the desired threshold length, above and below which the particles preferentially move in opposite directions. Explaining the origin of those forces is crucial for understanding the translocation process and for influencing it by experimental parameters, such as pore size, pore geometry, or (gate) voltage. Our model involves coupled partial differential equations (Poisson, Nernst-Planck, Stokes), which can only be tackled numerically, e.g. by employing finite element method.

Project Description

A. Completed Work (Publications [1, 2])

Our model system depicted in Fig. 1 consists of a cylindrical fluid chamber which is divided into two compartments by a thin solid-state membrane (typical thickness H ≈ 20 nm) with an hourglass-shaped pore (outer diameter D ≈ 20 nm, inner diameter d ≈ 10 nm, [3]) and a particle of radius R = 1.1 nm and length L = 2.2 - 50 nm, modeled as a cylinder with half spheres merged to the ends. For symmetry reasons and for the sake of numerical tractability, the particle is only allowed to move along the z-axis. The fluid chamber contains electrolyte solution with two oppositely charged

ionic species, assuming preset bulk concentrations far away from the membrane. Membrane and particle are modeled as insulators with constant surface charge densities σ_m and σ_p, respectively [4, 5], which are screened by the oppositely charged counterions in the electrolyte solution. Furthermore, the possibility of a gate electrode of thickness G within the membrane is indicated by dashed lines. An external voltage can be applied via the gray colored electrodes at the top and bottom of the system, the left/right electrode exhibiting a negative/positive potential.

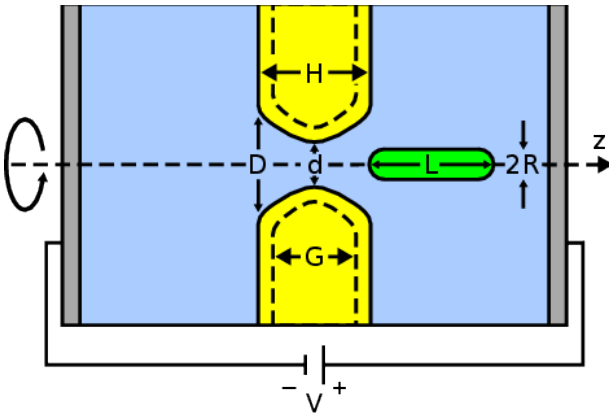

Fig. 1: Schematic illustration of the system. A membrane of thickness H (yellow) separates two compartments with electrolyte solution (blue) and contains an hourglass-shaped nanopore with minimal and maximal diameters d and D. The dashed lines indicate the possibility of an additional gate electrode of thickness G. A voltage V is applied to the electrodes (gray) and acts on a prolate particle with radius R and length L (green). The system is symmetric about the z-axis and z denotes the distance between pore and particle center. For further details see Refs. [1, 2].

The clear-cut time- and length-scale separation between the nanoparticle and the molecular degrees of freedom of the ambient fluid [6-8] allows us to take the particle position as a model parameter. Integrating the electrostatic and hydrodynamic forces acting on the particle at various positions yields the potential energy landscape, in which the particle is driven by thermal motion of the environment. For different particle lengths, a bulk concentration of 100mM, equal charge densities of particle and membrane ($\sigma p = \sigma m = -50$ mC/m^2 [4, 5]), and an external voltage of 100 mV, such energy landscapes are depicted in Fig. 2.

The two short (L < H) and long (L > H) particles take their energy minima on the left and right side of the membrane, respectively. This is so since there are two opposing forces acting differently on long and short particles: The potential drops almost exclusively in the pore, hence all forces induced by the electrical field arise in and close to the pore. First, because the (positively) charged fluid at the pore walls gets attracted by the external electric field, a fluid flow (electroosmosis) is generated, exerting drag forces as well as pressure forces on the particle.

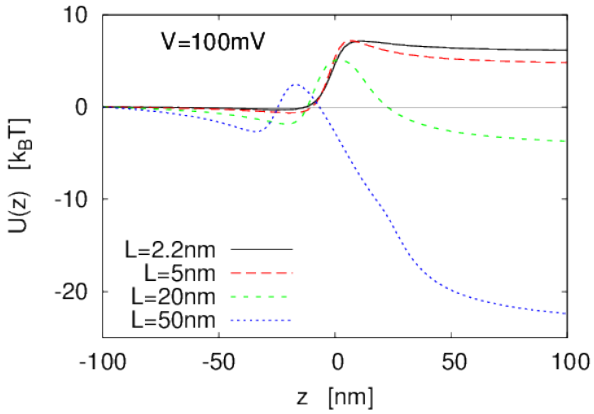

Fig. 2: The potential energy U(z) in units of the thermal energy k_BT of a particle at position z for different particle lengths L, V = 100 mV, and $\sigma_m = \sigma_p$ = -50 mC/m^2. The bulk concentration amounts to c_0 = 100 mM. (Figure adopted from Ref. [2].)

Second, the electric field also acts on the bare (negative) charge of the particle. As mentioned in the abstract, the forces mutually cancel for vanishing screening lengths, or equivalently, for high salt concentrations [2]. Now we consider the limit of a relatively small particle for finite screening lengths. One can show that for a sphere of radius R the electric and viscous forces scale like R^2 and R, respectively. Hence, in the limit $R \rightarrow 0$, the viscous force wins. Analogous scaling arguments are valid for small cylinders. Let us now turn to big particles, e.g. long cylinders. Then, there is ion exclusion in the pore, so that the electroosmotic flow (EOF) becomes weaker in comparison to the case of small particles. The electric force thus overwhelms the viscous force.

Reducing the absolute value of the membrane charge density to -40mC/m^2 results in the energy landscapes depicted in Fig. 3 (a). Because the EOF has become weaker (less charge), the curves are tilted to the right, according to the voltage sign convention in Fig. 1. For the same system but with an integrated gate electrode (Fig. 1) of thickness G = 16 nm and gate voltage of V_{gate} = -800 mV (relative to the external voltage), the energy landscapes are presented in Fig. 3 (b). The curves are clearly pushed up even in comparison to the case of equal charge densities (Fig. 2), because the gate potential effectively shifts the membrane charges, resulting in an increased EOF.

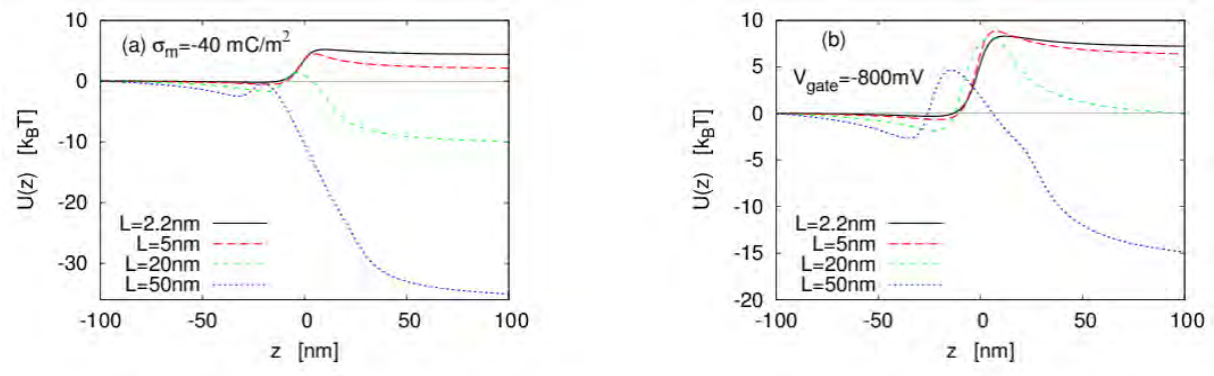

Fig. 3: (a) Same as in Fig. 2 (V = 100 mV, c0 = 100 mM) but now for an increased membrane surface charge density of σm = -40 mC/m2. (b) Same as in (a) but now for an additional membrane gate electrode of thickness G = 16 nm (see Fig. 1) with gate voltage Vgate = -800 mV.

B. Future Work

Currently we are investigating systems with several gate electrodes for purposes like transverse current sensing, or driving particles into energy minima near the pore walls. The first case aims at sensing individual nucleotides of DNA-molecules by measuring the transverse current through the molecule. This seems very promising because such local measurements yield signals with higher resolution. In the second case, translocation paths and combinations of multiple electrodes will be explored in order to influence the translocation velocity and the current through the pore. Both objectives require a numerical solution of the equations in three dimensions. Previously we confined ourselves to effectively two-dimensional cases to get around the huge numerical effort and associated computing time. In the near future we are planning to perform computations in three dimensions, using the COMSOL Multiphysics 4.3a finite element package running on the HPC Cluster at the Paderborn Center for Parallel Computing.

References

[1] Getfert, S.; Töws, T. and Reimann, P.: Phys. Rev. E **88**, 052710 (2013).
[2] Getfert, S.; Töws, T. and Reimann, P.: Phys. Rev. E **87**, 062710 (2013).
[3] Kowalczyk, S.W.; Grosberg, A.Y.; Rabin, Y. and Dekker, C.: Nanotechnology **22**,315101 (2011).
[4] He, Y.; Tsutsui, M.; Fan, C.; Taniguchi, M. and Kawai, T.: ACS Nano **5**, 5509 (2011).
[5] Behrens, S.H. and Grier, D.G.: J. Chem. Phys. **115**, 6716 (2001); Stein, D.; Kruithof, M. and Dekker, C.: Phys. Rev. Lett. **93**, 035901 (2004); Andersen, M.B.; Frey, J; Pennathur,S. and Bruus,H.: J. Colloid Interface Sci. **353**, 301 (2011).
[6] Bonthuis, D.J.; Zhang, J.; Hornblower, B.; Mathé, J.; Shklovskii, B.I. and Meller, A.: Phys. Lett. **97**, 128104 (2006).
[7] Kesselheim, S.; Sega, M. and Holm,C.: Comput. Phys. Commn. **182**, 33 (2011); Soft Matter **8**, 9480 (2012).
[8] Lubensky D.K. and Nelson, D.R.: Biophys. J. **77**, 1824 (1999); Reimann, P.: Phys. Rep. **361**, 57 (2002); Muthukumar, M. and Kong, C.Y.: PNAS **103**, 5273 (2006).

5.4.4 Reaction Dynamics of Photochromic Diarylethenes: Non-adiabatic Ab Initio Molecular Dynamics

Supervisor:	Jun.-Prof. Dr. Stefan Schumacher, Department of Physics and CeOPP, University of Paderborn
Members:	Christian Wiebeler, Department of Physics and CeOPP, University of Paderborn

Supported by:	Friedrich-Ebert-Stiftung and Deutsche Forschungsgemeinschaft through research training group GRK 1464 “Micro- and Nanostructures in Optoelectronics and Photonics”.

Abstract

Functionalization with molecular materials poses a promising route to the design of novel optoelectronic and photonic devices. Light-controlled, reversible molecular mechanisms add to the list of properties typically available in materials used in optical systems. One such molecular mechanism is photochromism, which is defined as a reversible transformation of a single chemical species between two forms with different absorption spectra. This transformation is induced in one or two directions via light irradiation [1]. In the past, azobenzene based polyelectrolytes were incorporated into tunable semiconductor microresonator structures [2]. Among the different photochromic materials that can reversibly and optically be switched between both of their forms, diarylethenes excel with high fatigue resistance, thermal stability, and high quantum yields [3]. Showing their photochromic functionality even in solid films, diarylethenes are promising to be used in solid-state photonic hybrid structures [4].

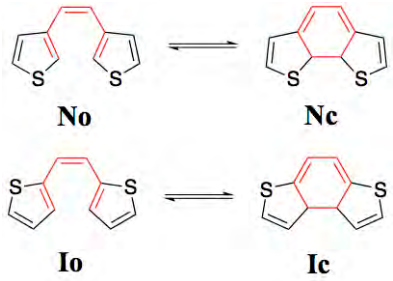

Scheme 1: Illustration of the two diarylethenes under study, normal-type (top) and inverse-type (bottom). Shown are open (left) and closed (right) ring forms. The reactive centers are highlighted.

Recently it was noted that the class of diarylethenes can be further divided into two subcategories: (i) normal-type diarylethenes in which the ethylene bridge is connected on both sides to a carbon atom of the thiophene ring that is in 3-position; and (ii) inverse-type diarylethenes in which the ethylene bridge is connected to a carbon atom in 2-position. The two structures are depicted in Scheme 1. The most important difference for prospective applications is that the quantum yield of the cycloreversion of I-type was recently found to be significantly higher than for the N-type [5].

To optimize photochromic materials further, it is crucial to understand the achievable reaction quantum yields and reaction time scales. However, these quantities typically only become accessible after a given substance has been synthesized. From a theoretical point of view, predicting reaction quantum yields involving excited electronic states usually poses a formidable task. Experimentally, reaction timescales are only accessible with advanced spectroscopic techniques. In the present study, we theoretically investigate the reaction mechanisms of I- and N-type diarylethenes. Our ab-initio calculations of the cycloreversion reaction dynamics are based on non-adiabatic Trajectory Surface Hopping (TSH). This approach gives us direct access to both reaction quantum yields and reaction time scales.

Project Description

The non-adiabatic ab-initio molecular dynamics was calculated along the lines given in Ref. [6]. Basis set and functional used were def2-SVP and PBE0, respectively. To generate a swarm of trajectories for the dynamical calculations with different initial conditions, the ground state of the rather rigid closed ring isomer was sampled using Born-Oppenheimer molecular dynamics. A timestep size of 50 a.u. was used and the ground state trajectories were calculated for a total of 4000 steps (≈ 4.84 ps). To ensure thermal equilibration, a Nosé-Hoover thermostat with a temperature of 300 K and a response time of 500 a.u. was used. Finally, 100 structures with corresponding nuclear velocities were randomly chosen to calculate the non-adiabatic ab initio molecular dynamics starting in the first excited singlet state based on Trajectory Surface Hopping. TD-DFT in Tamm-Dancoff approximation was used with a timestep of 40 a.u. and a total of 1000 timesteps (≈ 0.97 ps). The total energy was preserved during the time evolution. The implementation of the non-adiabatic dynamics calculations is based on linear response time-dependent density-functional theory. Only the non-adiabatic coupling between the first excited state and the ground state is included which can be easily justified here with the significant energy separation (≈ 0.6 eV) to higher-lying excited states as long as the system is found in the first excited state (cf. Figure 2, Figure 3, and Figure 4).

The calculations were performed with the SMP-version of Turbomole 6.5 and the parallelization described in reference [7] was used. Each trajectory of the non-adiabatic dynamics was run on a node of OCuLUS and in total 300 trajectories have been calculated to obtain the results presented in this study.

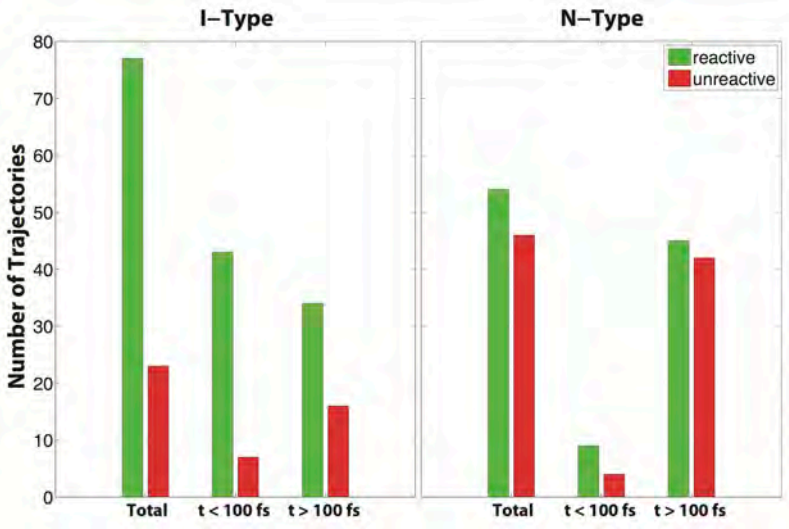

Fig. 1: Quantum yield of photoinduced cycloreversion of normal- (N) and inverse- (I) type diarylethenes

Having computed 100 trajectories for the cycloreversion reaction of normal- and inverse-type diarylethenes, statistics based on the results of the trajectories can be analyzed, see Figure 1. The numbers of trajectories that successfully lead to cycloreversion after relaxation into the S_0 ground state are shown in green. Out of these trajectories, for I-type a large number already shows a reaction on a very short time scale within the first 100 fs. For N-type, the reaction is considerably slower, so that only a few trajectories reach the ground state within the first 100 fs. Furthermore, the cycloreversion quantum yield is significantly lower in this case.

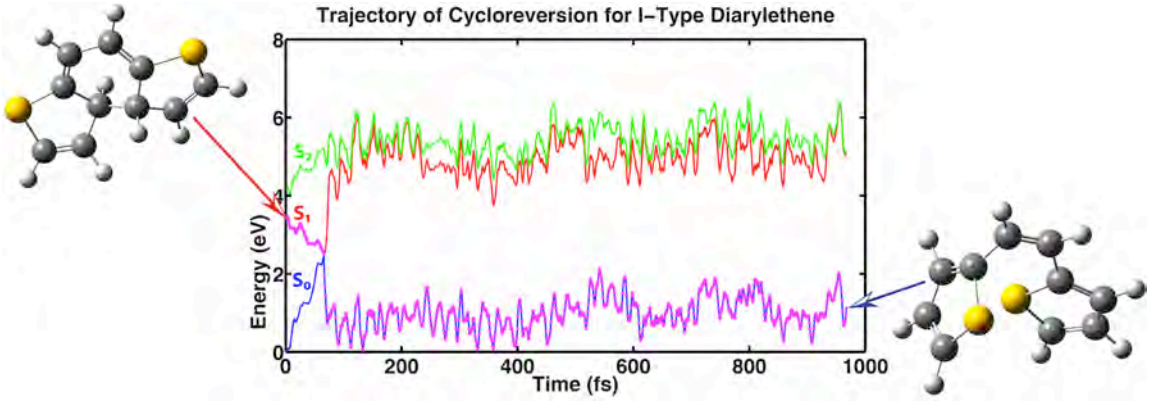

Fig. 2: Typical trajectory showing successful cycloreversion for the inverse-type diarylethene (representative of 43 % of trajectories)

To better understand the different outcomes of the dynamics, typical trajectories for both types of diarylethenes can be investigated. Figure 2 shows one of the 43 computed trajectories in which the inverse-type diarylethene reacts successfully within a very short time span of only 100 fs. Depicted are the respective energies of S_0, S_1, and S_2 states during the time evolution. After the system passes the conical intersection of S_0 and S_1, the energy separation between S_0 and S_1 significantly increases (compared to the initial separation at t = 0fs), indicative of the cycloreversion reaction. This is confirmed by the initial (closed ring form) and final

(open ring form) molecular geometries. The last remarks also hold for the trajectory of cycloreversion for normal-type diarylethenes as shown in Figure 3. However, in the first excited state the molecule is not as efficiently driven to the conical intersection as in the first case. Due to this, a successful reaction normally takes longer than for inverse-type diarylethenes. These findings explain the fundamental difference in the cycloreversion of normal and inverse type diarylethenes.

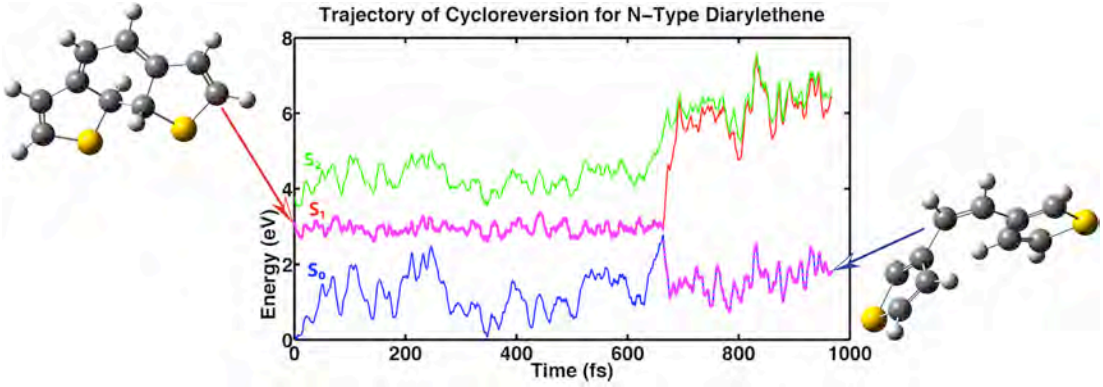

Fig. 3: Typical trajectory for successful cycloreversion for the normal-type diarylethene (representative of 44 % of trajectories)

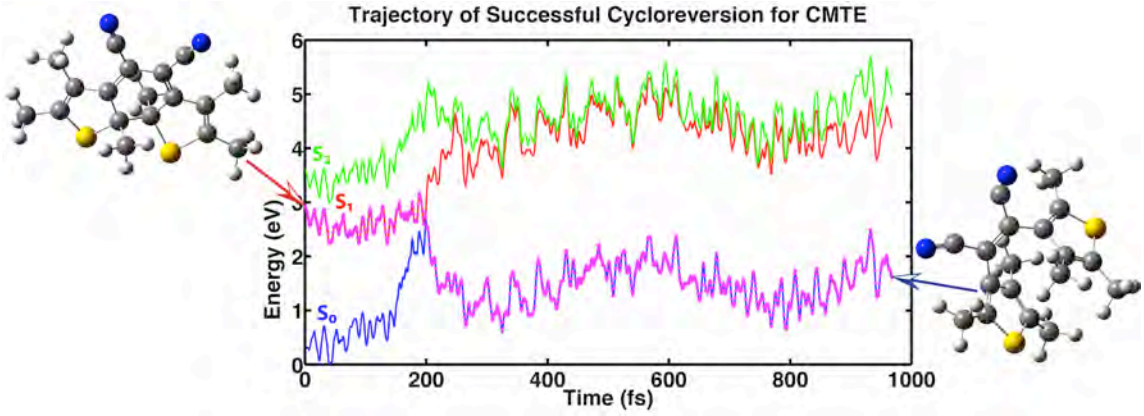

Fig. 4: Example showing a successful cycloreversion reaction for CMTE. The trajectory shown is representative for 11 of the 100 computed trajectories.

In a further study the cycloreversion of an experimentally relevant molecule, CMTE, is investigated. This molecule will be used for the functionalization of semiconductor microresonator structures [8, 9]. So, we calculated 100 trajectories for this significantly larger molecule and the quantum yield for cycloreversion we determine by our simulations is 0.11. This is in good agreement with previous values found experimentally, i.e. 0.07 ± 0.02 and 0.12 ± 0.02, respectively [10].

Inspired by these first calculations, there are many future directions that can be addressed. One promising aspect is to study the effect of substitutions at the reactive carbon atoms for N- and I-type diarylethenes for further optimization. Apart from its value to the specific field, the present study also constitutes a prime example of the

capabilities of available high-level quantum chemical methods in predicting reaction quantum yields and time scales for medium-sized molecular systems.

The results presented here were shown at two international conferences [11, 12]. Two full journal papers were recently submitted for publication [13, 14].

References

[1] Dürr, H. and Bouas-Laurent, H.: *Photochromism: Molecules and Systems,* ed Elsevier, 2003.

[2] Piegdon, K. A.; Lexow, M.; Grundmeier, G.; Kitzerow, H.-S.; Pärschke, K.; Mergel, D.; Reuter, D.; Wieck, A. D. and Meier, C.: *Opt. Express,* 2012, 20, 6060-6067.

[3] Yokoyama, Y. and Seki, T.: *New Frontiers in Photochromism,* ed. M. Irie, Springer Japan, 2013.

[4] Jean-Ruel, H.; Cooney, R.R.; Gao, M., Lu, C.; Kochman, M.A.: Morrison, C.A. and Miller, R. J. D.: *J. Phys. Chem. A*, 2011, 115, 13158-13168.

[5] Perrier, A.; Aloïse, S.; Olivucci, M. and Jacquemin, D.: *J. Phys. Chem. Lett.*, 2013, 4, 2190 -2196.

[6] Tapavicza, E.; Meyer, A.M. and Furche, F.: *Phys. Chem. Chem. Phys.*, 2013, 15, 18336-18348.

[7] Van Wüllen, C.: *J. Comput. Chem.*, 2011, 32, 1195-1201.

[8] Wiebeler, C.; Bader, C.A.; Meier, C. and Schumacher, S.: *Diarylethenes: Photochromism & Non-adiabatic Dynamics*, Meeting of the Graduate Program 1464 "Micro- and Nanostructures in Optoelectronics and Photonics", Paderborn, 2013.

[9] Bader, C.A.; Wiebeler, C.; Schumacher, S. and Meier, C.: *Photochromic Diarylethenes for Optically Tunable Microdisk Resonators*, Meeting of the Graduate Program 1464 "Micro- and Nanostructures in Optoelectronics and Photonics", Paderborn, 2013.

[10] Spangenberg, A.; Perez, J. A. P. ; Patra, A.; Piard, J.; Brosseau, A.; Métivier, R. and Nakatani, K.: *Photochem. Photobiol. Sci.,* 2010, 9, 188-193.

[11] Wiebeler, C.; Bader, C.A.; Meier, C. and Schumacher, S.: *Electronic and Optical Properties of Photochromic Diarylethenes,* 15th International Conference on Density Functional Theory and its Applications, Durham, 2013.

[12] Wiebeler, C. and Schumacher, S.: *Nonadiabatic Dynamics of the Cycloreversion of Diarylethenes: Normal- vs. Inverse-Type,* Excited States and Complex
Environments, Münster, 2013.

[13] Wiebeler, C. and Schumacher, S.: *Quantum yields and reaction times of photochromic diarylethenes: non-adiabatic ab initio molecular dynamics for normal and inverse type*, submitted.

[14] Wiebeler, C.; Bader, C.A.; Meier, C. and Schumacher, S.: *Optical spectrum, perceived color, refractive index, and non-adiabatic dynamics of the photochromic diarylethene CMTE*, submitted.

5.4.5 NANOHELIX

Supervisor:	Prof. Dr. Jens Förstner, University of Paderborn, Theoretical Electrical Engineering
Members:	Dr. Yevgen Grynko, University of Paderborn, Theoretical Electrical Engineering

Abstract

In this project we use computer simulations to solve the problem of light scattering by dielectric particles much larger than the wavelength of the incident light. Modeling of the scattering of light by realistic mineral particles is a complex task that appears in remote sensing of the Earth and Solar System bodies [1]. E. g., sands, clay clumps, planetary regoliths, atmospheric ice crystals can be relatively large which makes them a subject for massively parallel computations.

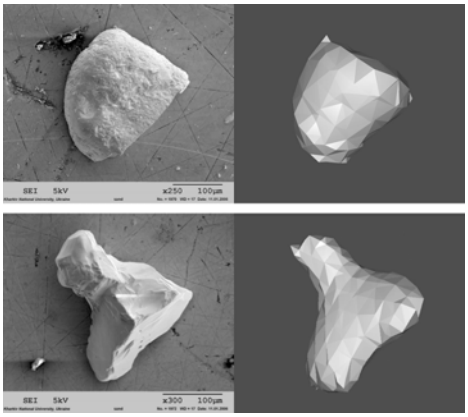

Fig. 1: Samples of real quartz sand particles and faceted models.

Various industrial applications, where the optical characterization of particles (color pigments, artificial aerosols, etc.) is employed, require similar considerations. Different approximations in modeling strongly depend on the specific conditions, e. g. the size, composition, and shape of the scattering particle of interest. Several numerical methods exist, which are more or less suitable in each specific case. Randomly irregular particles make the problem almost unsolvable if they are much larger than the wavelength of the incident light. There is no analytical solution of the electromagnetic problem for randomly irregular shapes. The only efficient approach here is to ignore wave effects and apply the geometrical optics (GO) approximation. More accurate numerical methods, e. g. the Discrete Dipole Approximation (DDA), T-matrix method or Finite Difference Time Domain (FDTD) method [2], which have little/no restrictions on the shape of the scatterer, require large computer resources if the size parameter $X = \pi d/\lambda$, where d is the particle size and λ is the wavelength, exceeds several tens.

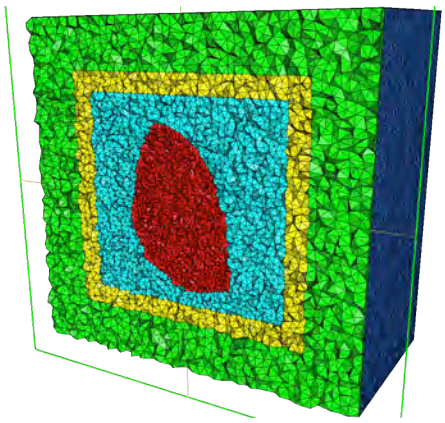

Fig. 2: Cross-section of the computational mesh with a model particle.

We apply the Discontinuous Galerkin Time Domain (DGTD) method [4, 5] and consider particles with size parameter $X = 60$ to approach the GO limit. Our results show that scattered intensity can be modelled with GO approximation already at this stage. Small absorption in the material significantly

improves the accuracy of GO. However, polarization still requires accounting for wave effects. In addition the DGTD method proved its parallel efficiency and performance in the simulation of light scattering by particles that are larger than the wavelength.

Project Description

The DGTD method is based on unstructured meshing that allows the optimal variation of spatial resolution throughout the computational domain. Additionally, the DGTD numerical scheme can be efficiently parallelized.

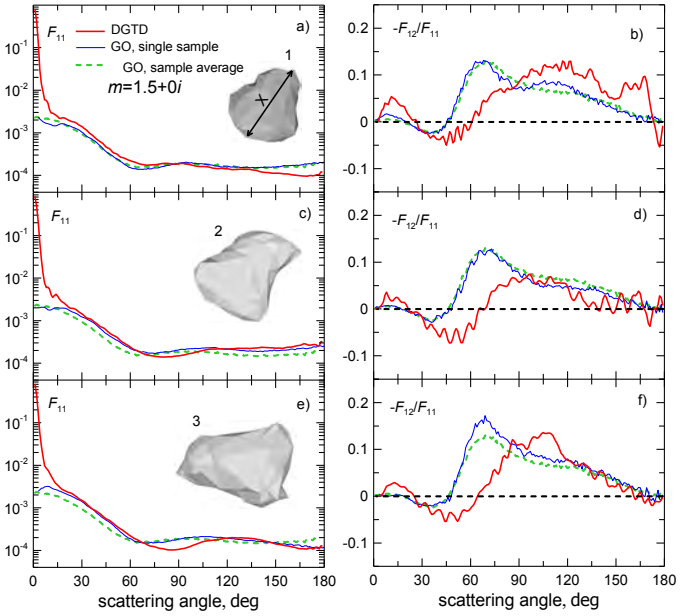

Fig. 3: Scattering angle curves of intensity (F_{11}, left) and degree of linear polarization ($-F_{12}/F_{11}$, right) for 3 arbitrary samples of GRF particles calculated with the DGTD method (m = 1.5 + 0.0i.) (thick solid lines), GO model (thin solid lines) and an average over 100 samples (dashed lines) calculated also with the GO model.

In a recent study [6] DGTD has been applied to simulate light scattering by large dielectric circular and hexagonal cylinders in 2-D regime. The results for size paramters X = 50 and 100 were found to be in good agreement with those provided by an improved geometric optics method (IGOM) [7, 8]. Here we consider 3-D scatterers and test a classic GO approximation against a wave optics.

Our implementation of the method is based on the example parallel DGTD code written by T. Warburton [9]. Our tests show very good scalability at least for up to 2000 CPU cores. For practical application of the code we implemented the source function, material mapping, total field/scattered field technique and the near-to-far-field transformation procedure. In essence, a particle placed in the computational domain is illuminated with a monochromatic wave until a steady state is reached. Then the scattered near field is Fourier-transformed and converted to the far field using the surface-integral method [10]. We found experimentally that a number of approximately 60 wave cycles is enough to reach the steady state for a given particles size and considered values of the refractive index.

In order to simulate numerically an open system with a finite computational domain we implemented an absorbing boundary condition using on the concept of the perfectly matched layer (PML) similarly to the formulation provided in ref. [11]

For all DGTD calculations we used the PC^2 clusters OCuLUS and Arminius with up to 2000 CPU cores in a single simulation. Based on these resources we take a size parameter of X = 60 (diameter of the circumscribing sphere) to realize orientation averaging in reasonable time. Previous studies, e.g. [12, 13] show that hundreds of orientations are required for reliably accurate result regarding the scattering matrix elements. In this work curves for each particle sample are averaged over 80 orientations only (including 180 scattering planes per orientation) to smooth out the spiky behavior of the scattering angle curves typical for large faceted particles.

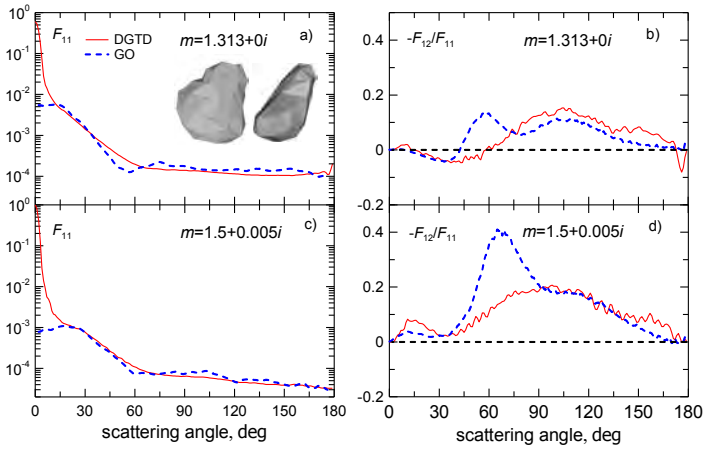

Fig. 4: Scattering angle curves of intensity (F_{11}, left) and degree of linear polarization ($-F_{12}/F_{11}$, right) calculated with the DGTD method (solid lines) and GO model (dashed lines) for sample 1 for two complex refractive indices m = 1.313 + 0.0i and m = 1.5 + 0.005i.

We here used the so-called Gaussian Random Field (GRF) particles [3]. They are generated with a 3-D GRF which can be considered as a 4-D single-valued surface with the Gaussian statistics of heights. We describe their surfaces by a set of triangular facets (200-300 facets per particle) and consider them as single independent scatterers, each within a computational domain. Tuning the particle generator parameters one can obtain shapes that are very similar to mineral grains like sand particles (see Fig. 1). In the last step a set of triangles representing the particle surface is used as an input for the tetrahedral mesh generator based on the TetGen library [14]. TetGen provides automatic generation of unstructured meshes with an option of local mesh refinement that can sufficiently reduce computational costs (see Fig. 2.).

Comparison of the accurate (DGTG) and approximate (GO) solutions for different samples in Fig. 3 reveals qualitative agreement in intensity between them. We note also that the intensity peak in the region of 0–15° formed solely by diffraction in the accurate solution is not present in the GO case as diffraction is totally ignored in our GO model. At the same time, polarization still requires accounting for wave effects at X = 60. The main discrepancy here is the maximum near 66° that is not reproduced by the accurate method at this particle size. The negative polarization branch at backscattering is definitely a wave effect. It varies from sample to sample but is persistently present for all of them.

In Fig. 4 we make a similar comparison for two different complex refractive indices for the particle shape 1 in Fig. 1. In the case of an “icy” material, m = 1.313 + 0i, (Fig. 2a,b) we see a slightly better agreement between two curves both in intensity and

polarization. Whereas the presence of absorption, $m = 1.5 + 0.005i$, leads to even better result (Fig. 2c,d) in the entire range of the scattering angles. This is consistent with previous results for cylinders. However, the 66°-feature in polarization still remains irreproducible at this size parameter.

In Fig. 5 we present six non-zero scattering matrix elements that are averaged for five samples of irregular particles. The sample averaging further improves performance of the GO model in intensity. This means that GO simulations can be used in the applications where high photometric accuracy is not critical. For instance,

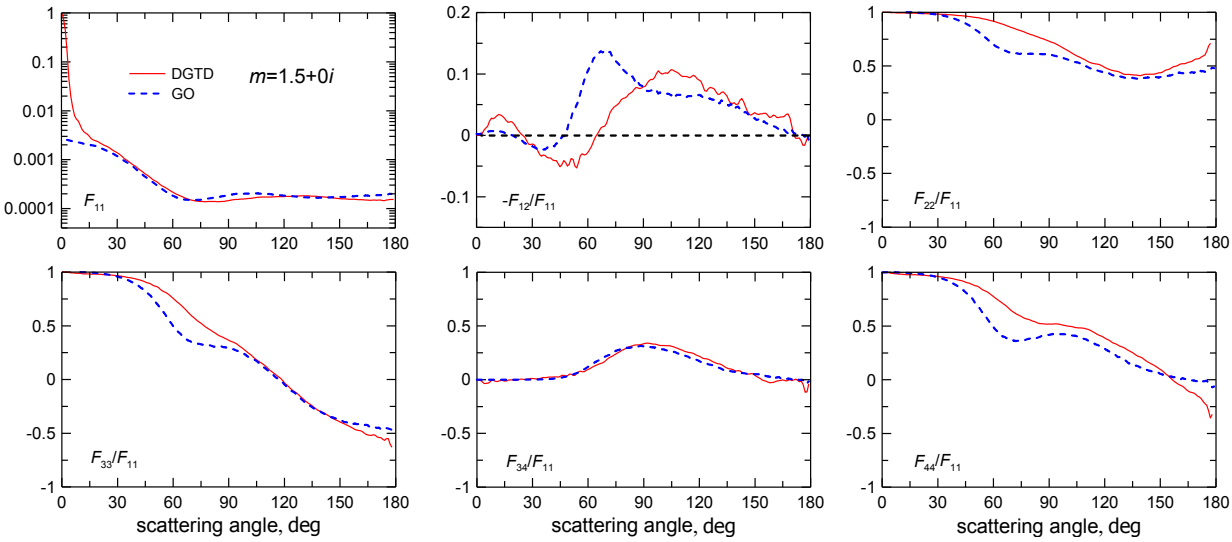

Fig. 5: Non-zero elements of scattering matrix calculated for five samples (all averaged over orientations) of GRF particles with the DGTD method (solid lines) and GO model (dashed lines) at $X = 60$, $m = 1.5 + 0i$.

one can carry out estimates in spectroscopy and photometry of mineral aerosols or surfaces formed by particles of this kind starting from $X = 60$ that corresponds to 6–10 μm in the visible range. The degree of linear polarization and other elements of the scattering matrix (Figs. 1–3) are more sensitive to the wave effects regardless if a single particle or a set of particles is considered. Especially this is seen near 66°. One can conclude that wave effects are very important in this domain. In order to decrease their role one should further increase the size parameter. Thus, we note that the GO approximation at $X = 60$ can be used for the analysis of polarization only at certain scattering angles (90º–180°).

We plan to consider larger size parameters of scaterrers in the future to reach the GO range at all scattering angles, including the the 66° positive polarization feature. Our first simulations for $X = 200$ show further improvement in the agreement between DGTD and GO. Such a scale required, however, the maximum of our resources that we have on the OCuLUS cluster. To realize this task to the full extent we will search for possible numerical optimizations.

References

[1] Videen, G.; Yatskiv, Y. and Mishchenko, M.: Eds. Photopolarimetry in remote sensing (Kluwer Academic Publishers, 2004).
[2] Kahnert, M. ; Quant, J. : Spectrosc. Radiat. Trans. 79, 775–824 (2003).
[3] Grynko, Y. and Shkuratov, Y.; Quant, J.: Spectrosc. Radiat. Trans. 78, 319-340 (2003).
[4] Hesthaven, J.S. and Warburton, T.; Comp, J.: Phys., 181, 186-221 (2002).
[5] Busch, K.; König, M. and Niegemann, J.: Laser & Phot. Rev., 5, 773-809 (2011).
[6] Tang, G.; Lee Panetta, R. and Yang, P.: Appl. Opt., 49, 2827-2840 (2010).
[7] Yang, P. and Liou, K.N.: Appl. Opt., 35, 6568-6584 (1996).
[8] Yang, P.; Feng, Q.; Hong, G.; Kattawar, G.W.; Wiscombe, W.J.; Mishchenko, M.I.; Dubovik, O.; Laszlo, I. and Sokolik, I.N.; of Aerosol, J.: Sci. 38, 995-1014 (2007).
[9] Warburton, T.: www.nudg.org
[10] Zhai, P. W.; Lee, Y. K.; Kattawar, G. W. and Yang, P.: Appl. Opt., 43, 3738–46 (2004).
[11] Niegemann, J.; König, M.; Stannigel, K.; Busch, K.: Photonics and Nanostructures – Fundamentals and Applications, 7, 2–11 (2009).
[12] Liu, C.; Lee Panetta, R.; Yang, P.; Macke, A. and Baran, A.J.: Appl. Opt., 52, 640-652 (2013).
[13] Um, J. and McFarquhar, G.M.; Quant, J.: Spectrosc. Radiat. Trans., 127, 207-223 (2013).
[14] Si, H.: tetgen.org.

6 PC² Bibliography

[1] Barrio, P.; Carreras, C.; Sierra, R.; Kenter, T. and Plessl,C.:
Turning control flow graphs into function calls: Code generation for heterogeneous architecture.
Proc. of the International Conference on High Performance Computing and Simulation (HPCS)*, 2012.*

[2] Beisel, T.; Wiersema, T.; Plessl, C. and Brinkmann, A.:
Programming and scheduling model for supporting heterogeneous accelerators in Linux.
Proc. of the Workshop on Computer Architecture and Operating System Co-design (CAOS), 2012.

[3] Berenbrink, P.; Brinkmann, A.; Friedetzky, T.; Meister, D. and Nagel, L.:
Distributing Storage in Cloud Environments.
Proc. of the High-Performance Grid and Cloud Computing Workshop (HPGC)*, 2013.*

[4] Birkenheuer, G.:
Risk Aware Overbooking for SLA Based Scheduling Systems.
PhD-Thesis, Paderborn Center for Parallel Computing, 2012.

[5] Birkenheuer, G.; Brinkmann, A.; Kaiser, J.; Keller, A.; Keller, M.; Kleineweber, C.; Konersmann, C.; Niehörster, O.; Schäfer, T.; Simon, J. and Wilhelm, M.:
Virtualized HPC: a contradiction in terms?
Software - Practice and Experience, 42(4):485-500, 2012.

[6] Congiu, G.; Grawinkel, M.; Narasimhamurthy, S. and Brinkmann, A.:
One Phase Commit: A Low Overhead Atomic Commitment Protocol for Scalable Metadata Services.
Proc. of the 4th Workshop on Interfaces and Architectures for Scientific Data Storage (IASDS), Beijing, China, 2012.

[7] Gesing, S.; Herres-Pawlis, S.; Birkenheuer, G.; Brinkmann, A.; Grunzke, R.; Kacsuk, P.; Kohlbacher, O.; Kozlovszky, M.; Krüger, J.; Müller-Pfefferkorn, R.; Schäfer, P. and Steinke, T.:
The MoSGrid Community – From National to International Scale.
EGI Community Forum, 2012.

[8] Gesing, S.; Herres-Pawlis, S.; Birkenheuer, G.; Brinkmann, A.; Grunzke, R.; Kacsuk, P.; Kohlbacher, O.; Kozlovszky, M.; Krüger, J.; Müller-Pfefferkorn, R.; Schäfer, P. and Steinke, T.:
A Science Gateway Getting Ready for Serving the International Molecular Simulation Community.
Proc. of Science, vol. PoS(EGICF12-EMITC2)050, 2012.

[9] Giefers, H; Plessl, C. and Förstner, J.:
Accelerating fine difference time domain simulations with reconfigurable dataflow computers.
Proc. of Int. Workshop on Highly Efficient Accelarators and Int. Workshop on Highly Efficient Accelerators and Reconfigurable Technologies (HEART), 2013.

[10] Grad, M. and Plessl, C.:
On the feasibility and limitations of just-in-time instruction set extension for FPGA-based reconfigurable processors.
Int. Journal of Reconfigurable Computing (IJRC), 2012.

[11] Graf, T.; Schäfers, L.; and Platzner, M.:
On Semeai Detection in Monte-Carlo Go.
Proc. of the Conference on Computers and Games, CG 2013, Yokohama, Japan, 2013.

[12] Grawinkel, M.; Süß, T.; Best, G.; Popov, I. and Brinkmann, A.:
Towards Dynamic Scripted pNFS Layouts.
Proc. of the 7th Parallel Data Storage Workshop (PDSW), Salt Lake City, Utah, USA, 2012.

[13] Grunzke, R.; Gesing, S.; Krüger, J.; Birkenheuer, G.; Wewior, M.; Schäfer, P.; Schuller, B.; Schuster, J.; Herres-Pawlis, S.; Breuers, S.; Balaskó, A.; Kozlovszky, M.; Szikszay Fabri, A.; Packschies, L.; Kacsuk, P.; Blunk, D.; Steinke, T; Brinkmann, A.; Fels, G.; Müller-Pfefferkorn, R.; Jäkel, R. and Kohlbacher, O.:
A Single Sign-On Infrastructure for Science Gateways on a Use Case for Structural Bioinformatics.
Journal of Grid Computing, 2012.

[14] Grunzke, R.; Birkenheuer, G.; Blunk, D.; Breuers, S.; Brinkmann, A.; Gesing, S.; Herres-Pawlis, S.; Kohlbacher, O.; Krüger, J.; Kruse, M.; Müller-Pfefferkorn, R.; Schäfer, P.; Schuller, B.; Steinke, T. and Zink, A.:
A Data Driven Science Gateway for Computational Workflows.
UNICORE Summit 2012, 2012.

[15] Herres-Pawlis, S.; Hoffmann, A.; Gesing, S.; Krüger, J.; Balaskö, A.; Kacsuk, P.; Grunzke, R.; Birkenheuer, G. and Packschies, L.:
User-Friendly Workflows in Quantum Chemistry.
IWSG, 2013.

[16] Herres-Pawlis, S.; Birkenheuer, G.; Brinkmann, A.; Gesing, S.; Grunzke, R.; Jäkel, R.; Kohlbacher, O.; Krüger, J. and Dos Santos Vieira, I.:
Workflow-enhanced conformational analysis of guanidine zinc complexes via a science gateway.
Studies in Health Technology and Informatics, IOS Press, vol. 175, pp. 142-151, 2012.

[17] Kaiser, J.; Meister, D.; Gottfried, V. and Brinkmann, A.:
Overcoming the Data Download Bottleneck in Data Centers.
Proc. of the 8th IEEE International Conference on Networking, Architecture, and Storage (NAS)*, 2013.*

[18] Kaiser, J.; Meister, D.; Brinkmann, A. and Effert, S:
Design of an exact data deduplication cluster.
Proc. of the 28th Symposium on Mass Storage Systems and Technologies (MSST), Pacific Grove, CA, USA, 2012.

[19] Kaiser, J.; Meister, D.; Hartung, T. and Brinkmann, A.:
ESB: Ext2 Split Block Device.
Proc. of the 18th IEEE International Conference on Parallel and Distributed Systems (ICPADS), Singapore, 2012.

[20] Kaufmann, P.; Glette, K.; Platzner, M. and Torresen, J.:
Compensating Resource Fluctuations by Means of Evolvable Hardware: The Run-Time Reconfigurable Functional Unit Row Classifier Architecture.
Intl. J. Adaptive, Resilient and Autonomic Systems (IJARAS), 3(4), pp.17-31, 2012.

[21] Kaufmann, P.; Glette, K.; Gruber, T.; Platzner, M.; Torresen, J. and Sick, B.:
Classification of Electromyographic Signals: Comparing Evolvable Hardware to Conventional Classifiers.
IEEE Trans. Evolutionary Computation, 17, pp. 46-63, 2012.

[22] Kasap, S. and Redif, S.:
Novel FPGA Architecture for Computing the Approximate EVD of Para-Hermitian Systems.
IEEE Transactions on Very Large Scale Integration (VLSI) Systems, doi: 10.1109/TVLSI*, 2013.*

[23] Kasap, S. and Redif, S.:
FPGA Implementation of a Second-Order Convolutive Blind Signal Separation Algorithm.
IEEE 21st Sig Process. Commun. Apps. Conf. (SIU), 2013.

[24] Kasap, S. and Benkrid, K.:
Parallel Processor Design and Implementation for Molecular Dynamics Simulations on a FPGA Parallel Computer.
Journal of Computers, 2012.

[25] Kenter, T.; Plessl, C. and Schmitz; H.:
Pragma based parallelization - Trading hardware efficiency for ease of use?
Proc. of the International Conference on ReConFigurable Computing and FPGAs (ReConFig), 2012.

[26] Meister, D.; Kaiser, J.; Brinkmann, A.; Kuhn, M.;Kunkel, J. and Cortes, T.:
A Study on Data Deduplication in HPC Storage Systems.
Proc. of the ACM/IEEE Conference on High Performance Computing (SC), Salt Lake City, Utah, USA, 2012.

[27] Meister, D.; Brinkmann, A. and Süß, T.:
File Recipe Compression in Data Deduplication Systems
Proceedings of the 11th USENIX Conference on File and Storage Technologies (FAST), 2013.

[28] Niehörster, O.:
Autonomous Resource Management in Dynamic Data Centers.
PhD Thesis, Paderborn Center for Parallel Computing, 2013.

[29] Niehörster, O.; Simon, J.; Brinkmann, A.; Keller, A. and Krüger, J:
Cost-aware and SLO Fulfilling Software as a Service.
Journal of Grid Computing, vol. 10, no. 3, pp. 553-577, 2012.

[30] Platzner, M; Boschmann, A. and Kaufmann, P.:
Wieder natürlich Gehen und Greifen.
ForschungsForum Paderborn, vol. 15, pp. 6-11, 2012.

[31] Popov, I.; Brinkmann, A. and Friedetzky, T.:
On the Influence of PRNGs on Data Distribution.
Proc. of the 20th Euromicro International Conference on Parallel, Distributed and Network-Based Processing (PDP), pp. 536-543, Munich, 2012.

[32] Redif, S. and Kasap, S.:
Parallel algorithm for computation of second-order sequential best rotations.
International Journal of Electronics 100(12), 2013.

[33] Riebler, H.; Kenter, T.; Sorge, C. and Plessl, C.:
FPGA-accelerated Key Search for Cold-Boot Attacks against AES.
Proc. of the International Conference on Field-Programmable Technology (FPT), 2013.

[34] Schlemmer, T.; Grunzke, R.; Gesing, S .; Krüger, J.; Birkenheuer, G.; Müller-Pfefferkorn, R. and Kohlbacher, O.:
Generic User Management for Science Gateways via Virtual Organizations.
EGI Technical Forum 2012, Prague, Czech Republic, 2012.

[35] Schumacher, T.; Plessl, C.; and Platzner, M.:
IMORC: an infrastructure and architecture template for implementing high-performance reconfigurable FPGA accelerators.
Microprocessors and Microsystems, vol. 36, no. 2, pp. 110-126, 2012.

[36] Thielemans, K.; Tsoumpas, C.; Mustafovic, S.; Beisel, T.; Aguiar, P.; Dikaios, N. and Jacobson, M.W.:
STIR: Software for Tomographic Image Reconstruction Release 2.
Physics in Medicine and Biology, 2012.

[37] Wistuba, M.; Schäfers, L. and Platzner, M.:
Comparison of Bayesian Move Prediction Systems for Computer Go.
Proceedings of the IEEE Conference on Computational Intelligence and Games, pp. 91-99, Granada, Spain, 2012.